

17.1 Introduction

The last four chapters have been concerned with tensile properties, the extension of fibres under loads applied along the fibre axis. The influence of forces in other directions is also interesting and of practical importance. The bending and twisting of fibres influence the behaviour of bulked yarn filaments and the drape and handle of fabrics. Recovery from bending is a factor in creasing. Twisting and bending both play a part in the arrangement of fibres in a yarn, and transverse compressive forces are involved when tension is applied to a twisted yarn. Bending strength and shear strength may be important in wear. It is these properties that will be considered in this chapter.

17.2 Bending of fibres

17.2.1 Flexural rigidity for small curvature

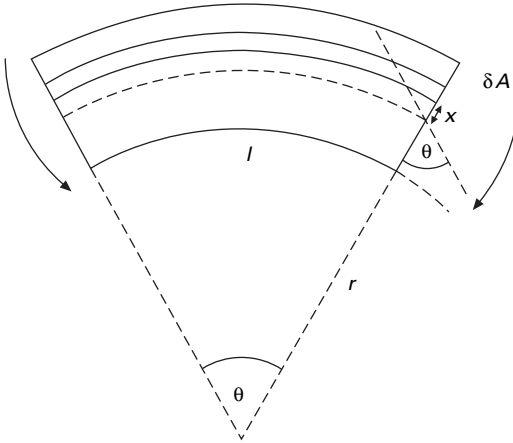
The flexural rigidity (or stiffness) of a fibre is defined as the couple required to bend the fibre to unit curvature. Curvature is the reciprocal of radius of curvature. By this definition, the direct effect of the length of the specimen is eliminated. The flexural rigidity may be calculated in terms of other fibre properties. The problem is similar to that of the bending of beams. Suppose we have a specimen of length l , bent through an angle θ to a radius of curvature r , as shown in Fig. 17.1. Its outer layers will be extended and its inner layers compressed, but a plane in the centre, known as the neutral plane, will be unchanged in length. As a result of the extension and compression, stresses will be set up that give an internal couple to balance the applied couple.

Consider an element of area of cross-section δA , at a perpendicular distance x from the neutral plane:

$$\text{elongation of element} = x \theta = \frac{xl}{r} \quad (17.1)$$

$$\text{tension in element} = \frac{xl/r}{E \delta A} \quad (17.2)$$

where E = Young's modulus,



17.1 Bending of a fibre.

the moment about an axis in the neutral plane

$$= \frac{x}{r} E \delta A x = \frac{E}{r} x^2 \delta A \quad (17.3)$$

$$\text{total internal couple} = \frac{E}{r} \sum (x^2 \delta A) = \frac{E A k^2}{r} \quad (17.4)$$

$$\text{where } A = \sum \delta A = \text{area of cross-section and } k^2 = \sum (x^2 \delta A) / \sum \delta A. \quad (17.5)$$

$E A k^2$ is often referred to as $E I$, where I is the moment of inertia of the cross-section. The parameter k is analogous to a radius of gyration, taken about the neutral plane. It may be related to a shape factor η , which is 1 for a circular fibre, by the expression:

$$k^2 = \frac{1}{4\pi} \eta A \quad (17.6)$$

$$\text{Since } A = \frac{c}{\rho} \quad (17.7)$$

where ρ = density and c = linear density of filament,

$$\text{and } E = \rho E_s \quad (17.8)$$

where E_s = specific modulus

$$\text{total couple} = \frac{1}{4\pi} \frac{\eta E_s c^2}{r \rho} \quad (17.9)$$

$$\text{flexural rigidity}^1 = \frac{1}{4\pi} \frac{\eta E_s c^2}{\rho} \quad (17.10)$$

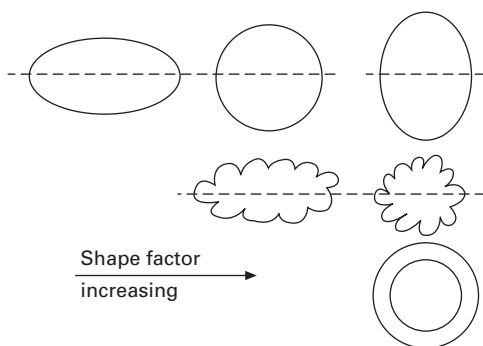
¹It should be noted that this equation is in a consistent set of units. In SI: E_s in N/kg m; c in kg/m; ρ in kg/m³; and flexural rigidity in N m². In likely practical units, with E_s in N/tex, c in tex, and ρ in g/cm³, the equation becomes: flexural rigidity = $(1/4\pi) (\eta E_s c^2) / \rho \times 10^{-3}$ N mm².

It follows from this relation that the flexibility of a fibre depends on its shape, its tensile modulus, its density and, most of all, its thickness.

The densities of the ordinary textile fibres range only between 1.1 and 1.6 g/cm³, so that this is not a very large factor. Values of the modulus obtained in tensile tests have been given in Chapter 13. They range from over 200 N/tex for HM–HT fibres to about 10 N/tex for polyester fibre and as low as 2 N/tex for wool. The shape factor becomes greater, and the rigidity increases, the more distant the material is from the centre. This is illustrated in Fig. 17.2. It will be seen that with an asymmetrical shape there may be a difference according to the direction of bending. In practice, the fibres will usually twist so as to bend about the easiest direction. For simple shapes, values of η may be obtained by integration from a relation derived from equations (17.5) and (17.6). For more complicated shapes, either numerical computation or experiment will be necessary. Table 17.1 gives some typical values.

Since the fineness comes in as a squared term, and in view of the range of values occurring in practice, from around 0.01 tex for microfibrils and smaller for nanofibrils to 1 tex for a coarse wool and higher for some hair fibres and manufactured monofilaments, it will be the most important factor in determining the flexural rigidity. The choice of fibre linear density is thus important in deciding flexibility.

In order to compare material properties, it is convenient to introduce a quantity that is independent of the fineness of the specimen. We may call this quantity the



17.2 Shape factors.

Table 17.1 Flexural rigidity (after Finlayson [1])

Fibre	Shape factor η	Specific flexural rigidity R_1 (mN mm ² /tex ²)
Viscose	0.74	0.19
Acetate	0.67	0.08
Wool	0.80	0.20
Silk	0.59	0.19
Nylon	0.91	0.14
Glass	1.0	0.89

specific flexural rigidity R_f , which is the flexural rigidity of a fibre of unit linear density². It equals (couple/curvature)/(linear density)² and is given by:

$$R_f = \frac{1}{4\pi} \frac{\eta E_s}{\rho} \quad (17.11)$$

Values of R_f obtained by using values of the modulus obtained in tensile tests are given in Table 17.1. They show the great flexibility of acetate filaments and the stiffness of glass.

The above analysis assumes that the fibre modulus E (or E_s) is constant. In reality, fibre stress–strain curves are mostly non-linear, so that the analysis applies only to small strains, namely to the relation between the initial flexural rigidity and the initial tensile modulus. For a neutral plane in the centre of the fibre, the maximum tensile strain, which will be positive on the outside and negative on the inside of the bend, equals r/R in a circular fibre, where r = fibre radius and R = radius of curvature of bend. Since fibres are so fine, quite small values of R (high curvature) result in fairly small strains, so that, in many practical situations, though not in severe creasing, it is only the initial flexural rigidity that is relevant.

17.2.2 Non-linearity at large curvatures

For more severe bending, the behaviour is represented by a moment–curvature relation. Non-linearity of stress–strain relations must then be taken into account. For most fibres, yield occurs at a lower stress in compression than in tension. This means that resistance to deformation will be less on the inside of a bend than on the outside. Consequently, in order to minimise strain energy, the neutral plane will move towards the outside. If the fibre shape and the stress–strain curves in tension and compression are known, the position of the neutral axis and the resistance to bending can be calculated.

A common procedure is to calculate an effective bending modulus E_B (or E_{Bs}) from the above equations. The difference from the modulus measured in tension gives an indication of the difference between compressive and extensional resistance.

Chapman [2] developed this approach by presenting his results as bending ‘stress–strain’ curves. This is a convenient way of normalising the information to eliminate the direct effect of fibre dimensions. He defined the bending strain as b/R , where b is half the thickness in the plane of bending. If the neutral plane is in the mid-way position, this is the maximum strain in the fibre. However, there will be lower strains in other parts of the fibre, with a complicated distribution if the fibre is irregular in shape. If the neutral plane shifts from the mid-position, the maximum strain (at the greater distance from the neutral plane) will be larger.

Equation (17.4) may be written as:

²The consistent SI units for specific flexural rigidity are $\text{N m} \times \text{m}/(\text{kg m}^{-1})^2$ or $\text{N m}^4 \text{kg}^{-2}$. If E is in N/tex and ρ in g/cm^3 , then $R_f = (1/4 \pi) (\eta E_s/\rho) \times 10^{-3} \text{ N mm}^2/\text{tex}^2$.

$$\text{moment} = M = \left(\frac{EAk^2}{b} \right) \left(\frac{b}{R} \right) \text{ or } \left(\frac{Mb}{Ak^2} \right) = E \left(\frac{b}{R} \right) \quad (17.12)$$

This equation is analogous to Hooke's law, and (Mb/Ak^2) has the dimensions of stress. Chapman therefore terms it the 'bending stress' and uses it in the more general non-linear situation.

Lee [3] has modified the standard analysis and derived the bending moment versus curvature relation for rectangular, elliptical and hollow cross-sections with a power law relation for the stress-strain properties of the material. In a later paper [4], he treats a greater variety of cross-sections. Jung and Kang [5] also analyse the large deflection of fibres with non-linear elastic properties. He and Wang [6] treat the buckling of fibres with irregular cross-sections.

17.2.3 Measurement of bending

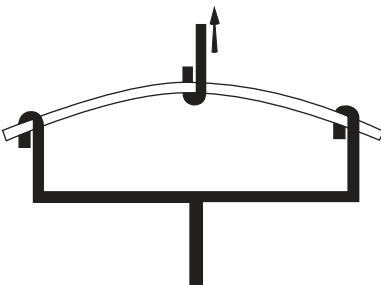
The flexural rigidity of coarse monofilaments may be measured by supporting the specimen at either end and finding the deformation due to a load at the centre. A tensile tester may be modified as shown in Fig. 17.3 [7].

Peirce [8] suggested studying the deformation of loops under an applied load. Carlene [9] used this method for viscose rayon filaments. A circular ring was suspended and loaded by a rider, as shown in Fig. 17.4. Peirce showed that:

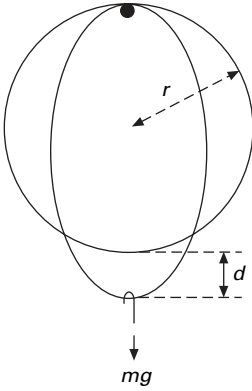
$$\text{flexural rigidity} = 0.0047mg(2\pi r)^2 \frac{\cos \theta}{\tan \theta} \quad (17.13)$$

where mg = weight of rider, r = radius of ring, $\theta = 493d/2\pi r$ and d = deflection of lower end of ring.

Guthrie *et al.* [10], following a method devised by Khayatt and Chamberlain [11], measured the deflection of short lengths (from a fraction of 1 mm to 2.5 mm) of filaments clamped at one end and loaded at the other. The loading was applied by pressing the specimen against a razor edge attached to the arm of a torsion-balance. The deflection could be measured by a microscope with a micrometer eyepiece. If the deflection was small, it could be shown that:



17.3 Adaptation of tensile tester for measurement of flexural rigidity of coarse fibres.



17.4 Measurement of flexural rigidity by a loop.

$$\text{flexural rigidity} = \frac{Fl^3}{3d} \quad (17.14)$$

where F = force applied to specimen, l = length of specimen from clamp to razor-edge and d = deflection of specimen.

The flexural rigidity may also be measured dynamically [12, 13]. One end of a specimen is vibrated transversely, and the frequency is varied until the position of resonance, at which the amplitude of vibration of the specimen is a maximum, is reached. At least 0.5 cm of straight fibre is required for a test, and it may be observed with a microscope. The method may be used at frequencies between about 20 Hz and 10 kHz. The air damping may usually be neglected, and the rigidity is then given by:

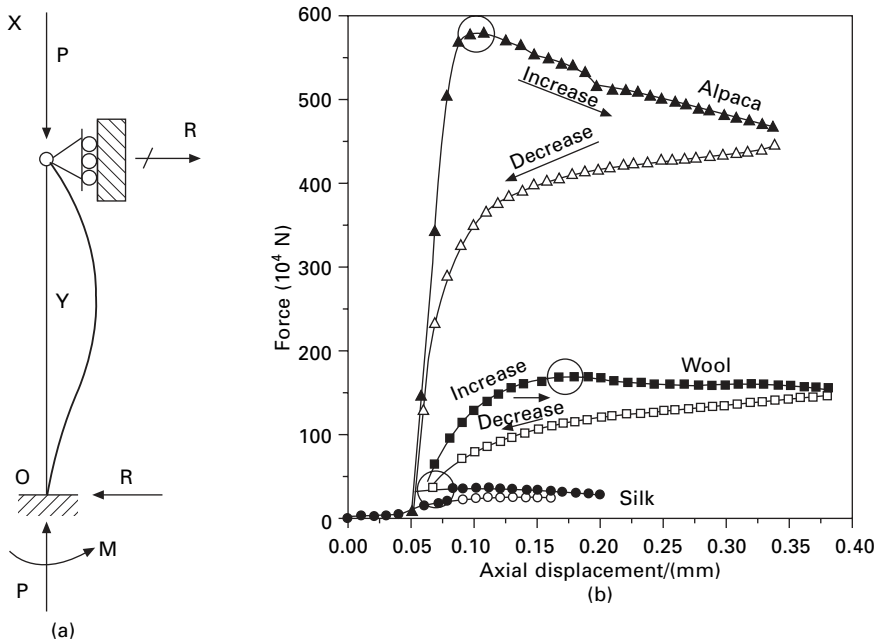
$$\text{flexural rigidity} = \frac{4\pi^2 A\rho l^4 f^2}{h^4} \quad (17.15)$$

where A = area of cross-section of specimen, ρ = density of specimen, l = length of specimen, f = resonant frequency and m depends on the harmonic that is being excited and is a solution of the equation $\cos h \times \cosh h = -1$ (for the fundamental $m = 1.8751$).

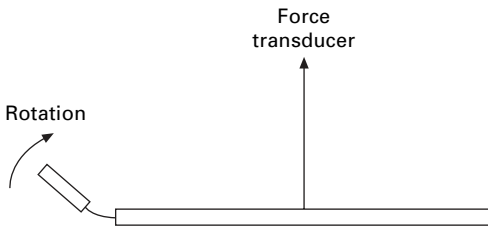
The loss modulus or $\tan \delta$ may be determined from the width of the resonance peak, as described in Section 16.5.3.

Yu and Liu [14] used a buckling test shown in Fig. 17.5(a) to measure bending resistance. Figure 17.5(b) shows the variation of displacement with axial compressive force. The force rises to a maximum, which is the critical value at which buckling occurs. Yu and Liu solve the differential equations for the bending mechanics and show that the effective bending modulus can be determined from the linear plot of critical stress against (D^4/L^2) , where D = fibre diameter and L = fibre length.

There are three experimental difficulties in measuring the full bending moment versus curvature relations: the manipulation of fine fibres at small radii of curvature; the measurement of small moments; and the maintenance of a uniform curvature in the specimen (most simple methods of bending lead to a variable curvature, as is apparent for example, from Figs 17.3, 17.4 and 17.5). Chapman [15] has described



17.5 (a) Axial buckling test. (b) Force displacement plots with critical condition circled. From Yu and Liu [14].



17.6 Principle of Chapman's fibre-bending tester [15].

an apparatus that overcomes these difficulties. It is based on a principle introduced in a fabric-bending test by Livesey and Owen [16]. The essential features of Chapman's method are shown in Fig. 17.6. Curvature is applied by rotation of one fibre mount, and the couple is determined by using a sensitive electronic microbalance to measure the force on a lever arm attached to the other mount. Provided that the lever arm is long, the errors due to non-uniform curvature are negligible.

17.2.4 Experimental results

Table 17.2 gives examples of the results of experiments on bending obtained by Owen [17], using a double-pendulum method. If the fibre is non-uniform, one would expect a difference between the moduli found in bending tests and those found in tensile tests, since the outer layers play a larger part in bending than do the centres

Table 17.2 Flexural and torsional properties of fibres 65% r.h.20 °C [18]

Fibre	Specific flexural rigidity (mN mm ² /tex ²)	Modulus GPa		Specific torsional rigidity (mN mm ² /tex ²)	Shear modulus (kN/mm ²)
		bending	tension		
Cotton	0.53		7.7	0.16	
Viscose rayon					
<i>Fibro</i> (staple)	0.35	10	8.7	0.058–0.083	0.84–1.2
<i>Vincel</i> (high wet modulus)	0.69	20		0.097	1.4
Secondary acetate	0.25		4.2	0.064	
Triacetate	0.25		3.8	0.091	
Wool	0.24	3.9	5.2	0.12	1.3
Silk	0.60		14	0.16	
Casein					
<i>Fibrolane</i>	0.18		2.3	0.11	
Nylon 6.6 (3 types)	0.15–0.22	2.5–3.6	1.9–3.8	0.041–0.060	0.033–0.48
Polyester fibre					
<i>Terylene</i>	0.30	7.7	6.2	0.067	0.85
Acrylic fibre (3 types)	0.33–0.48	6.0–8.1	4.9–7.0	0.12–0.18	1.0–1.6
Polypropylene	0.51	5.2	2.4	0.14	0.75

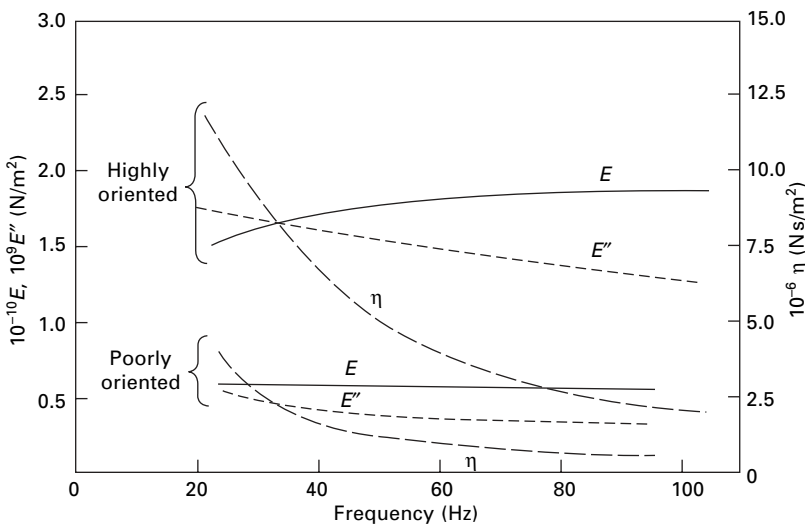
of the fibre. In practice, Guthrie *et al.* [10] found that the modulus in bending tests was greater than that in tensile tests at similar rates of loading for acrylic, polyamide and polyester fibres. K arrholm and Schr oder [19] obtained the same results for viscose rayon, but Khayatt and Chamberlain [11] found the bending moduli in wool to be lower than the tensile moduli. Yu and Liu [14], using the buckling test, found bending moduli of 1.47 GPa for wool, 2.15 for alpaca and 4.58 for silk.

In dynamic tests, Guthrie *et al.* [10] found that the modulus of viscose rayon was constant between 40 Hz and 7 kHz; but Horio *et al.* [20] observed a drop in the modulus near 20 Hz. This is shown in Fig. 17.7, together with values of E'' and η (see Section 16.5.2). This suggests that there is a peak in the absorption and a drop in the modulus at a low frequency.

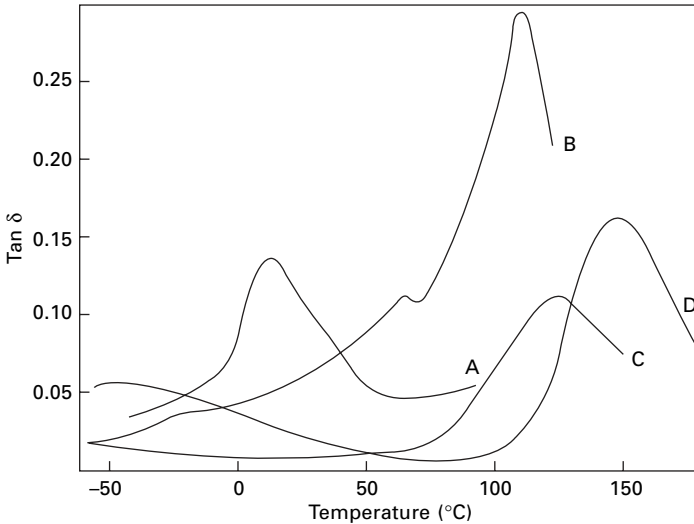
Meredith [18] reported dynamic-bending measurements of $\tan \delta$, as shown in Fig. 17.8 for four synthetic fibres, with peaks in the important range between 0 and 150 °C. He also reported rather complicated results for cellulosic and protein fibres. Other results have been given by Meredith and Hsu [13].

Elder [21] reported on the effect of temperature and humidity on the bending modulus of some synthetic monofilaments. It is interesting to note that nylon 6 and 6.6, polyethylene, and polypropylene are on the lower part of a sigmoidal curve between 20 and 80 °C, but polyester fibres are on the upper part. For example, at 65% r.h., the bending modulus of nylon 6 falls from 3 GPa at 15 °C to 1.3 GPa at 40 °C but then changes less, whereas *Terylene* polyester fibre is close to 13 GPa between 20 and 40 °C but falls to 10.3 GPa at 80 °C. A change in relative humidity of from 30 to 85% at 20 °C causes the bending modulus of nylon to fall from 5.5 to 1.5 GPa.

Experimentally, for viscose rayon, the flexural rigidity has been found to be proportional to $(\text{tex})^n$, where the index n is slightly less than the theoretical value of 2. Guthrie *et al.* [10] found $n = 1.96$ for Fibro staple fibre, and Carlene [9] found $n = 1.80$ and 1.82 for other specimens of viscose rayon.



17.7 Values of E , E'' and η in in bending of two viscose rayon monofilaments [20].



17.8 Tan δ measured in dynamic bending of fibres at 0% r.h at frequencies of 200–300 Hz: A polypropylene; B, acrylic fibre; C, nylon; D polyester fibre.

Skelton [22] reported that the bending recovery of 15 denier (1.67 tex) nylon fell steadily from close to 100 % for small curvature to about 20 % at high curvature.

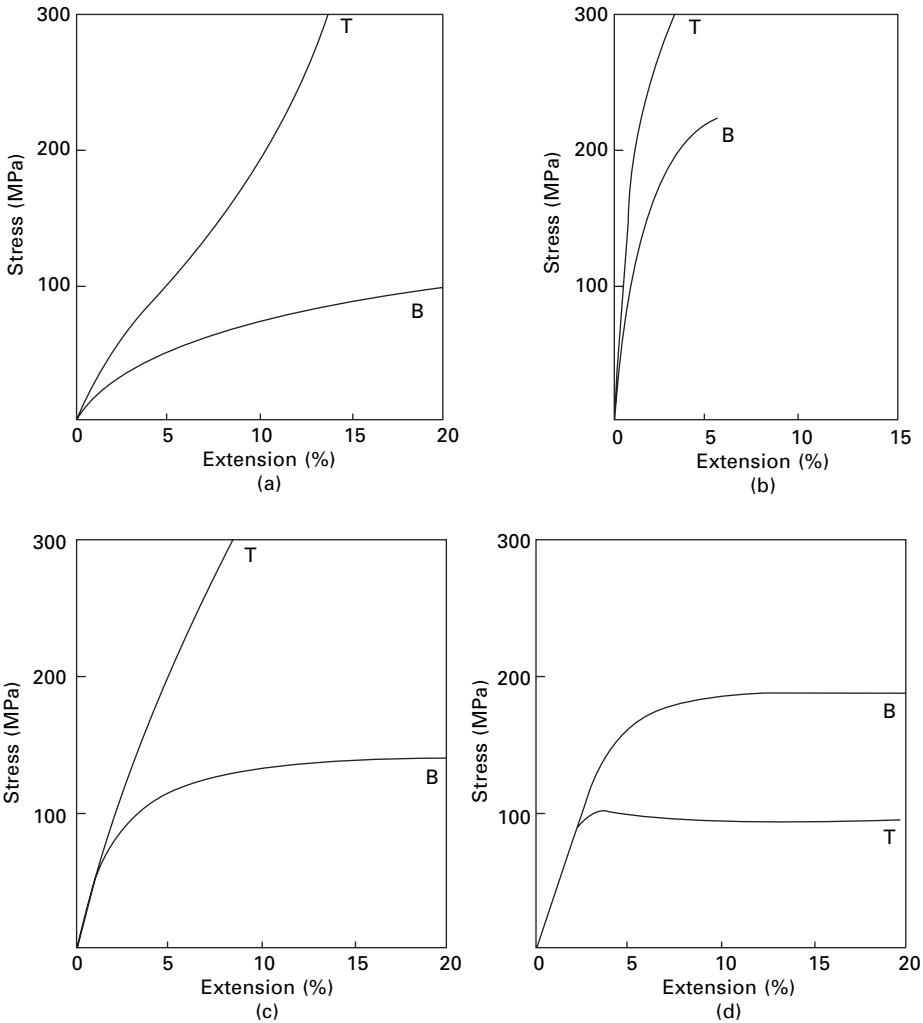
17.2.5 Bending stress–strain relations

Love [23] showed from elasticity theory that a modulus defined as the ratio of bending stress to bending strain is identical with the tensile modulus for a uniform, transversely isotropic beam. In the absence of other complications, the bending and tensile stress–strain curves should coincide near the origin.

If the fibres being tested are elliptical, with semi-axis a perpendicular to the plane of bending and semi-axis b in the plane of bending, then the bending strain is (b/R) as defined above, and the bending stress is $(4M/\pi b^2 a)$.

A comparison of bending stress–strain curves with tensile stress–strain curves is shown in Fig. 17.9. Generally similar results were found by Chapman with finer fibres, though it was not possible to carry the tests to such large bending strains.

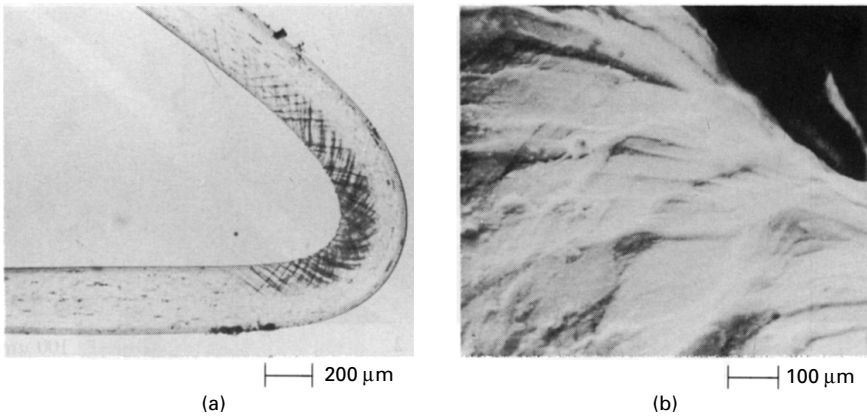
In all the manufactured fibres, the bending stress–strain curves lay below the tensile curves and indicated that yield in bending, due to yield on the compression side of the bend, occurred more easily than yield in tension. This was accompanied by the development of kink-bands on the inside of the bend. Observations of these kink-bands were described by Bosley [24] and Jariwala [25, 26]. Typical examples are shown in Fig. 17.10. Application of tension after a single bend removes the visible kink-bands and there is no loss of strength. The occurrence of kink-bands depends on test conditions. In polyester fibres, kink-bands develop in a single bend at 20 °C but not at 100 °C, whereas in nylon they appear at 100 °C but not at 20 °C. The development of kink-bands into flex fatigue failure, including the effect of temperature and humidity, is discussed in Section 19.5.2.



17.9 Bending (B) and tensile (T) stress–strain curves from Chapman [2]: (a) nylon 6 fishing line; (b) high-tenacity polyester fibre filament; (c) polypropylene monofil; (d) horse hair.

However, in horsehair (and wool), the bending curve is higher. If the yield behaviour were the same in compression as in tension, Chapman showed that the bending yield stress would be about 1.7 times as great as the yield stress in a tensile test. In fact, the bending yield stress in horsehair is twice the tensile value, and this indicates that the yield stress in compression is larger than the yield stress in tension. In this situation, the neutral plane will move towards the outside of the bend, whereas in the synthetic fibres it will move towards the inside.

Chapman [2] also studied the influence of ambient conditions in bending modulus and found, as would be expected, a decrease in stiffness with increase in temperature and humidity. In another paper, Chapman [27] described studies of bending-stress



7.10 Kink-bands in bent polyester fibres: (a) shown by polarised light microscopy; (b) visible on the surface in scanning electron microscopy.

Table 17.3 Loop and knot strengths

Fibre	$\frac{\text{Loop strength}}{\text{Tensile strength}} \times 100$	$\frac{\text{Knot strength}}{\text{Tensile strength}} \times 100$
Cotton		91
Viscose rayon		58
High-tenacity viscose rayon	96.5	63
Acetate		95
Wool		85
Silk		88
Nylon	82.5	86
Orlon acrylic fibre	80.9	
Dacron polyester fibre	72.8	
Fibreglas	8.4	5
	(from Coplan [28])	(from Bohringer and Schieber [29])
		(from Berry [30])

relaxation and recovery. Whereas wool and nylon usually did show complete recovery in time, polyester fibres were left with a permanent set, probably as a result of the compressive yielding.

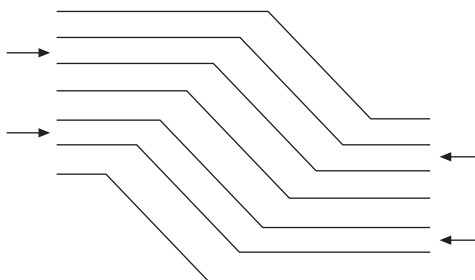
17.2.6 Loop strength and knot strength

If a filament is loaded in a bent state, it will break more easily than when it is straight. This is due to the initiation of breakage by the high extension of the outside layers. The reduction in strength, of which some values are given in Table 17.3, is greatest in fibres with the lowest elongation at break. A similar effect is observed when there is a knot in the filament, and values for the decrease in strength due to this cause are also given in Table 17.3.

17.2.7 Compression and bending in high-performance fibres

There is a major difference between different types of HM–HT fibres in their resistance to bending, which is related to their resistance to axial compressive stresses. Yielding in compression with the formation of kink-bands, which is described above for nylon and polyester fibres, is a more severe problem in highly oriented linear-polymer fibres. Yielding occurs by internal buckling of cylindrical elements. This is really a manifestation of the Euler buckling of a column, which occurs under a low stress when the aspect ratio L/D of the element is long. The simple Euler treatment is for a single element, but analogous effects occur in multiple assemblies provided that the interaction between the elements is not so high that shear between elements is prevented. For single rods or bundles without any lateral cohesion, the buckling will be into a smooth bending curve; but, where there is some interaction between neighbouring elements, it is more likely to occur as sharp kinks of the form indicated in Fig. 17.11. Details of the occurrence of kink-bands in aramid fibre filaments have been discussed by van der Zwaag *et al.* [31]. Such effects can occur at any structural level: fibres in a yarn or a composite; fibrils or other elements within a fibre; or the linear molecules themselves. Sometimes, the forms may be biased by particular structural features, such as crystal twinning or particular molecular conformations; but this is essentially a secondary effect and merely reflects that the yield will occur in the easiest of various possible ways.

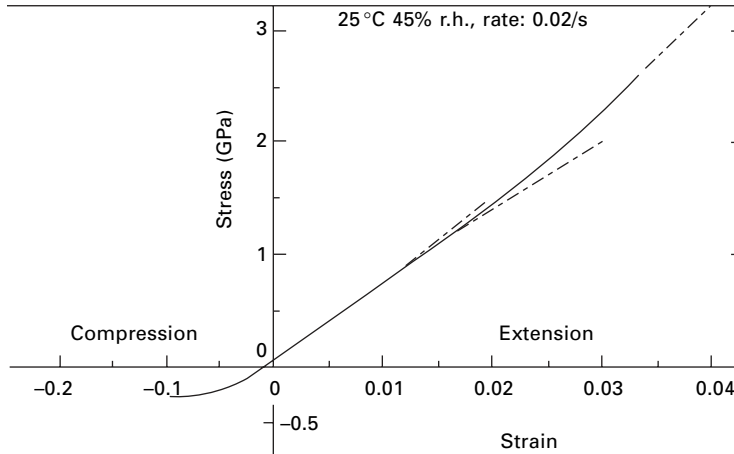
It is, of course, difficult to study single fibres in compression because, except at impossibly short test lengths, they buckle as a whole before the internal yielding occurs. However, the formation of kink-bands in compression can be demonstrated by the dynamic effects of snap-back after breakage. Quantitative estimates of compressive strength can be obtained from tensile recoil measurements [32], and some experimental results are listed in Table 17.4. Values of compressive strength can also be inferred from loop tests, and van der Zwaag and Kampschoer [33] found that the compressive strength of aramid fibres ranged from 0.5 GPa for a low-modulus type to 0.9 GPa for a high-modulus type. The values for HMPE were much lower. Compressive yield can also be shown in composites. For example, although the initial moduli in tension and compression of a *Kevlar 49*/epoxy unidirectional composite are almost the same, there is yield in compression at a strain of about 0.3% at a stress of about one-fifth of the tensile breaking stress. The yield determines the



17.11 Compressive deformation to a kink-band.

Table 17.4 Comparison of tensile strength and compressive strength measured in recoil [32]

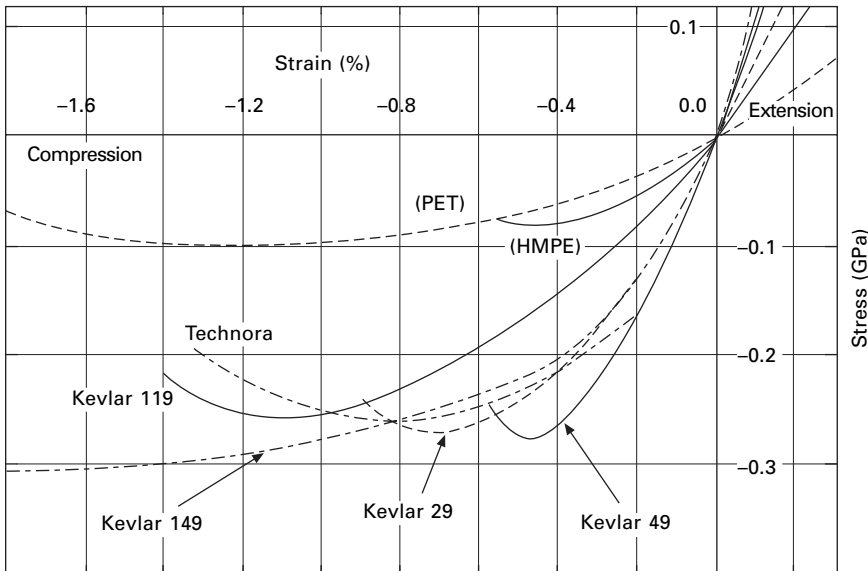
Fibre	Tensile strength (GPa)	Compressive strength (GPa)
<i>Kevlar 29,49</i>	3.4	0.37
Polyethylene, gel-spun	2.7	0.07
Carbon, <i>Magnamite AS4</i>	3.6	1.4
<i>Thornel P-55</i>	2.1	0.4



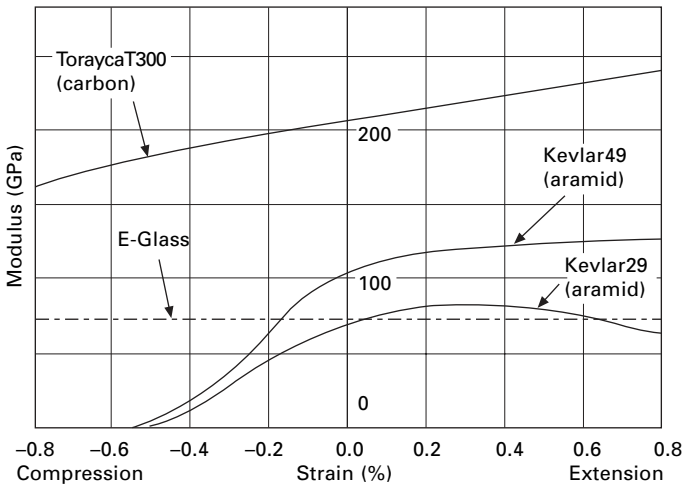
17.12 Aramid (*Kevlar 29*) fibre in axial extension and compression. From Kawabata [35].

maximum stress that an oriented linear polymer fibre can sustain. Consequently, the compressive strength is the same low value as the compressive yield stress.

Kawabata [34] developed a microcomposite method for measuring axial compression of fibres. A fibre bundle, which has been dipped in liquid epoxy resin is pulled into a *Teflon* tube with an inner diameter of 1 mm. After curing, the composite, which has a fibre volume fraction of 0.8 to 0.85, is extracted and cut into 5 mm lengths. Compression forces up to 2 kN are applied through a steel plunger giving deformations of less than 2 μm , which can be measured on an LDVT. The fibre stress is calculated from a simple mixture law. Figure 17.12, which includes axial extension, shows the low yield stress in axial compression. Results for a number of fibres are shown in Figure 17.13. HMPE and polyester fibres have a lower compressive yield stress than aramids. Another way of presenting the data by plotting the tangent modulus against strain is shown in Fig. 17.14. The low compressive modulus of the *Kevlar* fibres corresponds to the approach to the minima in Fig. 17.13. Glass shows a constant modulus, indicating linearity in extension and compression. The ceramic fibre *Tyranno* is also linear in extension and compression. The carbon fibre shows an increasing modulus, indicating a constant upward curvature in the stress–strain curve from compression to extension.



17.13 Axial compression behaviour of aramid fibres compared with HMPE and polyester. From Kawabata [34].



17.14 Longitudinal modulus as a function of strain. From Kawabata [34].

In contrast to the easy compressive yield of the one-dimensional structures, the three-dimensional bonding in ceramic and glass fibres allows no mechanism for compressive yield. If there is a high degree of three-dimensional interlocking in carbon fibres, there will be no mechanism for yield in compression, and the compressive strength will be high. But, in more perfect graphitic structures, the compressive strength will be lower.

The counterpart to the low compressive strength of the oriented linear polymer

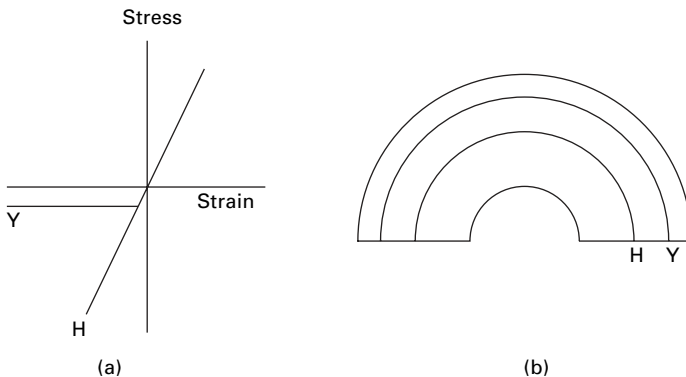
fibres is that they can suffer severe bending without breaking, whereas the three-dimensionally bonded fibres cannot do so.

Materials such as carbon, glass and ceramic fibres, which are linear elastic in tension and compression, follow the classical behaviour in bending, as shown in Fig. 17.1. The neutral plane remains central and leads to equal and opposite tensile and compressive strains on the outside and inside of the bend. If the radius of curvature of the bend is R and the fibre radius is r , the maximum strain present is r/R , and, when this equals the breaking strain, rupture will occur. Consequently, DuPont's alumina FP fibre with a breaking extension of 0.4% cannot be bent into a curvature tighter than 250 fibre diameters without breaking.

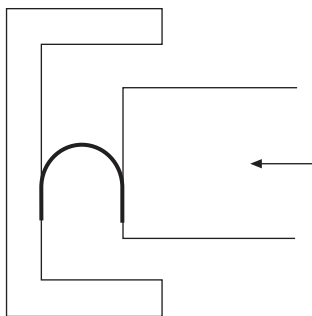
In contrast to this, when there is yield in compression, the neutral plane will move out to allow most of the deformation to occur by the easier compression mode. The situation is illustrated in Fig. 17.15. Mathematically, equation (17.2) has to be modified because the compressive force on an element on the inside of the bend, beyond the small region of elastic deformation, will be given by $f_y \delta A$, instead of $(x/R) Y \delta A$, where f_y is the yield stress and Y is Young's modulus. The division of area between the tension side, δA_t , and the compression side, δA_c , will be given by a minimisation of the deformation energy, U_b , where:

$$U_b = \sum 1/2(x/r)^2 Y \delta A_t + \sum f_y (x/r) \delta A_c \quad (17.16)$$

Schoppee and Skelton [36] have developed the bending–breakage test shown in Fig. 17.16, and this confirms that *Kevlar* fibres can be bent back on themselves without breaking. If the neutral plane had remained central, this would have implied a tensile strain of 100%. Values for various fibres are shown in Table 17.5. The fibres that do not yield in compression break at curvature levels close to those that would be predicted from the tensile breaking extensions. It is reasonable that the breaking strains calculated from bending tests should be larger than those from tensile tests, since they are effectively made on a very short test length, comparable with the fibre diameter.



17.15 (a) Stress–strain relations for Hookean material (H) and material yielding in compression (Y). (b) Bending response: H, neutral plane central; Y, neutral plane moving out.



17.16 The bending test developed by Schoppee and Skelton [36].

Table 17.5 Rupture in bending [36]

Fibre	Breaking strain in tensile test (%)	Maximum apparent strain in bending (%)
Glass	6.2	7.3
Graphite HM-S	0.8	1.4
HT-S	1.4	2.8
Kevlar 49	3.0	100

17.3 Twisting of fibres and the shear modulus

17.3.1 Torsional rigidity

The torsional rigidity of a fibre, its resistance to twisting, is defined as the couple needed to put in unit twist, that is, unit angular deflection between the ends of a specimen of unit length. The shear modulus is defined as the ratio of shear stress to shear strain, the shear strain being measured in radians.

The torsional rigidity can be obtained in terms of the shear modulus (or modulus of rigidity) in the same way that the flexural rigidity can be obtained in terms of the tensile modulus, since twisting bears the same relation to shearing as bending does to stretching.

We consider the twisting of a cylinder of length l , as shown in Fig. 17.17. After it has been twisted through an angle θ , a line AB has been sheared through an angle ϕ to the new position AC. The shear stresses set up give an internal couple opposed to the applied torque. The shear angle, which is zero at the centre, increases in proportion to the distance from the centre, x . Consider an element of area δA at a distance x from the centre:

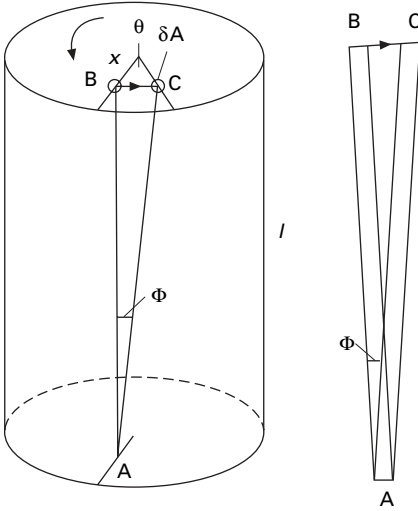
$$\text{shearing force} = v\phi\delta A = v(\theta x/l)\delta A \quad (17.17)$$

where v = shear modulus (force/unit area). Therefore:

$$\text{moment about the centre line} = v(\theta x/l)\delta A \cdot x = v\theta x^2\delta A/l \quad (17.18)$$

$$\text{total torque} = (v \theta / l) \sum x^2\delta A = vAk^2\theta/l \quad (17.19)$$

$$\text{where } Ak^2 = \sum x^2\delta A \quad (17.20)$$



17.17 Twisting of a fibre.

We can define a shape factor, ϵ , by the relation:

$$k^2 = \frac{\epsilon A}{2\pi} \quad (17.21)$$

This gives $\epsilon = 1$ for a circular fibre. The shape factor ϵ is different from η in bending, since, in equation (17.19), x is the distance from the centre line, whereas in equation (17.5), x is the distance from the neutral *plane*.

When equation (17.18) is converted to a relation involving specific shear modulus n , linear density c , density ρ and twist per unit length τ , it becomes:

$$\text{total torque} = \left(\frac{\epsilon n c^2}{\rho} \right) \tau \quad (17.22)$$

The torsional rigidity may be defined *either* as the torque to produce unit twist in radians per unit length, when it will equal $(\epsilon n c^2 / 2\pi\rho)$, or as the torque to produce one turn per unit length, when it will equal $(\epsilon n c^2 / \rho)$. The expression shows the effect of shape, density, modulus and fineness on the torsional rigidity of a fibre. As in bending, since fineness comes in as a squared term, it is the most important factor. It is convenient to introduce a quantity, the torsional rigidity of a specimen of unit linear density (in tex), independent of the fineness of the particular specimen, and this may be called the specific torsional rigidity³, R_t . It is given by:

$$R_t = \left(\frac{\epsilon n}{\rho} \right) \quad (17.23)$$

We have no direct values of the shear modulus, since these are found by torsional measurements, as described in the next section.

³See footnotes 1 and 2 on pages 415 and 417 for notes on units.

The determination of shape factor has been discussed by Meredith [37]. For simple shapes, the value of the shape factor may be obtained theoretically by integration, no measurement on the fibre being necessary. For slightly more complicated shapes, there are expressions for the shape factor that require the substitution of certain parameters of the fibre cross-section, for example, the major and minor axes of elliptic cross-section, or the relative areas of wall and void in hollow fibres.

For very complicated shapes, such as that of rayon, an experimental analogy may be used. If a membrane is formed across a hole having the same shape as the cross-section of the fibre and is then distended by air pressure, the shape factor will be proportional to the volume between the film and the plane of the plate containing the hole. This analogy depends on the fact that both problems are governed by equations of the same form. The experiment may be carried out by having a burette communicating with a vessel fitted with two plates, one having a hole of circular cross-section and the other a hole of the shape of the cross-section that is being investigated. The holes are covered with a soap film, and the volume needed to raise the circular membrane to a given height (and thus to a given air pressure) is measured first with both soap films being distended, and then with the irregular hole sealed off. Thus the volumes contained under the two membranes can be determined. The areas of the holes are also measured, and the shape factor is given by:

$$\epsilon = \left(\frac{V_1}{V_2} \right) \left(\frac{A_2}{A_1} \right)^2 \quad (17.24)$$

where V_1 and A_1 are the volume and area for the irregular hole, and V_2 and A_2 are the volume and area for the circular hole.

Table 17.6 gives expressions for the shape factor for various cross-sections and shows the values given by Meredith [37]. Lee [38] provides a more detailed analysis of the torsional rigidity of fibres with a generalised elliptical cross-section.

The above analysis is only valid for small twist. In Figure 17.17, $AC = AB \sec \phi$, which causes a tensile strain of $(\sec \phi - 1)$, increasing from the centre to the outside, where ϕ equals the twist angle α . Table 17.7 compares the shear strain, equal to $\tan \alpha$, with the tensile strain. At low twists, tensile strain can be neglected, but it must be taken into account at high twists, particularly as tensile modulus is greater than shear modulus. The tensile strains will be strongest for twisting at constant length. Figure 17.18 shows the development of torque and tension in a nylon monofilament twisted at constant length. At zero tension, the fibre will contract on twisting, reducing the tensile strain at the outside but giving a compressive strain at the centre.

17.3.2 Experimental methods

A method used by Morton and Permanyer [40] for measuring torque–twist relations is indicated in Fig. 17.19. The specimen is mounted between a rotating head A and a torsion-wire of known properties, which is connected to another rotating head C. The principle of the method is that, as the specimen is twisted by the rotation of A, the other head, C, is rotated so as to maintain the pointer B freely in a constant position, marked by the indicating pointer D. Owing to the absence of rotation of B,

Table 17.6 Shape factors for torsion (after Meredith [37])

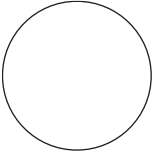
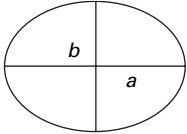
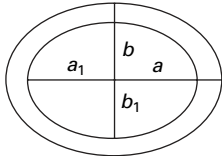
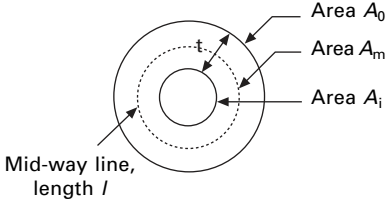
Cross-section	Expression for shape factor ϵ	Fibres approximating to the cross-section	Shape factor ϵ
Circular 	1	Cuprammonium rayon, nylon, casein, Ardil, Terylene, Saran, glass, polythene, etc.	1
Elliptical, $l = b/a$ 	$\frac{2}{e + 1/e}$	Wool	>0.977
Thin elliptical tube of constant thickness $a/a_1 = x$, $b_1/a_1 = e$ 	$\frac{(2e - 1 + x)^2 (1 + x)^2}{2(e + x)^3 (1 - x)}$	Kapok	5.07 (mean of 10 values)
Thick tube, constant wall thickness 	Approximately $\frac{4\pi A_m l}{(A_o - A_i)l}$	Cotton Flax Ramie	0.71 0.96, 0.92 0.77 (mean values)

Table 17.6 (Continued)

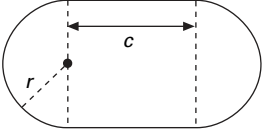


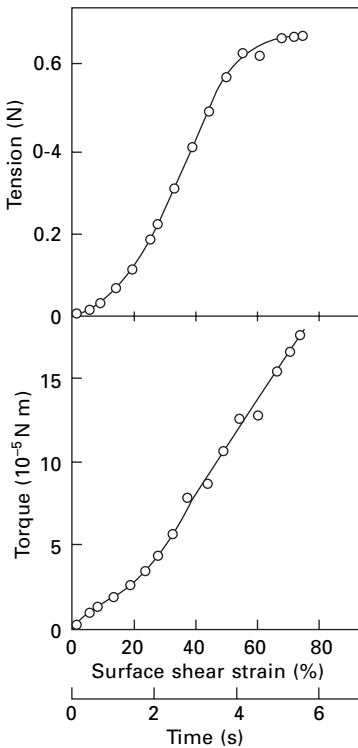
Cross-section	Expression for shape factor ϵ	Fibres approximating to the cross-section	Shape factor ϵ
Irregular, determined by soap-film method		Viscose { <i>Fibro</i> viscose rayon <i>Tenasco</i>	0.95 0.93 0.94
		Fortisan	0.97
		Acetate { <i>Celanese</i> <i>Seraceta</i>	0.73 0.69
Race-rack, $e = c/2r$	 $\frac{3(4e + \pi)^2}{\pi[3\pi(1 + 2e^2) + 8e(e^2 + 3)]}$	<i>Orlon</i> <i>Vinylon</i> <i>Vinyon</i>	0.57 0.66 0.67
Rectangular, $e = b/a$	 $\frac{2\pi e(1 - 0.63e)}{3}$	Tussah silk Calcium alginate	0.35 0.51
Quadrant of circle	 0.84	Silk	0.84

Table 17.7 Comparison of shear and tensile strains at surface of a circular fibre

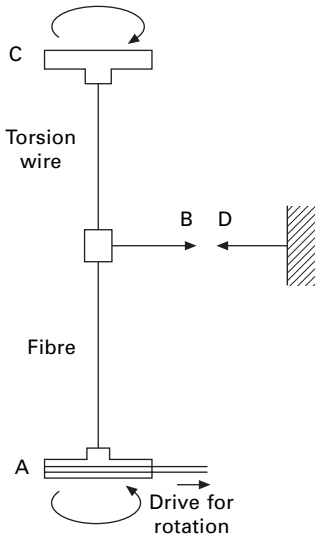
Twist angle α	Shear strain (%) $\tan \alpha$	Tensile strain (%) $\sec \alpha - 1$
1°	0.17	0.015
5°	8.7	0.4
10°	18	1.5
45°	100	41



17.18 Development of tension and torque in an 80 μm diameter nylon monofilament twisted at 5 turns/second. From Sikorski *et al.* [39].

the twist in the specimen is given by the number of turns taken by A, which may be rotated at a constant rate. The torque is obtained from the twist of the torsion wire, which is calculated from the angle turned through by C. Values are noted at intervals as the test is in progress. The same apparatus can be used for measuring the relaxation of torque. With sensitive transducers, the method could be automated [41].

A torque transducer suitable for fibres is described by Sikorski [42, 43] as part of the flexible thermomechanical analyser (FTMA) described in Section 18.5.2. It incorporates semiconductor strain gauges in a commercially available flexible pivot. Twist is directly inserted. The instrument is computer controlled to give programmed changes in two independent variables selected from tension, torque, elongation and twist together with temperature control. Another sensitive torsion tester is described by Kawabata [44].



17.19 Measurement of torque–twist relation [40].

Values of the torsional rigidity can also be found dynamically, by observing the oscillations of a torsion pendulum, which consists of a bar suspended by the fibre. It may be shown that:

$$\text{torsional rigidity of fibre} = \frac{8\pi^3 Il}{t^2} \quad (17.25)$$

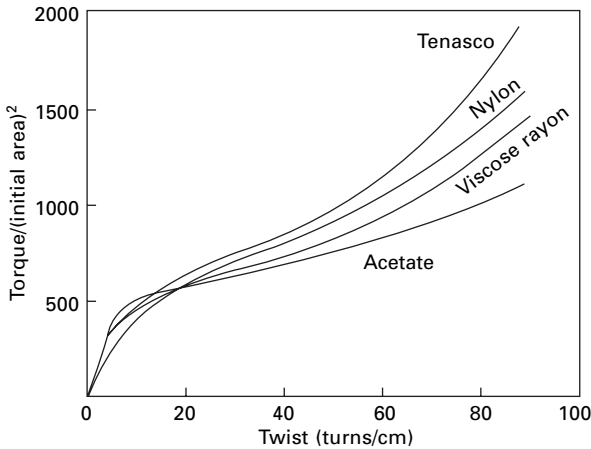
where I = moment of inertia of the bar about the fibre axis, l = length of fibre and t = period of the oscillation, corrected, if necessary, for the damping.

Meredith [37] used 1.5 cm lengths of fibre with light-alloy inertia-bars, ranging in mass from 16 to 110 mg and in length from 1.3 to 2.6 cm. By a suitable choice of bar, the tension on the filament could be kept between 0.49 and 1.96 mN/tex, and the period of oscillation between 4 and 10 s. Under these conditions, the damping was negligible. Owen [17] used a double-pendulum method.

17.3.3 Results of torsional experiments

Figure 17.20 shows torque–twist relations obtained by Morton and Permanyer [41]. They are similar to tensile stress–strain curves. Table 17.2 includes values of the specific torsional rigidity and shear modulus of fibres determined in Owen’s dynamic tests [17], in which the strain was small. The results are directly comparable with Owen’s bending results in Table 17.2. The specific torsional rigidities range from 0.05 to 2 mN mm²/tex².

Meredith [37] found a very low value for specific torsional rigidity of polyethylene (0.054 mN mm²/tex²) and high values for glass (6.4 mN mm²/tex²), as expected from its material properties, and kapok (73 mN mm²/tex²), due to its hollow form. Shear moduli are typically five to ten times lower than tensile moduli, but in the ratio is



17.20 Torque–twist relations for various fibres at 65% r.h. and 20 °C [41].

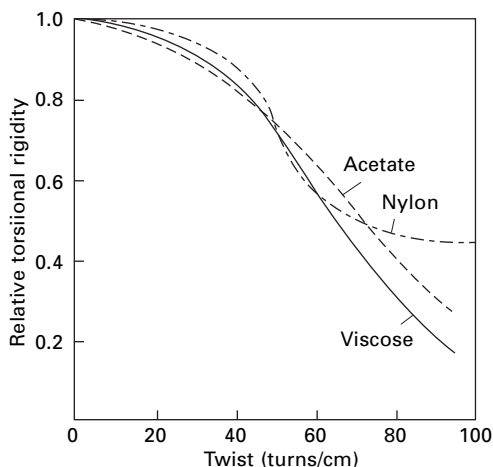
Table 17.8 Tensile and torsional properties. From Zeronian *et al.* [46]

Fibre	Tensile modulus– E (GPa)	Torsional modulus– v (GPa)	E/v	Breaking twist angle (°)
Polyester (PET) experimental filament	9.01	0.85	10.5	44
Polyester (PET) high-speed spun (POY)	1.98	0.65	3.05	77
Polyester (PET) drawn POY	8.81	0.85	10.4	32
Nylon 6 filament	3.41	0.49	6.96	48
Polypropylene filament	2.09	0.57	3.67	60
Gel-spun polyethylene (HMPE)	93.7	0.84	111	22
Polybenzimidazole (PBI) staple fibre	6.78	1.37	4.95	25
Aramid (PPTA) <i>Kevlar</i> 49 filament	94.2	1.60	58.9	17
Polyphenylenesulphide (PPS) staple <i>Vectran</i> M filament	4.62	1.39	3.32	46
<i>Vectran</i> HS heat-set filament	62.2	0.56	111	18
	69.5	0.56	124	20

greater in highly oriented fibres, such as flax and *Tenasco* (28). Muraki *et al.* [45] found shear moduli of 1.28 to 1.42 GPa for wool compared with tensile moduli of 3.55 to 3.73 GPa.

Table 17.8 gives values of tensile and shear moduli of fibres measured with a torsion pendulum by Zeronian *et al.* [46]. Values of the shear moduli cover a three-fold range from 0.5 to 1.6 GPa, but the tensile moduli cover a 50-fold range, reflecting the much higher orientation of the HM–HT fibres.

Torsional rigidity is very much affected by moisture, fibres being easier to twist as their regain increases. This is shown by the results in Fig. 17.21, in which the torsional rigidity, compared to a value of 1 when dry, is plotted against the relative humidity. Clayton and Peirce [48] found that the rigidity of cotton fibres decreased as the temperature increased; the temperature coefficient was 0.28% per °C in the dry state, rising to 1.48% per °C at 8.3% regain.



17.21 Variation of torsional rigidity with humidity [47].

Meredith [37] found that the torsional rigidity was independent of tension for the acrylic fibre *Orlon* between 0.98 and 9.80 mN/tex, increased slightly for nylon; and increased by 1.3% for an increase of tension of 0.98 mN/tex in crimped wool, where the configuration of the fibre would be altered.

Guthrie *et al.* [10] found that the torsional rigidity of viscose staple *Fibro* was proportional to $(\text{tex})^{1.9}$. The difference from the theoretical index of 2 can be accounted for by a difference of shape in fibres of different fineness.

Chamberlain and Khera [49] found that the specific torsional rigidity increased as the outer layers of viscose rayon filaments were removed. Meredith [18] found that the average coefficient of variation of shear modulus was 22% for cellulosic fibres, 15% for protein fibres, and 12 for synthetic fibres.

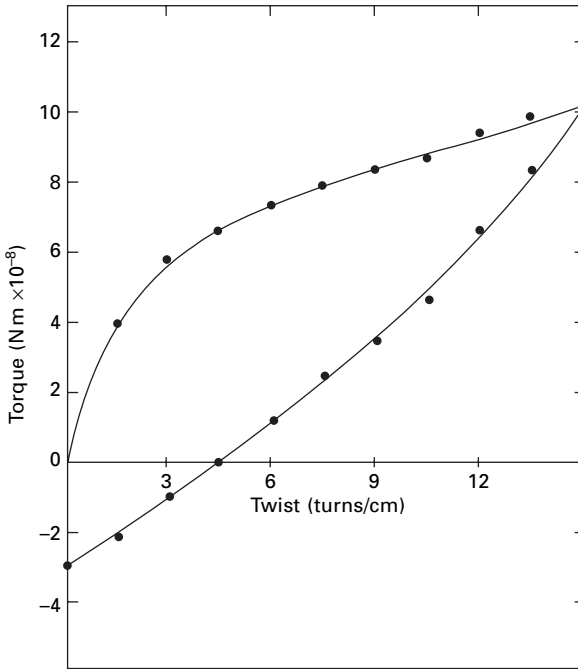
Skelton [50] reported that the torsional recovery of nylon falls from 100% for low strains to 60% for high strains. Figure 17.22 shows torque–twist and recovery response of a polypropylene fibre.

17.3.4 Torsion and time

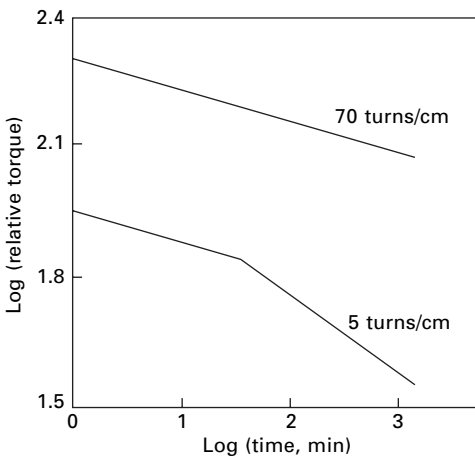
Creep and relaxation will occur in twisting just as they do in extension. Fig. 17.23 gives examples of the relaxation of torque found by Permanyer [47]. When $\log(\text{torque})$ is plotted against $\log(\text{time})$, straight lines are found. At low twists, there is a change of slope at about 30 minutes. Figure 17.24 shows stress relaxation and inverse relaxation after recovery in a nylon monofilament.

If determined in tests made over a wide frequency range, the dynamic modulus would also be expected to vary, but Meredith [37] found no change in nylon for periods of oscillation between 5 and 16 seconds. He also found that the damping of the oscillations was very small when the period of oscillation was long.

Kawabata *et al.* [51] found torsional creep compliance of *Kevlar 29* to be about 300 times greater than the longitudinal compliance.



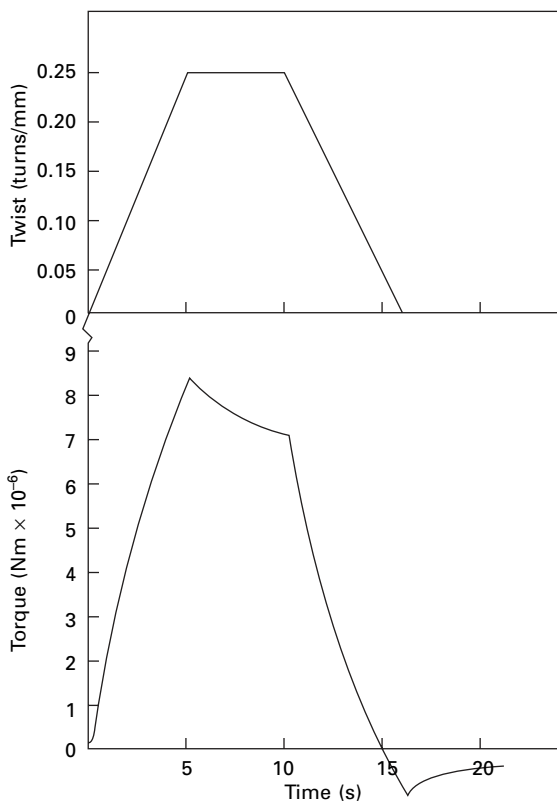
17.22 Torque–twist and recovery of 0.54 tex polypropylene fibre. From Sikorski *et al.* [39].



17.23 Relaxation of torque [47].

17.3.5 Breaking twist

If a fibre is twisted far enough, it will eventually rupture. The twist for which this occurs may be called the breaking twist. It has been confirmed experimentally by Schwab [52] and Koch [53] that, as would be expected theoretically, the number of turns to rupture is inversely proportional to the fibre diameter. To obtain a characteristic



17.24 Torque–twist behaviour for a 75 μm diameter nylon monofilament, followed by stress relaxation, recovery and inverse relaxation. From Sikorski *et al.* [39].

property of the fibre material, one may use the breaking twist angle α . This is the angle through which the outer layers are sheared and is given by:

$$\tan \alpha = \pi d \tau_b \quad (17.26)$$

where d = diameter of fibre and τ_b = breaking twist in turns per unit length.

Typical values of breaking twist angles found by Koch [53] are given in [Table 17.9](#). The general pattern of the results is the same as that for breaking extensions. The effects of some changes of testing conditions are given in [Table 17.10](#).

[Table 17.8](#) includes breaking twist angles measured at constant length by Zeronian *et al.* [46] using an apparatus described by Ellison *et al* [55]. The breaking twist angles correlate with break extensions, which reflects the fact that break is triggered by the elongation at the fibre surface.

17.4 Shear strength

It would be difficult to measure directly the relation between shear stress and shear strain. Finlayson [56] made direct measurements of shear strength by using a bundle of fibres placed in a hole passing through both jaws of the apparatus. The jaws are

Table 17.9 Breaking twist angle [53]

Fibre	Range of α°
Casein	58 $\frac{1}{2}$ –62
Polyamide fibre, staple	56–63
Polyamide fibre, continuous-filament	47 $\frac{1}{2}$ –55 $\frac{1}{2}$
Polyester fibre, staple	59
Polyester fibre, continuous-filament	42–50
Acetate	40 $\frac{1}{2}$ –46
Wool	38 $\frac{1}{2}$ –41 $\frac{1}{2}$
Silk	39
Viscose rayon, normal	39 $\frac{1}{2}$ –35 $\frac{1}{2}$
Cotton	37–34
Polyacrylonitrile fibre	33–34 $\frac{1}{2}$
Viscose rayon, high-tenacity	31 $\frac{1}{2}$ –33 $\frac{1}{2}$
Flax	29 $\frac{1}{2}$ –21 $\frac{1}{2}$
Viscose rayon, very high-tenacity	23
Glass fibre	2 $\frac{1}{2}$ –5

Test conditions 65% r.h.; room temperature; 1 cm lengths; tensile stress of 10 N/mm²; 240 turns/min.

Table 17.10 Effect of conditions on breaking twist angle [54]

Change in condition	Change in breaking twist angle	
	Viscose rayon	Acetate
Test length, 5 → 60 mm	25.2 → 28.7°	—
Rate of twisting, 30 → 565 turns/min	Negligible	Negligible
Humidity, 65% r.h. → wet	None	28 → 36°

then pulled apart and the force required to break the bundle is measured. Breakage must occur through shear. It was found that the breaking load was proportional to the total count of the bundle, which indicated that any composite specimen effect was small. The tensile strength was measured on the same specimens, and the results are given in Table 17.11. It will be seen that shear strength is less than tensile strength, the difference being particularly great in a stretched rayon.

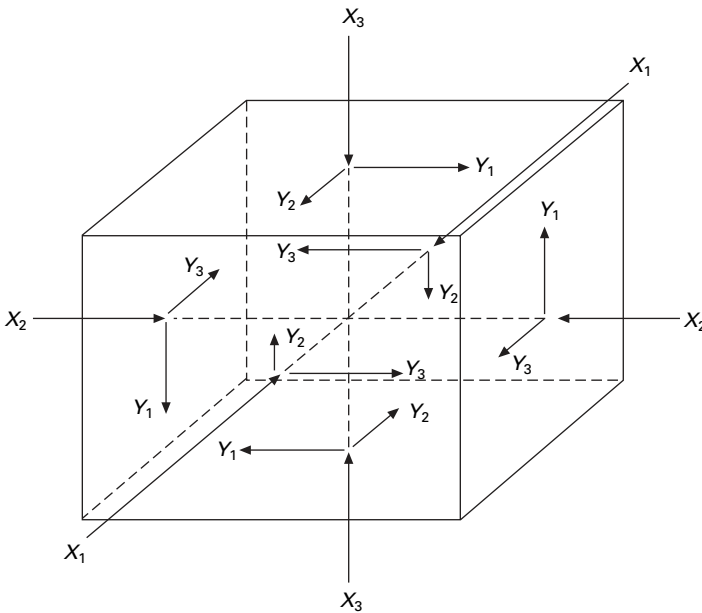
17.5 General elastic deformation

17.5.1 Elastic constants

For small strains, the properties of a homogeneous, perfectly elastic, but anisotropic material may be expressed in terms of a number of elastic constants [23, 57–59]. As indicated in Fig. 17.25, there are three tensile stresses, perpendicular to each face of a cube, and three shear stresses, paired together in two perpendicular directions in the plane of each face. These are related to six possible strains, extension in three mutually

Table 17.11 Shear strength [29]

Fibre	Shear tenacity (mN/tex)		Tensile tenacity (mN/tex)	
	65% r.h.	Wet	65% r.h.	Wet
Highly oriented cellulose	104.0	94.2	706	589
Nylon	111.8	95.2	392	353
Flax	81.4	73.6	255	284
Vinyon	98.1	94.2	275	245
Viscose rayon	63.8	31.4	177	69
Silk	115.8	88.3	314	245
Cotton	84.4	76.5	235	216
Acetate	57.9	50.0	118	78



17.25 Direction of principal stresses.

perpendicular directions and shear about three mutually perpendicular axes. Consequently, there are 36 elastic constants in the stress–strain matrix. However, the matrix is symmetrical, so that the number reduces to 21 for the most asymmetric structure. As the symmetry of the material increases, the number of constants decreases, until, in a completely isotropic material, only four constants (Young’s modulus, Poisson ratio, shear modulus and bulk modulus), of which only two are independent, are usually considered.

It is rare for fibres to be isotropic, and the simplest assumption, which is likely to hold reasonably well for many fibres, is that there is no difference in properties between different directions at right angles to the fibre axis, although these are different from the properties parallel to the fibre axis. Under these conditions, which

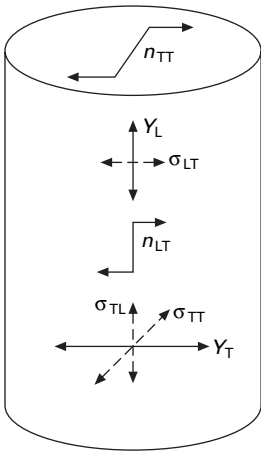
may be called transversely isotropic, the number of common constants may be reduced to seven: two Young's moduli, Y_L and Y_T ; two shear moduli, n_{LT} and n_{TT} ; and three Poisson ratios, σ_{LT} , σ_{TL} and σ_{TT} . Their directions are illustrated in Fig. 17.26. Of these, Y_L is the modulus measured in tensile or bending tests and n_{LT} the shear modulus involved in torsional rigidity. The number of independent constants is reduced to five by the relations:

$$n_{TT} = \frac{Y_T}{2(1 + \sigma_{TT})} \frac{\sigma_{LT}}{Y_L} = \frac{\sigma_{TL}}{Y_T} \tag{17.27}$$

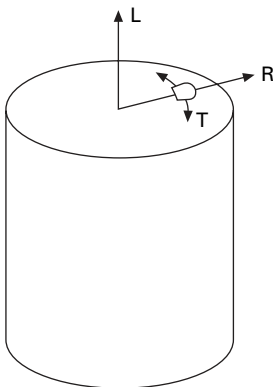
For this system, the bulk modulus, k , that is, the ratio of a hydrostatic stress to the resulting volume strain, is given by:

$$k = \frac{Y_T}{2 + (\sigma_{TL}/\sigma_{LT}) - 2(\sigma_{TT} + 2\sigma_{TL})} \tag{17.28}$$

In a fibre with radial symmetry, as illustrated in Fig. 17.27, all that is justified is the orthotropic system with three mutually perpendicular axes of symmetry. With



17.26 Elastic constants of a transversely isotropic fibre.



17.27 Directions of principal axes in a fibre with radial symmetry.

orthogonal curvilinear coordinates, the directions are taken as longitudinal, radial and tangential. There are 12 constants

$$Y_L, Y_R, Y_T; n_{LR}, n_{RT}, n_{TL}; \sigma_{LR}, \sigma_{RT}, \sigma_{TL}; \sigma_{RL}, \sigma_{TR}, \sigma_{LT}$$

with three relations between them:

$$\begin{aligned} \frac{\sigma_{LR}}{Y_L} &= \frac{\sigma_{RL}}{Y_R} \\ \frac{\sigma_{RT}}{Y_R} &= \frac{\sigma_{TR}}{Y_T} \\ \frac{\sigma_{TL}}{Y_T} &= \frac{\sigma_{LT}}{Y_L} \end{aligned} \quad (17.29)$$

A detailed account of orthotropic elasticity is given by Jayne [60].

In fibres, particularly natural fibres, with an internal structure, a simple model is not a true representation. Transversely isotropic or orthogonal symmetry may apply locally but the elastic constants vary from place to place. This gives rise to complicating effects. For example, in cotton the helical orientation of the molecules leads to an untwisting, namely a shearing, of the fibre under axial tension. In wool the properties will differ in ortho- and para-cortex and in the cuticle (and in meso-cortex and medulla, if present). However, for experiments on whole fibres, it may be convenient to present results as if the simple model was valid.

It may also be noted that the particular elastic constants mentioned are not the only ones that could be defined. It is quite common to use compliances, ratio of strain to stress, instead of moduli. The transverse deformation may be given by the ratio of transverse strain to axial stress instead of by the Poisson ratio, which is the ratio of transverse strain to axial strain. Moduli could be defined as at zero transverse strain, with another constant to give transverse stress developed, instead of at zero transverse stress, and so on. The constants also serve as surrogates for full stress–strain relations.

17.5.2 Measured properties

Tensile tests account for the overwhelming majority of studies of the mechanical properties of fibres. In addition, as already described, there have been a number of studies of torsional behaviour. Thus the only moduli (or more generally the stress–strain relations) for which information is easily available are Y_L and n_{LT} .

Bending, as described earlier, also involves Y_L , but, while tensile behaviour is averaged over the whole fibre, bending is influenced more by outer layers. Comparison of the two gives information on variations in modulus, particularly between skin and core. Bending also gives information on behaviour in compression. Marlow [61] reports that the initial moduli in tension and compression are equal: indeed, a discontinuity at the origin would be highly improbable. This result was confirmed by Elder [62], who examined various synthetic fibre monofilaments in tension, compression, and bending up to 1% strain. However, Chapman's results in Section 17.2.5 show that at larger strains the yielding behaviour is different.

Direct studies of axial compression have been made by cutting sections of fibres or monofilaments and compressing them between plates. Miles [63] found that, although nylon bristle shows the same modulus in tension and compression, the compressive stress–strain curve deviates markedly from the tensile stress–strain curve at strains greater than 1.5%. Whereas the tensile stress–strain curve is approximately linear up to a stress of 0.2 N/tex and a strain of 15%, the compression curve bends over to reach a stress level of 0.04 N/tex, which is substantially constant above 5% compression.

Compression between plates may also be used to study the transverse properties and obtain information on Y_T . Figure 17.28 shows the principles of the test.

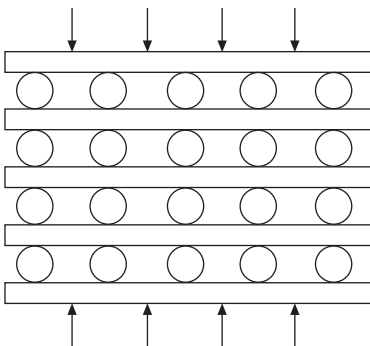
The Poisson ratio σ_{LT} (transverse contraction for imposed extension) can be studied, with some difficulty, by several methods: direct microscopical examination; diffraction methods [65]; and methods involving the insertion of a fibre in a tube and noting the change in electrical conductance [66] or fluid flow. Values of about 0.39 have been reported for nylon. Banky and Slen [67] found values between 0.42 and 0.63 for wool.

A complete study of elastic constants was made by Hadley *et al.* [68], who obtained values of the five independent elastic constants for several manufactured fibre monofilaments, with diameters of 100–300 μm . The experimental methods used were as follows:

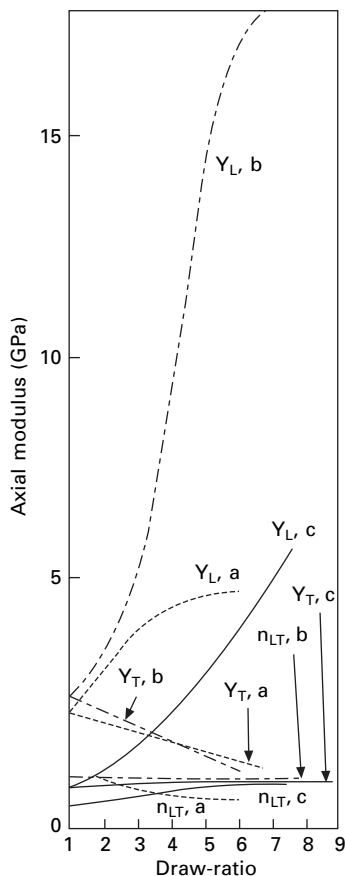
- axial extension, by applying loads and measuring length changes with a travelling microscope, 1 minute after loading, to obtain the axial modulus Y_L ;
- axial Poisson ratio σ_{LT} by measuring the change of diameter of monofilament by means of a microscope with a calibrated eyepiece;
- transverse compression to give thickness of contact between monofilament and plates and change in diameter parallel to plane of contact (the former is mainly dependent on the transverse modulus Y_T ; the latter is related to the transverse Poisson ratio σ_{TT} by an extension of Hertzian contact theory);
- torsion measurements with a vibration pendulum, giving the shear modulus n_{LT} .

By calculation from these observations, the values of all the constants can be obtained.

Figure 17.29 shows how the three moduli vary with the draw-ratio. In general, the tensile modulus changes most rapidly in the range of draw-ratio values that are



17.28 Principle of method of measurement of transverse moduli [64].



17.29 Variation of moduli with draw-ratio: a, nylon; b, polyester fibre; c, polypropylene fibre [68].

commonly found. Consequently, the ratio of tensile to shear modulus, which plays an important part in the buckling of filaments in bulked yarns, can be varied considerably. Table 17.12 collects a set of values, including all the usual constants, together with values of the moduli obtained by Morris [64] under wet and dry conditions.

In spruce wood, which has orthotropic symmetry, Barkas [57] found the values given in Table 17.13. The wood had a density of 0.5 g/cm^3 and a regain of 12%. It will be noted that $Y_T \ll Y_L$, $n_{TT} \ll n_{LT}$, and $\sigma_{TL} \ll \sigma_{LT}$ or σ_{TT} , as would be expected for a material that is highly oriented along the fibre axis.

In the highly oriented HM–HT fibres, such as aramids HMPE and PBO, the weak bonding between the molecules will give low values of the transverse modulus, Y_T , both shear moduli, n_{LT} and n_{TT} , and the Poisson ratio, σ_{TL} . The PIPD ‘M5’ fibre has the somewhat higher shear modulus of 7 GPa due to the hydrogen bonding.

In perfect graphite, there is a very high degree of anisotropy, as shown by Fig. 17.30. The maximum Young’s modulus, for extension within the planes of atoms, is estimated to be 1060 GPa, but across the planes it is only about 37 GPa [69]. The

Table 17.12 Elastic constant data for drawn nylon and drawn and undrawn polyester fibre [68] and for three other fibres [64]

Constant*	Nylon	Undrawn polyester fibre	Polyester fibre A†	Polyester fibre B‡
Y_L	3.45	2.27	9.09	14.08
Y_T	1.37	2.50	1.12	0.62
n_{LT}	0.61	0.93	0.74	0.74
n_{TT}	0.54	0.89	0.39	0.23
σ_{LT}	0.48	—	0.43	0.44
σ_{TL}	0.19	—	0.05	0.02
σ_{TT}	0.27	0.38	0.44	0.37

Constant*	Nylon	Courtelle acrylic fibre	Viscose rayon
Y_L dry	2.50	2.80	2.85
wet	0.95	2.77	0.15
Y_T dry	0.91	0.21	0.14
wet	0.74	0.20	0.0075

*Values of Y and n are expressed in GPa.

†Drawn to a birefringence of 0.153.

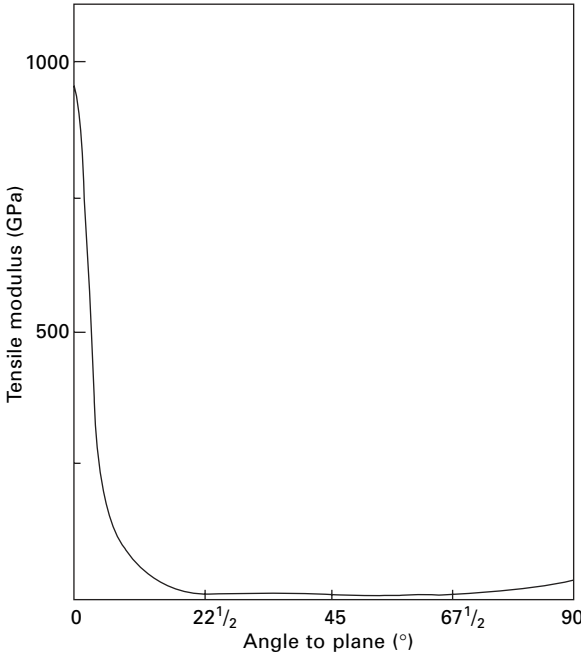
‡Drawn to a birefringence of 0.187.

Table 17.13 Elastic constants of spruce wood [57]

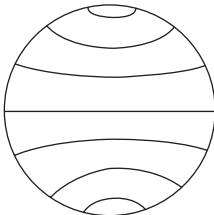
	Moduli (kN/mm ²) and Poisson ratios	
Young's moduli	Y_L $Y_L = 16.6$	Y_T $Y_R = 0.85$; $Y_T = 0.69$
Shear moduli	n_{LT} $n_{LT} = 0.84$; $n_{LR} = 0.63$	n_{TT} $n_{RT} = 0.037$
Poisson ratios	σ_{LT} $\sigma_{LR} = 0.36$; $\sigma_{LT} = 0.52$	σ_{TT} $\sigma_{RT} = 0.43$; $\sigma_{TR} = 0.33$
	σ_{TL} $\sigma_{RL} = 0.018$; $\sigma_{TL} = 0.023$	

shear modulus between planes is estimated to be 4 GPa, but that within planes, 180 GPa and, through planes is estimated as 15 GPa. These properties must be reflected in carbon fibres, though the exact effect will depend on the extent of disorder, disorientation, and interconnection between the planes. Good orientation of planes parallel to the fibre axis implies that the shear modulus (n_{LT} in Fig. 17.26), which determines torsional rigidity, will be low. If the overall arrangement of planes is such that the fibre is transversely isotropic, the transverse modulus Y_T and the shear modulus n_{TT} will be an average of high and low values; but, if the structure is layered, as in Fig. 17.31, which approximates to the form of pitch fibres, there will be substantial transverse anisotropy.

Glass and ceramic fibres are isotropic, so their Young's modulus Y will be the same in all directions. Poisson ratios σ have typical values of around 0.3, and, since there are only two independent elastic constants in an isotropic material, the shear modulus n will equal $Y/2(1 + \sigma)$, namely about 40% of the tensile modulus. There will be no directions of particular weakness in the structure.



17.30 Variation of modulus of perfect graphite crystal with direction [7].

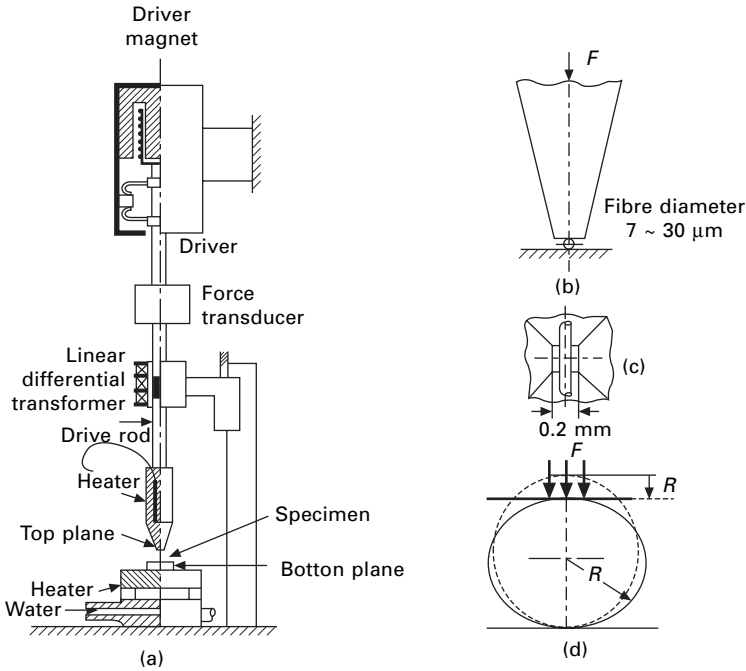


17.31 Carbon fibre oriented in layers across the fibre.

17.5.3 Transverse compression

Kawabata [70] developed the instrument shown in Fig. 17.32(a) for measuring transverse compression on single fibres. As indicated in Fig. 17.32(b) and (c), the fibre is compressed between a top plane, $0.2 \times 0.2 \text{ mm}^2$, and a bottom plane. Both surfaces are mirror finished steel. Other features of the instrument are the driver, force transducer, LDVT for deformation, and provision for heating and wetting. The displacement resolution is $0.05 \mu\text{m}$, which is adequate for testing fibres with a diameter of $5 \mu\text{m}$ or more. Figure 17.32(d) shows the deformation geometry for a fibre of radius R (diameter D) for a contraction U under a force F per unit length. Kawabata modifies the analysis used by Ward *et al.* [71, 72] to give the following equations between measures of stress $f = F/D$ and strain $u = U/D$:

$$u = \left(\frac{4f}{\pi} \right) \left[\left(\frac{1}{E_T} \right) - \left(\frac{\sigma_{LT}^2}{E_L} \right) \right] \left[0.19 + \sinh^{-1} \left(\frac{R}{b} \right) \right] \quad (17.30)$$



17.32 (a) Transverse compression instrument. (b) Section through compression zone. (c) Plan of compression zone. (d) Compression geometry. From Kawabata [70].

$$b^2 = \left(\frac{8fR^2}{\pi} \right) \left[\left(\frac{1}{E_T} \right) - \left(\frac{\sigma_{LT}^2}{E_L} \right) \right] \quad (17.31)$$

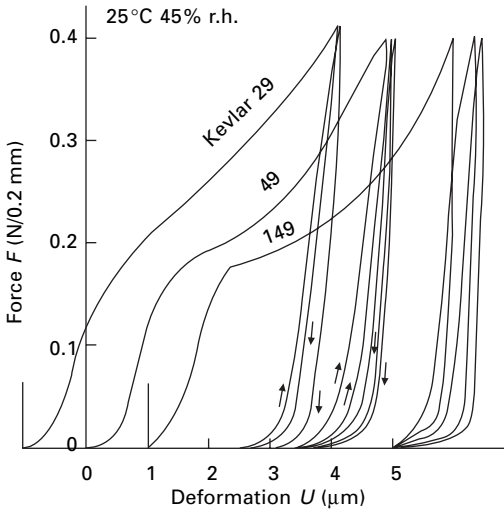
If $(\sigma_{LT}^2/E_L) \ll (1/E_T)$, i.e. when longitudinal modulus \gg transverse modulus, the equations simplify to:

$$u = \left(\frac{4f}{\pi E_T} \right) \left[0.19 + \sinh^{-1} \left(\frac{R}{b} \right) \right] \quad (17.32)$$

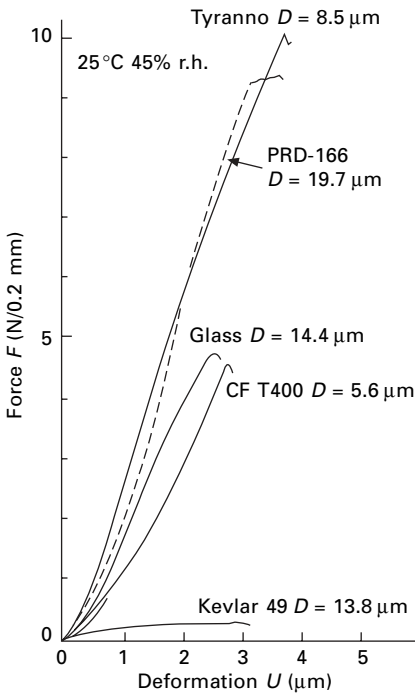
$$b^2 = \frac{8fR^2}{\pi E_T} \quad (17.33)$$

A finite element computation showed good agreement with predictions of the equations used by Kawabata [70]. The \sinh^{-1} term causes little divergence from linearity except for small values of f . The experimental results for *Kevlar 48* diverged from the relation between f and u at low stresses, probably due to an artefact of mounting the specimen, and at high stresses, which would be a change in material properties. Calculated moduli were obtained from intervals along the linear part of the experimental curve.

Figure 17.33 shows force/deformation plots for aramid fibres in transverse squashing and recovery and Fig. 17.34 shows the much larger resistance to deformation in

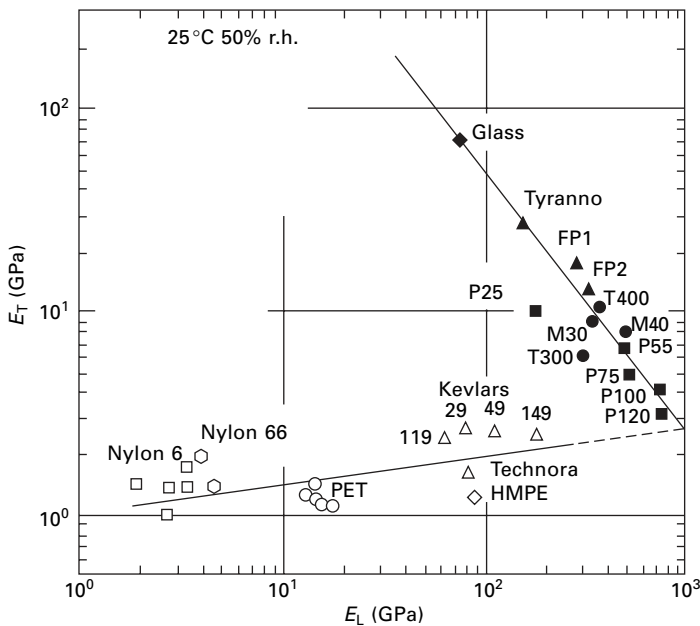


17.33 Deformation and recovery of aramid fibres in transverse compression. From Kawabata [70].



17.34 Inorganic fibres in transverse compression, with *Kevlar* for comparison. *Tyranno* is a silica fibre. PRD-166 is an alumina/zirconia fibre (not commercialised), CF 1400 is a carbon fibre. From Kawabata [70].

inorganic fibres. The log–log plot of axial and transverse moduli in Fig. 17.35 shows a comparatively small difference between the moduli in nylon, which is in agreement with earlier data. There are only small increases in transverse modulus in going to polyester and HM–HT fibres, but the axial modulus increases greatly. In the glass fibre, the moduli are almost equal, but other inorganic fibres show anisotropy with the axial moduli increasing and the transverse moduli decreasing. This is to be expected in carbon fibres where the graphitic planes are axially oriented, but is surprising in the ceramic fibres. Table 17.14 gives values of transverse and axial moduli and strengths. Transverse creep compliance was about 600 times greater than axial compliance [51].



17.35 Comparison of transverse moduli E_T and axial moduli E_L . Brittle type: • carbon (PAN), ■ carbon (pitch), ▲ ceramic, ◆ glass. Yielding type: ○ PET, □ nylon 6, ○ nylon 66, △ kevlar, ◇ HMPE From Kawabata [70].

Table 17.14 Elastic moduli measured by Kawabata [45, 70]

Fibre type	Transverse modulus (GPa)	Axial modulus (GPa)	Transverse strength (GPa)	Axial strength (GPa)
PAN-based carbon	6.03–10.08	235–343	0.95–3.34	3.08–5.19
Pitch-based carbon	3.08–9.95	126–379	0.079–0.64	2.35–4.73
Alumina	12.7	341	2.34	1.34
Silica	26.5	160	6.73	3.34
Aramid	1.59–2.59	63.4–179	0.042–0.077	2.18–3.57
Wool	0.97–1.01	3.55–3.73		

17.5.4 Interactions of stresses

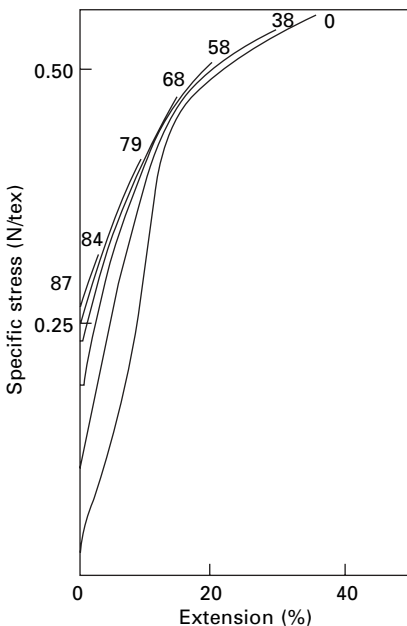
For small stresses and strains, it is assumed in elasticity theory that the effect of each stress is independent and that the total effect of a complex stress situation can be obtained by summing the separate effects of all the stresses. Thus the initial tensile modulus of a fibre would be unaffected by slight twisting. But, when the strains become large, there will be an interaction between the effects.

Dent and Hearle [73] examined the tensile properties of twisted single fibres. The experiments were performed in two ways: with constant length during twisting and with a constant low tension during twisting. Twist values are given as the twist factor $\tau\sqrt{c}$ ($\text{tex}^{1/2}\text{cm}^{-1}$), where τ is the twist in turns/cm and c is the linear density in tex. This is related to the twist angle α by the relation:

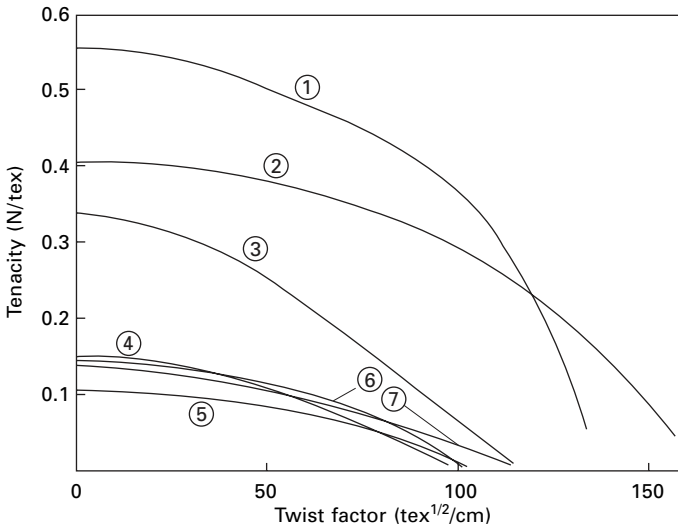
$$\sigma\sqrt{c} = \frac{1}{2}\sqrt{(10^5/\pi v)} \tan \alpha \quad (17.34)$$

where v is the fibre specific volume in cm^3/g .

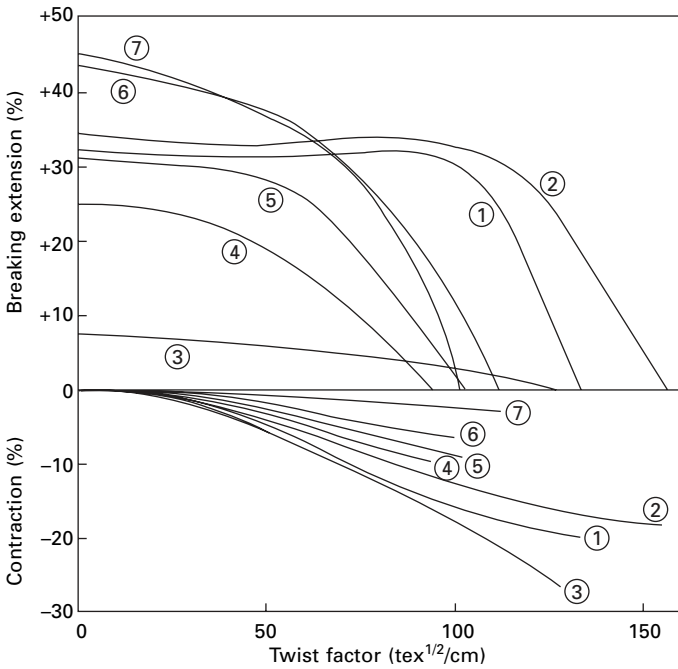
Figure 17.36 illustrates the effect of twist on the stress–strain curves, with constant length twisting. The tendency to contract during twisting displaces the start of the curve up the stress axis. The initial moduli become less at high twists, and the breaking point occurs much earlier when the twist factor becomes large. A comparison of results obtained in constant tension twisting is given in Fig. 17.37. In most fibres, though not in cotton and wool, the strength is fairly constant up to twist factors of between 30 and 50 $\text{tex}^{1/2}/\text{cm}$ but then decreases rapidly. Failure due to twist alone occurs at twist factors between 50 and 120 $\text{tex}^{1/2}/\text{cm}$.



17.36 Stress–strain curves of nylon fibre twisted to various levels at constant length [73].



(a)



(b)

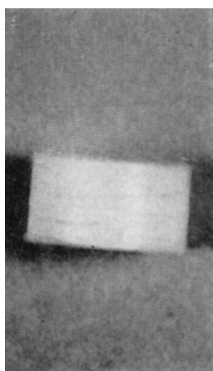
17.37 (a) Change of tenacity, based on linear density before extension, of fibres twisted at constant tension [73]. (b) Change of breaking extension, based on length in twisted state before extension, and of contraction, based on length before twisting, of fibres twisted at constant tension: 1, nylon; 2 *Terylene* polymer; 3, cotton; 4, viscose rayon; 5, acetate; 6 *Acrilan* acrylic; 7, wool [73].

Hearle and Zhou [74] have reported a study of the effect of combined torque and tension on *Kevlar*. The effects are generally similar, except that, in constant-length twisting, the strength of *Kevlar* falls to zero at a twist factor of $30 \text{ tex}^{1/2}/\text{cm}$, which is about half the value found in nylon and polyester fibres.

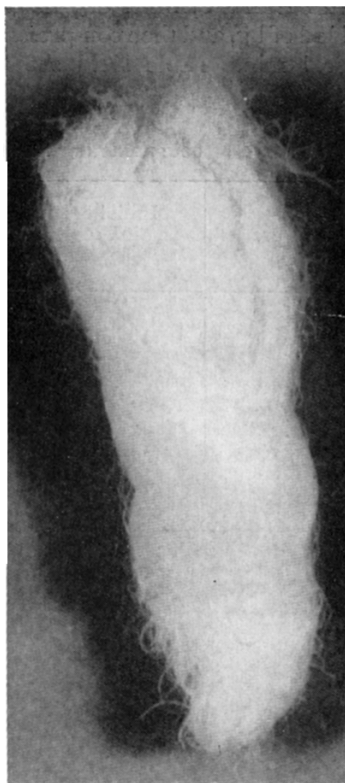
Table 17.15 Compression of fibre mass [76]

Fibre	Initial height, in., under 1-gf load*	15 min recovery (%)
<i>Saran</i>	0.80	100
Nylon	1.00	90
Wool	1.00	31
Casein	0.50	24
<i>Orlon</i> acrylic fibre	1.20	17
<i>Dacron</i> polyester fibre	1.10	14
Acetate	0.84	11
Viscose rayon	1.30	8

*1 gf = 9.81 mN; 1 in. = 2.54 cm.



(a)



(b)

17.38 Recovery of compressed rayon staple on wetting: (a) immediately after immersion; (b) 30 s later After Kolb *et al.* [76].

Another example of the application of combined stresses is in the observation by Wilson [75] of a change in the breaking extension of nylon under combined axial and transverse stress.

17.6 Compression stresses on fibre masses

One other type of stress that has been studied is the application of a compressive stress to a mass of staple fibres. Kolb *et al.* [76] placed 0.3 g of fibres in a cylinder of 13 mm ($1/2$ in). diameter, measured the height under a load of 1 gf, and then compressed it under a pressure of 689 MN/mm² (100 000 lbf/in²) for 1 min. Table 17.15 shows values of the initial height and of the recovery after 15 min. It will be noted that fibres that show good tensile recovery also show high recovery after compression. The fibres showed a crushed appearance where they crossed one another. By contrast, the nylon is seen to be little affected. The synthetic fibres recovered better in hot air, and viscose rayon recovered 100% in water. The photographs in Fig. 17.38 show the effect of water on the rayon staple.

17.7 References

1. D. Finlayson. *J. Text. Inst.*, 1946, **37**, P168.
2. B. M. Chapman. *J. Text. Inst.*, 1973, **64**, 312.
3. K. Lee. *J. Textile Inst.*, 2002, **93**, Part 1, 293.
4. K. W. Lee. *Textile Res. J.*, 2005, **75**, 710.
5. J. H. Jung and T. J. Kang. *Textile Res. J.*, 2005, **75**, 713.
6. W. He and X. Wang. *Textile Res. J.*, 2002, **72**, 573.
7. P. W. Carlene. *J. Text. Inst.*, 1947, **38**, T38.
8. F. T. Peirce. *J. Text. Inst.*, 1930, **21**, T377.
9. P. W. Carlene. *J. Text. Inst.*, 1950, **41**, T159.
10. J. C. Guthrie, D. H. Morton, and P. H. Oliver. *J. Text. Inst.*, 1954, **45**, T192.
11. R. Khayatt and N. H. Chamberlain. *J. Text. Inst.*, 1948, **39**, T185.
12. J. W. Ballou and J. C. Smith. *J. Appl. Phys.*, 1949, **20**, 493.
13. R. Meredith and B. S. Hsu. *J. Polymer Sci.*, 1962, **61**, 271.
14. W. Yu and Y. Liu. *J. Appl. Polymer Sci.*, 2006, **101**, 701.
15. B. M. Chapman. *Text. Res. J.*, 1971, **41**, 705.
16. R. G. Livesey and J. D. Owen. *J. Text. Inst.*, 1964, **55**, T516.
17. J. D. Owen. *J. Text. Inst.*, 1965, **56**, T329.
18. R. Meredith In *Proceedings of Fifth International Congress on Rheology*, University of Tokyo Press, Tokyo, Japan, 1969, Volume 1, p. 43.
19. E. M. K arrholm and B. Schr oder. *Text. Res. J.*, 1953, **23**, 207.
20. M. Horio, S. Onogi, C. Nakayama and K. Yamomoto. *J. Appl. Phys.*, 1951, **22**, 966.
21. H. M. Elder. *J. Text. Inst.*, 1966, **57**, T75.
22. J. Skelton. *J. Text. Inst.*, 1965, **56**, T454.
23. A. E. H. Love. *A Treatise on the Mathematical Theory of Elasticity*, Cambridge University Press, Cambridge, 4th edition, 1927.
24. D. E. Bosley. *Text. Res. J.*, 1968, **38**, 141.
25. B. C. Jariwala. MSc thesis, University of Manchester, 1971.
26. B. C. Jariwala. PhD thesis, University of Manchester, 1974
27. B. M. Chapman. *J. Appl. Polymer Sci.*, 1973, **17**, 1693.

28. M. J. Coplan. USAF Report No. 1134, Part III, March, 1952. Cited by E. R. Kaswell in *Textile Fibers, Yarns, and Fabrics*, Reinhold, New York, 1953, p. 61).
29. H. Bohringer and W. Schieber. Cited by H. F. Schiefer, L. Fourt and R. Kropf. *Text. Res. J.*, 1948, **18**, 18.
30. J. K. Berry. *Text. Rec.*, 1946, **64**, Sept., 52.
31. S. van der Zwaag, S. J. Picken and C. P. van Sluijs. Paper presented at Rolduc Polymer Conference, 1988.
32. S. R. Allen. *J. Mater Sci.*, 1987, **22**, 853.
33. S. van der Zwaag and G. Kampschoer. Paper presented at Rolduc Polymer Science Conference, 1987.
34. S. Kawabata. *J. Textile Inst.*, 1995, **86**, 347.
35. S. Kawabata. In *Modern Textile Characterization Methods*, M. Raheel (Editor), Marcel Dekker, New York, 1996, Chapter 19, 311.
36. M. M. Schoppee and J. Skelton. *Text. Res. J.*, 1974, **44**, 968.
37. R. Meredith. *J. Text. Inst.*, 1954, **45**, T489.
38. K. W. Lee. *Textile Res. J.*, 2005, **75**, 377.
39. M. E. Sikorski, C. P. Buckley, J. W. S. Hearle and S. K. Mukhopadhyay. *Rev. Sci. Instrum.*, 1993, **64**, 1947.
40. W. E. Morton and F. Permyner. *J. Text. Inst.*, 1947, **38**, T54.
41. W. E. Morton and F. Permyner. *J. Text. Inst.*, 1949, **40**, T371.
42. M. E. Sikorski. PhD thesis, University of Manchester, 1986.
43. M. E. Sikorski and C. P. Buckley. *Proc. 35th Int. Symp. Instrument Soc. America*, Orlando, FL, 1989.
44. S. Kawabata. *Proc. 4th Japan-USA Conf. Composite Materials*, 1988, p. 253.
45. C. Muraki, M. Niwa, N. Amino and S. Kawabata. *J. Textile Inst.*, 1994, **85**, 12.
46. S. H. Zeronian, G. Buschler-Diller, S. Holmes and M. K. Inglesby. *J. Textile Inst.*, 1994, **85**, 293.
47. F. Permyner. Ph.D. Thesis, University of Manchester, 1947.
48. F. H. Clayton and F. T. Peirce. *J. Text. Inst.*, 1929, **20**, T315.
49. N. H. Chamberlain and M. P. Khera. *J. Text. Inst.*, 1952, **43**, T123.
50. J. Skelton. *J. Text. Inst.*, 1965, **56**, T443.
51. S. Kawabata, M. Sera, T. Kotani, K. Katsuma, M. Niwa and C. Xiaoxin. ICCM 9, 1993, **VI**, 671.
52. R. Schwab. *Kleppzig's Textil-Z.*, 1939, **42**, 397.
53. P.-A. Koch. *Textil-Rdsch.*, 1949, **4**, 199; 1951, **6**, 111.
54. K. Breuer. *Kunstseide*, 1939, **21**, 202.
55. M. S. Ellison, S. H. Zeronian, K. W. Alger, S. M. Aboul-Fadl and T. M. Soler. *Polymer Eng. Sci.*, 1989, **29**, 1738.
56. D. Finlayson. *J. Text. Inst.*, 1947, **38**, T50.
57. W. W. Barkas. *The Swelling of Wood under Stress*, HMSO, London, 1949, Chapter 2.
58. J. C. Jaeger. *Elasticity, Fracture, and Flow*, Methuen, London, 1956, pp. 63-67.
59. J. W. S. Hearle. *J. Text. Inst.*, 1958, **49**, T389.
60. B. A. Jayne. *Theory and Design of Wood and Fiber Composite Materials*, Syracuse University Press, Syracuse, NY, 1972, Chapter 2.
61. P. F. Marlow. *J. Text. Inst.*, 1958, **49**, T40.
62. H. M. Elder. *J. Text. Inst.*, 1966, **57**, T8.
63. J. B. Miles. *Text. Res. J.*, 1971, **41**, 108.
64. S. Morris. *J. Text. Inst.*, 1968, **59**, 536.
65. V. V. Davis. *J. Text. Inst.*, 1959, **50**, T688.
66. F. I. Frank and A. L. Ruoff. *Text. Res. J.*, 1958, **28**, 213.
67. E. C. Banky and S. B. Slen. *Text. Res. J.*, 1956, **26**, 204.

68. D. W. Hadley, P. R. Pinnock and I. M. Ward. *J. Mater. Sci.*, 1969, **4**, 152
69. W. N. Reynolds. *Physical Properties of Graphite*, Elsevier, Amsterdam, 1968.
70. S. Kawabata. *J. Textile Inst.*, 1990, **81**, 432.
71. D.W. Hadley, I. M. Ward and J. Ward. *Proc. Roy. Soc.*, 1965, **A285**, 275.
72. P. R. Pinnock, I. M. Ward and J. M. Wolfe. *Proc. Roy. Soc.*, 1965, **A291**, 267.
73. R. W. Dent and J. W. S. Hearle. *Text. Res. J.*, 1960, **30**, 805.
74. J. W. S. Hearle and C. Y. Zhou. *Text. Res. J.*, 1987, **57**, 7.
75. N. Wilson. *Nature*, 1963, **198**, 474.
76. H. J. Kolb, H. E. Stanley, W. F. Busse and F. W. Billmeyer. *Text. Res. J.*, 1953, **23**, 84.

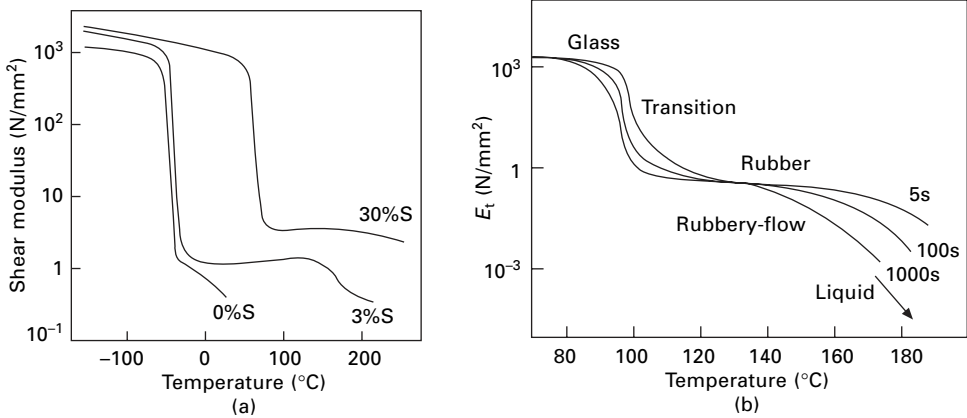
18.1 Introduction

18.1.1 Changes of state in polymers

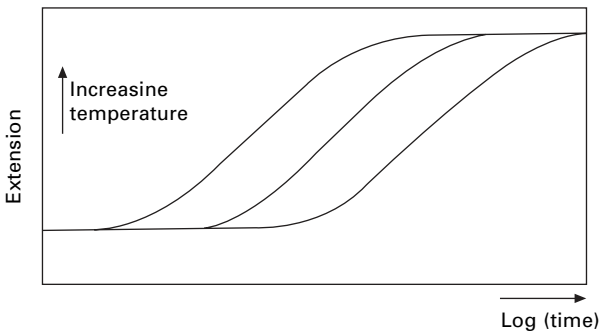
Most materials are characterised by transitions between three states: solid, liquid and gas. Melting and boiling occur so sharply that they can define the limits of temperature scales or be used to identify chemical substances. Polymers behave differently. Firstly, the molecules are so large that decomposition occurs before there could be any possibility of vapourisation. In many polymers, such as cellulose and aramids, decomposition occurs before melting can take place. Secondly, when it occurs, melting is not sharp. There is a gradual softening before a viscous melt forms. The flow properties change strongly with temperature, so that melt-spinning conditions must be carefully chosen. Thirdly, there are important transitions in the solid state. Different allotropic crystal forms are also found in many materials and are of minor importance for fibre behaviour. Transitions within amorphous regions and more subtle effects in crystalline regions play a major role in the processing and use of fibres.

Simple amorphous polymers show one important transition in the solid state. At low temperatures, they are glassy solids; at high temperatures, they are elastomeric. In natural and synthetic rubbers, the transition occurs below room temperature. In plastics, such as polystyrene or polyvinyl chloride, the transition is above room temperature. There are complications. Firstly, the transitions are time dependent as well as temperature dependent. Secondly, unless the polymer molecules are very long and entangled or are lightly crosslinked, the rubbery state merges into viscous flow. There are two other polymeric states. At high degrees of crosslinking, the materials are rigid thermoset resins. Regular polymers can form crystals. All of these features are involved in thermal transitions of fibres, many of which combine crystalline and amorphous material.

Figure 18.1 illustrates the above effects. Below -20°C , natural rubber (Fig. 18.1(a)), is a hard solid with a shear modulus over 1 GPa. It then falls sharply to a value over a thousand times smaller. If there is no crosslinking, the viscoelastic modulus continues to fall as temperature rises. However a moderate degree of vulcanisation forms crosslinks through sulphur bridges and the material has good rubbery properties from -20°C to 150°C . With more crosslinks, the transition from the glassy to the rubbery state moves to higher temperatures. In polystyrene (Fig. 18.1(b)), the transition from glass



18.1 (a) Change with temperature of shear modulus in dynamic tests at about 1 Hz for natural rubber with varying degrees of cross-linking by sulphur(s). From Schneider and Wolf [1]. (b) Tensile relaxation modulus of polystyrene after various times at different temperatures. s is for second From Tobolsky [2].



18.2 Creep curves over a wide range of times at different temperatures.

to rubber occurs at around 100 °C. The influence of rheology is shown by the change in transition temperature and the change to rubbery flow according to the time available. For large changes in rate, from milliseconds to years, the changes in transition temperature will be much larger. The sigmoidal creep curves in Fig. 18.2 could represent the behaviour of a given polymer at different temperatures.

18.1.2 The nature of transitions

Melting of crystals and boiling of liquids are first-order transitions. The structure changes from the regular packing in crystals to the mobile disorder in a liquid and then to the dispersion into the available volume for a vapour. In addition to the transformation of mechanical state, they are characterised by latent heats and changes of volume.

A thermodynamic second-order transition involves no change of molecular

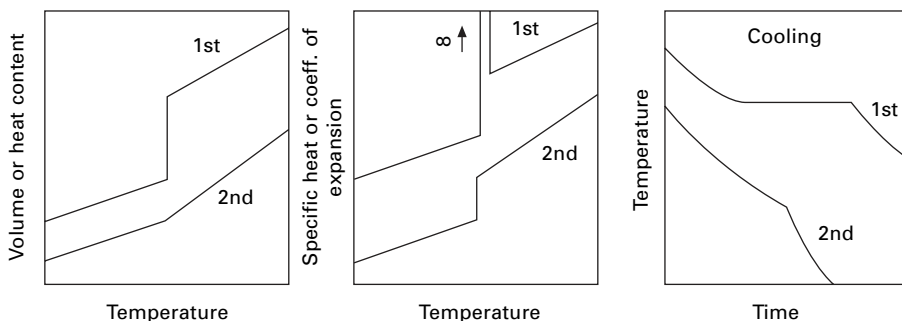
arrangement. Snapshots of the molecular arrangement above and below the transition would be virtually the same. But there is a change in response of the structure, shown up by changes in the second-order quantities, namely the rate of thermal expansion (dV/dT), the specific heat (dH/dT), and so on. The difference between first- and second-order transitions is shown graphically in Fig. 18.3.

The change in amorphous polymers from the glassy to the rubbery state has many of the characteristics of a second-order transition, but is not as sharp and is time dependent. The transition would not be obvious to anyone merely watching a polymer such as polystyrene being heated (in contrast to the clear indication of the melting of wax). It would be apparent if the material were allowed to deform, since it suddenly becomes flexible.

There is a distinction between sharp and broad transitions. This may be, and often is in polymer materials, merely a reflection of local variations in structure, for example, in crystal size or perfection or in local packing, so that the observed effect is really a collection of sharp transitions spread over a range of temperatures. Even in a uniform system, transitions vary in sharpness depending on the extent to which they are cooperative. A highly cooperative transition with a large total energy change, such as the change from crystal lattice to liquid disorder, will be sharp. It makes no sense to say that a crystal is half-melted (except in terms of a molten region progressively spreading over the crystal with sharp boundaries between the regions), since the only way of defining the crystal is by saying that a large number of neighbouring molecules are packed regularly together. However, at the other extreme, the dissociation of a molecule into two parts (e.g. $H_2 \rightarrow H + H$) is not at all cooperative: each molecule splits independently of the rest and the degree of dissociation can change steadily from 0 to 100% over a broad transition range of temperature. Some of the transitions in fibres lie between these two extremes.

18.1.3 Observation of transitions

Melting can be directly observed, for example by putting a fibre on the hot stage of a microscope and noting when it flows. However, the change may not be very sharp. Softening of the material, which leads to fibres sticking together, gives an impression of melting. Values of melting points for a given fibre vary. For example, in earlier

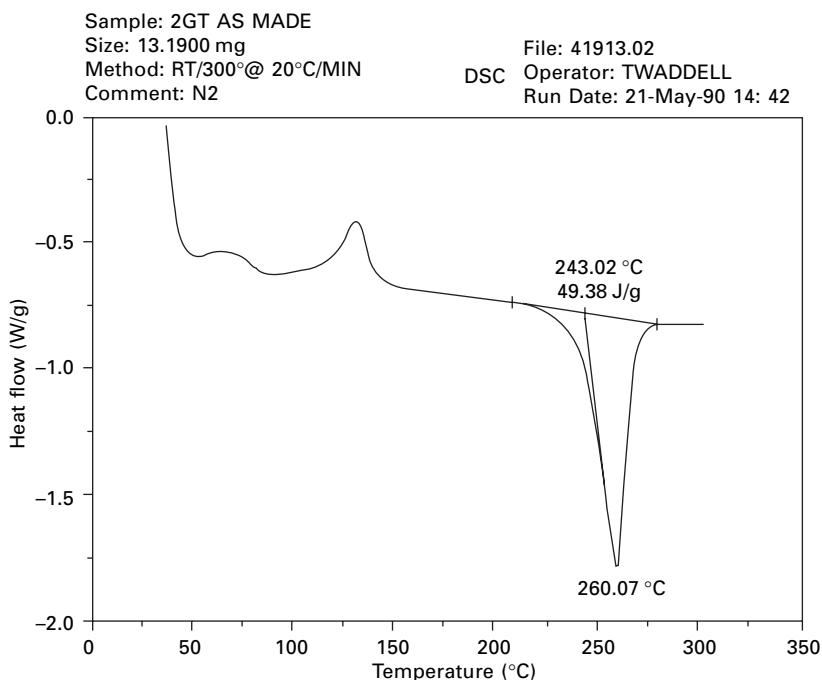


18.3 Changes occurring in first- and second-order transitions.

accounts the melting point of nylon 66 is given as 250 °C but later to values between 255 and 265 °C.

More information can be obtained from thermo-analytical techniques using commercial instruments. In differential scanning calorimetry (DSC), the heat required to increase the temperature of a sample is compared with a reference. The heat flow is controlled to maintain a constant heating rate and to keep both temperatures the same. A plot of heat flow against temperature would indicate the value of the specific heat¹. Since latent heat is ideally taken up at a constant temperature, it should show as an infinite negative spike. Experimental limitations would spread the spike to a limited extent, but in a typical fibre test as shown in Fig. 18.4 the spread is much larger, indicating the range over which melting occurs. The positive spike at about 120 °C indicates some additional crystallisation or increased crystal perfection. The broad peak above 50 °C may be due to some rearrangement of the structure to a lower energy state. The initial rapid decrease is an artefact of the start of heating. The heat flow rate between peaks and troughs gives values of specific heat and integration of the peak or trough gives values of latent heat of crystallisation or melting.

An alternative to DSC is differential thermal analysis (DTA) in which heat flow is maintained constant. Differences in temperature between sample and reference give similar information to DSC and enable specific and latent heats to be computed.



18.4 A typical print-out from a DSC scan of a polyester fibre melting around 260 °C. Courtesy of Du Pont.

¹For a given heating rate, heat flow in J/s (watt) can be converted to J/°C, and knowing the mass of the sample to specific heat in J/°C/g.

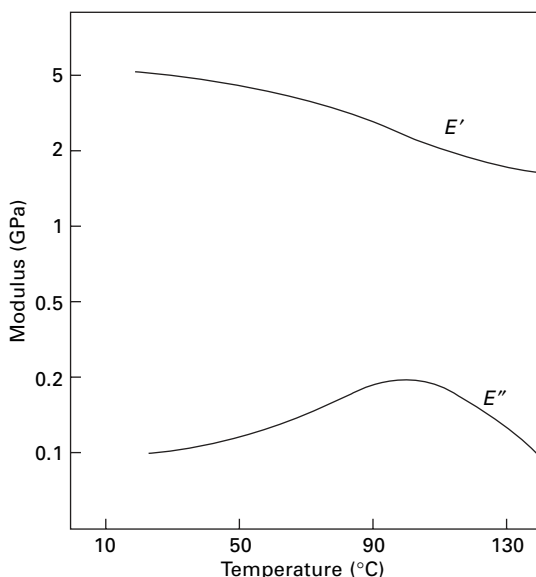
Measurements of volume or other dimensional changes with temperature are not very convenient for fibres. The most instructive way of studying the secondary transitions in the solid state is by measurement of dynamic mechanical analysis (DMA), as described in Section 16.5.3, with the typical plot in Fig. 18.5 showing the decrease in the modulus E' and paer in the modulus E'' in the transition region. Measurements of dielectric constant and dielectric loss can be made, but while these are good for polymer films or blocks, they are not well suited to fibres. Changes of dielectric properties with frequency and temperature are included in Chapter 21.

Thermomechanical analysis (TMA) measures changes in length at constant tension or vice versa and has been less used on fibres than DMA. The other common thermal measurement, thermogravimetric analysis (TGA), measures chemical decomposition through loss of weight and is not relevant to this book.

18.2 Melting

18.2.1 Characteristic features

Melting is an obvious phenomenon. The fibre loses its identity and contracts to a molten globule. In bulk, the molten material is a viscous liquid, quite different from a collection of solid fibres. Melting can also be detected in other ways, though different experimental methods do give slightly different values of melting point, particularly if the heating rate changes. The fibre loses strength, so that, at the melting point, a small weight suspended by the fibre will fall. At the melting point, the fibre becomes sticky. And on melting, the material takes up its latent heat, detectable as an endotherm peak in calorimetry, as described above.



18.5 Real and imaginary dynamic moduli of nylon 6.6 fibres: plotted on a logarithmic scale. From Murayama *et al.* [3].

The melting of textile fibres is an essentially irreversible process. To some extent, this is true of all materials: a wax statuette cannot be reformed without the mould. But in fibres, it is not only the external form but also the fine structure that cannot be reproduced without repeating the manufacturing sequence of extrusion, drawing and other treatments. Typical values of fibre melting points are given in Table 18.1.

Apart from differences attributed to experimental error, there are differences between different specimens of the same type of fibre as a result of structural differences. A major source of difference is the size and perfection of crystalline regions. Thermodynamically, the melting point is the temperature at which the values of the free energy F in the crystalline and molten states are the same, so that they are in equilibrium together. We therefore have:

$$\Delta F = \Delta U - T_m \Delta S = 0 \quad (18.1)$$

$$T_m = \frac{\Delta U}{\Delta S} \quad (18.2)$$

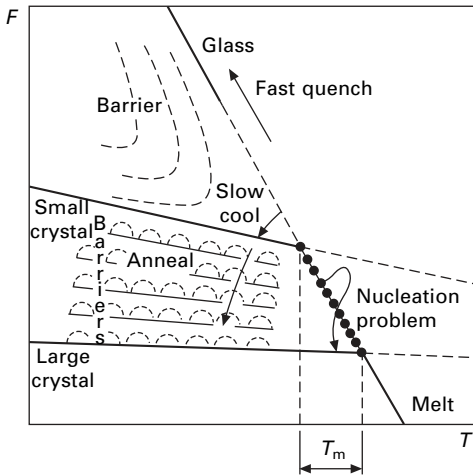
where Δ refers to the difference between the states, U is the internal energy, S is the entropy and T_m is the melting point.

The situation is shown graphically in Fig. 18.6. In a small or imperfect crystal, which forms on initial crystallisation, the internal energy is not as low as in large perfect crystals, owing to the surface or defect energy contributions. The melting point is therefore low, but increases as crystals grow and defects are eliminated on annealing. An example of this effect is shown in Fig. 18.7, in which the variation of melting point with the thickness of polyethylene single crystal lamellae is plotted. It may be noted that a value of about 140 °C is usually quoted for bulk linear polyethylene, with values of about 110 °C for branched polyethylene, where the crystals are necessarily less perfect. The extrapolated value for large perfect crystals is 146 °C.

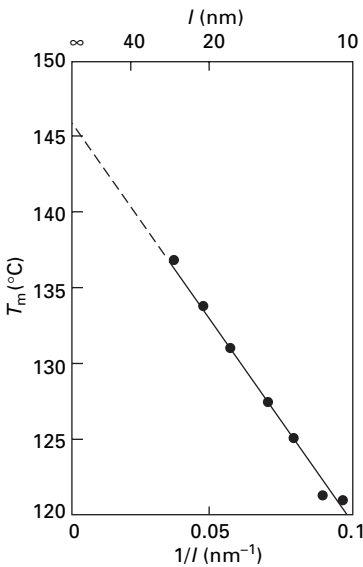
The dependence of melting point on crystal size and perfection is important in melt-spun synthetic fibres, because, as a result of their formation by rapid quenching and drawing, they will contain many small imperfect crystals. Annealing, by exposure to temperatures approaching the quoted melting point, will serve to melt the smallest and least perfect crystals and allow larger, more perfect ones to grow or, more generally, will allow a molecular rearrangement, with a removal of defects, which leads to bigger and better crystalline regions. There will also be some increase in total crystallinity, although this will be relatively small, since, to a considerable

Table 18.1 Fibre melting points (approximate values)

Polyethylene – low density 120 °C
– high density 135 °C
Polypropylene 170 °C
Secondary acetate 250 °C
Cellulose triacetate 300 °C
Nylon 6 215 °C
Nylon 6.6 260 °C
Polyester fibre 260 °C
(Cellulosic and protein fibres decompose before melting)



18.6 Classical free energy diagram for melting and annealing.



18.7 Variation of melting point of polyethylene single crystals with lamellar thickness. From Bair *et al.* [4].

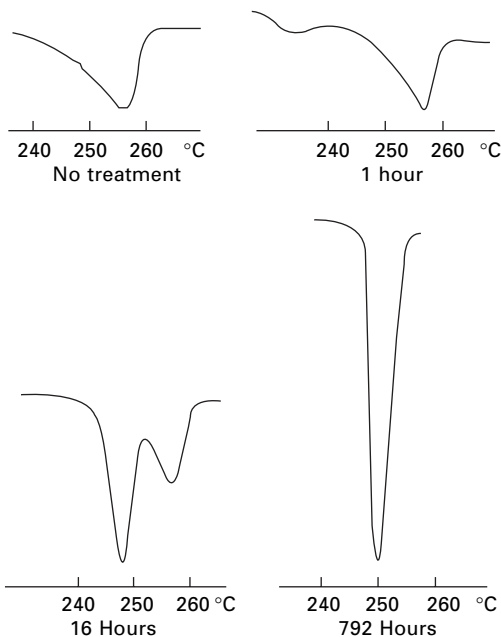
degree, an increase in ordering in one region of a structure of long chains can only be achieved by accumulating disorder in other regions.

Another well-known phenomenon is the depression of the melting point in the presence of impurities. This shows up in fibres as a lowering of the melting point in the presence of water, as is shown experimentally by observing the melting of fibres enclosed in a glass capsule full of water. In nylon, the wet melting point is 80 °C lower than the dry melting point, and even in polyester fibres it is 35 °C lower [5].

A situation that is specific to polymers is the strong dependence of melting point, particularly the internal melting during annealing, on the state of stress on the system. The cause of this is the existence of the tie-molecules that link the crystalline regions. If these are under tension, then the melting of part of the chain will relieve the tension in the tie-segment and allow its entropy to increase. There is thus not only the usual contribution to ΔS from the portion transferring from crystal to melt but also a contribution from the change in the linked segment. The latter part will be greater if the chains are under tension. Looking at it another way, one can say that stress from the tie-molecules will help to break up the smaller crystals.

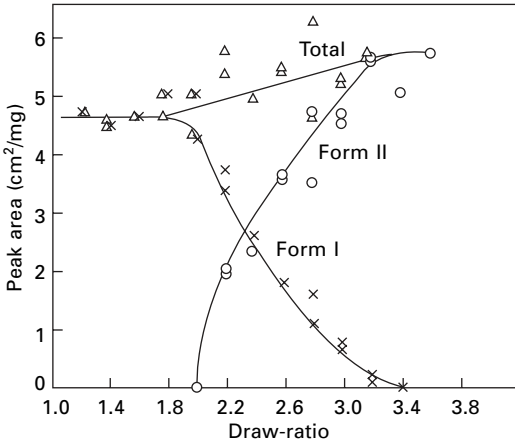
18.2.2 Multiple melting phenomena

Nylon and polyester fibres, among other polymeric materials, show interesting effects of multiple melting in differential calorimetry. When a fibre sample is heated, a negative peak is indicative of the absorption of latent heat and thus of melting. Figure 18.8 shows such data for undrawn nylon yarn as received and after annealing at 220 °C. In the untreated yarn, the peak is at 256 °C, but on annealing a second peak appears below 240 °C. With further annealing this becomes more prominent and rises in temperature level, to reach 260 °C eventually. This suggests that there are two structures with different melting behaviour. Bell [6] calls the first, produced by rapid melting, form I and the second, given by annealing, form II. There is a point at which both give a peak at 256 °C, but the two can be distinguished by seeing if annealing

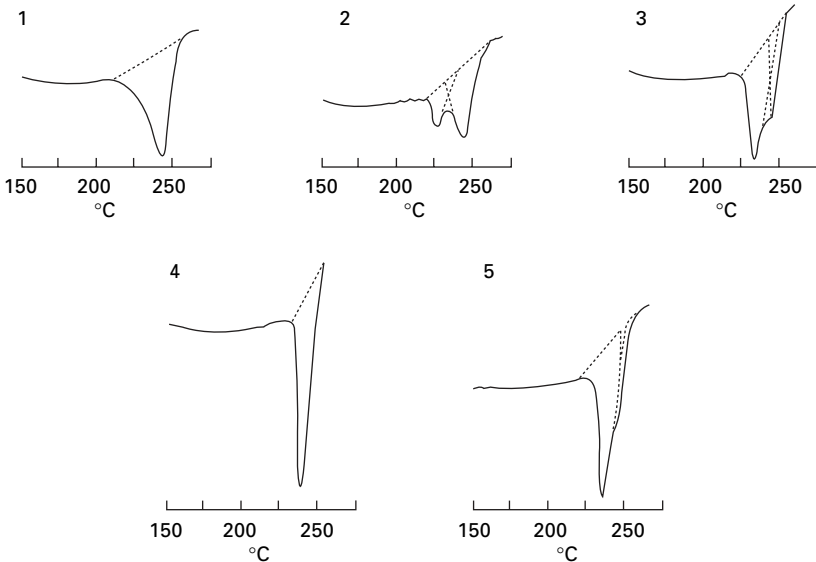


18.8 DSC data for undrawn nylon 6.6 yarn after annealing at 220 °C for various times. From Bell *et al.* [6].

causes the second peak to appear or not. The change from form I to form II also occurs on cold drawing, as shown in Fig. 18.9. Similar effects are found for polyester (PET), (Fig. 18.10). Even after a day's annealing, form II melting has only reached about 240°C, whereas the drawn fibre in Fig. 18.4 has an endotherm at 260°C. Presumably the higher stiffness of the polyester molecule hinders the growth of larger perfect crystals except in an oriented structure where the molecules are more nearly parallel.

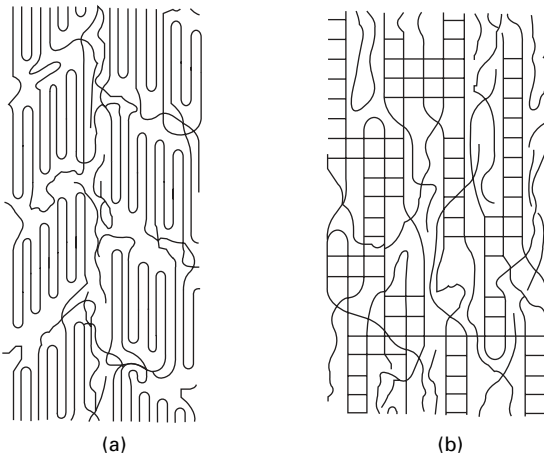


18.9 Change in areas of melting endotherms with draw ratio for nylon 66. From Bell and Murayama [7].

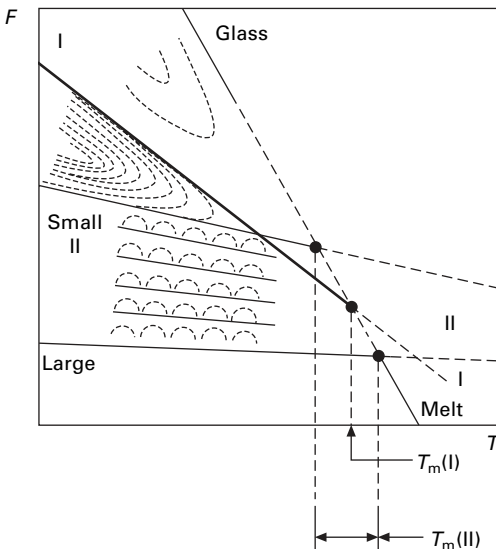


18.10 Effect of annealing time at 220°C on DTA plots for polyester (PET) that had been crystallised for 0.5 h at 110°C: 1, no annealing; 2, 0.25 h; 3 2 h; 4, 6.5 h; 5, 23.5 h. From Bell and Murayama [7].

The experimental evidence on the subject was reviewed by Hearle and Greer [8]. They suggested that form II consists of crystalline micelles, as in Figs 1.16 and 18.11, which become larger on annealing, whereas form I is another state of the solid polymer in which many individual chain repeat units will be in register with neighbouring units, but interspersed with disorder so that there are no separate crystalline and non-crystalline regions, as in Fig. 1.18(c). Although there are problems in applying thermodynamics to metastable states, they explained the effects in terms of changes in free-energy, $F = (U - TS)$. Hearle [10] took the argument further, as shown in Fig. 18.12. As temperature increases, $(-TS)$ becomes numerically greater leading to a

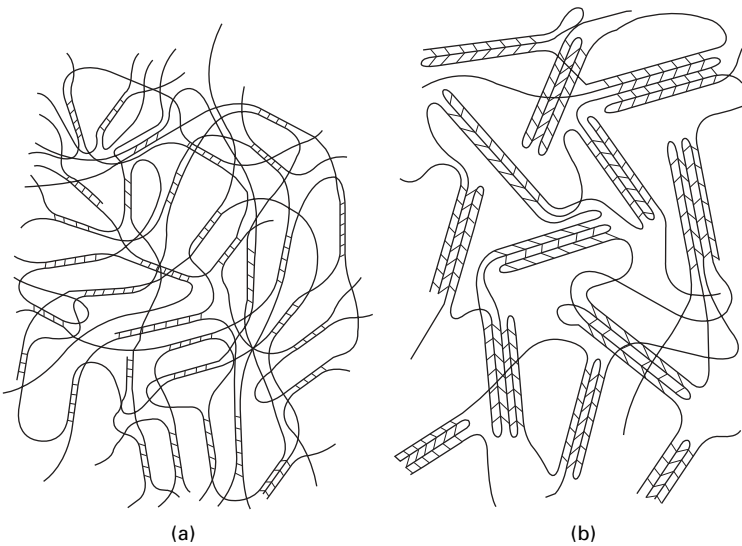


18.11 (a) A fringed micellar model proposed by Hearle and Greer [9]. (b) An alternative form, from Hearle [10].

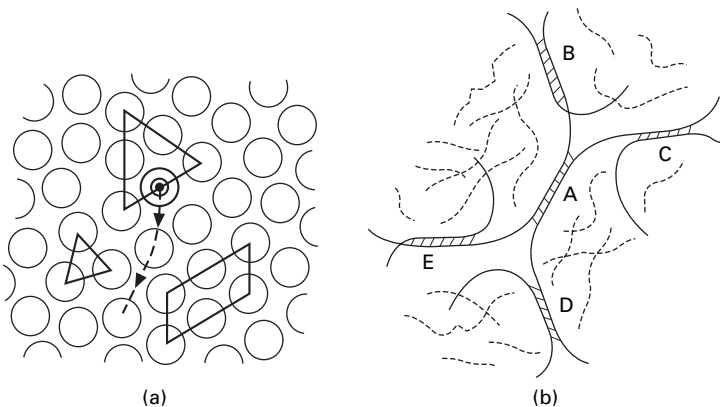


18.12 Free energy of various forms. From Hearle [10].

decrease in free energy along the glass→liquid line. The lines for form II correspond to the effect of annealing with the melting point increasing as crystals grow and become more nearly perfect, as shown in Fig. 18.6. There is nothing remarkable in this. The question is where form I fits in. Hearle [10] made the controversial suggestion that form I is a *dynamic crystalline gel*. Figure 18.13(a) is a schematic view of a form I structure in unoriented polymer, which anneals to form II shown in Fig. 18.13(b). The dynamics are as follows. In a liquid near the melting point (Fig. 18.14(a)), molecules are locally in crystallographic register but are continually changing position in a state of dynamic equilibrium. In the polymer form II (Fig. 18.14(b)), the locally



18.13 Schematic of possible structures of (a) form I and (b) form II in unoriented polymer. For clarity, the packing is much more open than in reality. From Hearle [10].



18.14 (a) Molecules locally in crystallographic register in a liquid. (b) Chain segments locally in register in form I. From Hearle [10].

linked segments would also be in a state of dynamic equilibrium. However, when the segments (A) separated, the neighbours (B, C, D, E) would still be linked. This would be happening all over the material with links breaking and re-forming, but always maintaining the continuity of a solid. The entropy of this form would be greater than the static structure of form II, so that the slope of the free energy diagram would be steeper, as shown in Fig. 18.12 and would intersect with the liquid line to give the melting point of form I. However, annealing would allow the material to fall through the energy barriers to form II with small imperfect crystals having a lower melting point. Further annealing would give larger and better crystals with a higher melting point, eventually passing that of form I. The changes between the several structures in various circumstances are shown in Fig. 18.15(a), with the thermodynamic justification in Fig. 18.15(b).

Whether or not the above explanations are correct, the important practical point is to note the complexity of melting behaviour and the difference in forms that can occur. Commercial fibre samples may be in either form I or form II, depending on their thermomechanical history.

18.2.3 Sticking and bonding

At temperatures below the melting point as defined above, thermoplastic fibres stick together. For example, in early studies of false-twist texturing, Burnip *et al.* [11] found that nylon yarn would pass through the heater at 255 °C but emerged as solid rod. The filaments had not become liquid but they had merged together. The sticking temperature is sometimes referred to as the meting point, since it implies a degree of molecular mobility that is not normally found in a solid.

This property of fibres is utilised in thermal bonding of nonwovens. Mukhopadhyay *et al.* [12] used the flexible thermomechanical analyser described in Section 18.5.2 to measure the strength of thermal bonds. Figure 18.16 shows the experimental arrangement. Fibre loops are held together at specified tension, temperature and time.

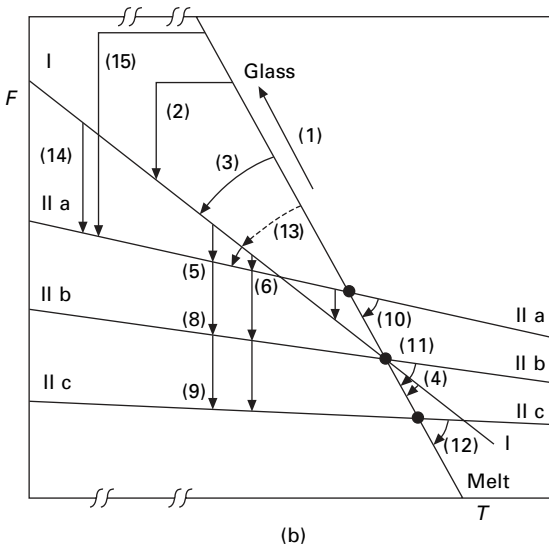
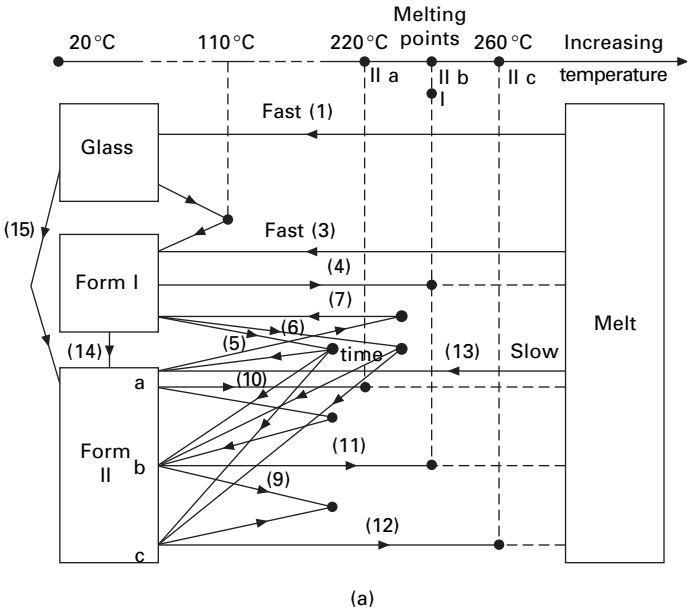
After cooling to room temperature, two arms are then cut and the force required to break the bond is measured. Table 18.2 shows measurements of bond strengths of four polypropylene fibre types and one copolyester. Except for the low bond strength for PP4, where an SEM picture shows that the material has become too nearly molten, the bond strengths correlate with commercial bonding performance. For optimum bonding, it is clearly necessary to choose the right fibre and the right bonding conditions. In a later paper, Mukhopadhyay [13] showed that pre-wetting polypropylene fibres gave good bonding at a lower temperature.

Kim *et al.* [14] present computaonal analysis of thermal bonding in bicomponent fibres.

18.3 Dynamic mechanical responses

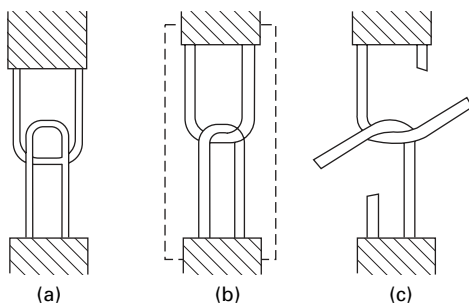
18.3.1 Dynamic moduli

As described in Section 16.5.2, the real (storage) modulus depends on the elastic part of the deformation, and the imaginary (loss) modulus or $\tan \delta$ depends on the time-



18.15 (a) Schematic of changes between various forms. (b) Changes between forms on free energy diagram. From Hearle [10].

dependent part. Above and below the transition region, the elastic deformation, with high or low modulus, is dominant. In the transition, the structural response is sluggish, so that there is substantial energy absorption, which gives the peak in loss modulus and the phase difference between stress and strain given by the peak in $\tan \delta$.



18.16 Testing bond strength: (a) fibres as mounted; (b) in heated chamber under controlled tension; (c) ready to measure bond strength. From Mukhopadhyay *et al.* [12].

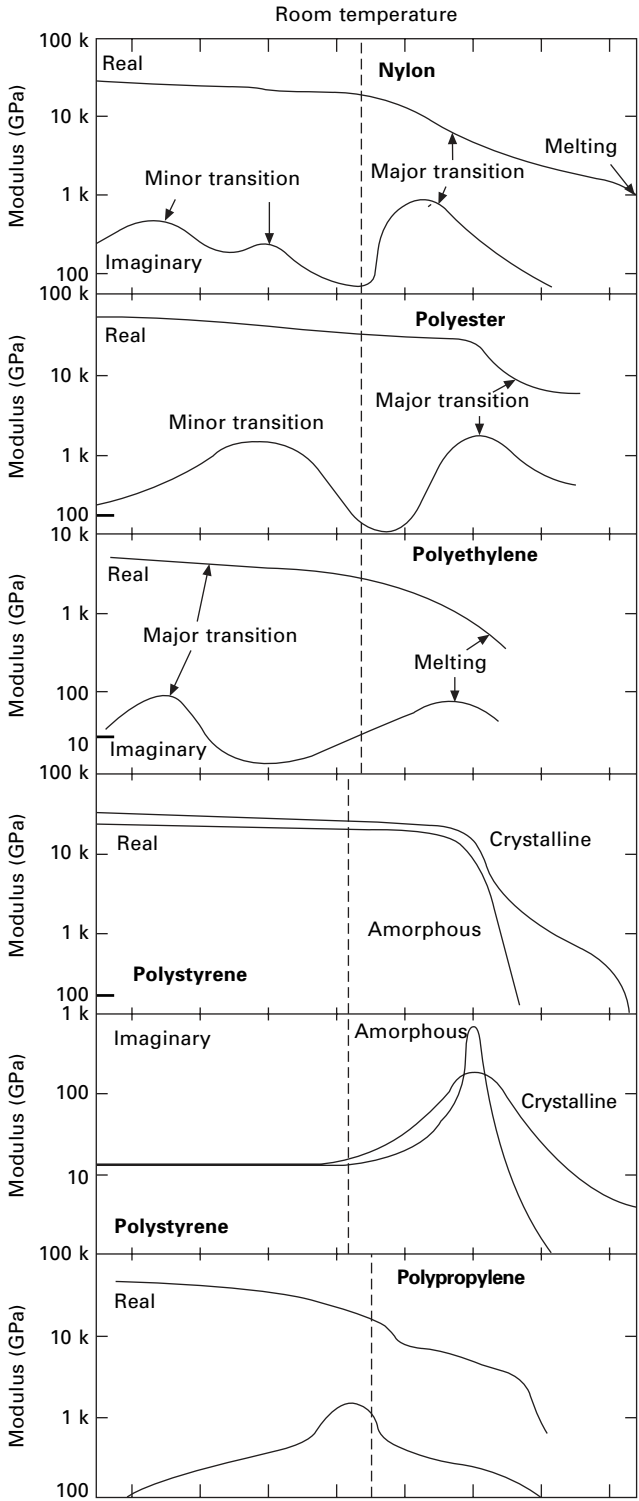
Table 18.2 Thermal bonding of four polypropylene fibres and a copolyester. 10 mN tension gives 17 mN/tex on each arm. From Mukhopadhyay *et al.* [12]

Bonding conditions					Fibre properties		Commercial thermobonding performance
Temperature (°C)	160	100	150	150	20	150	
Time (seconds)	60	60	60	60			
Tension (mN)	10	20	10	20			
Fibre type	Bond strength mN/tex				Fibre strength mN/tex		
PP1		96			391	125	Very poor
PP2		124			355	113	Poor
PP3		240	134	191	308	113	Good
PP4		161	168	224	255	101	Very good
Co-polyester	103, 132	Fibre broke			122	70	Good

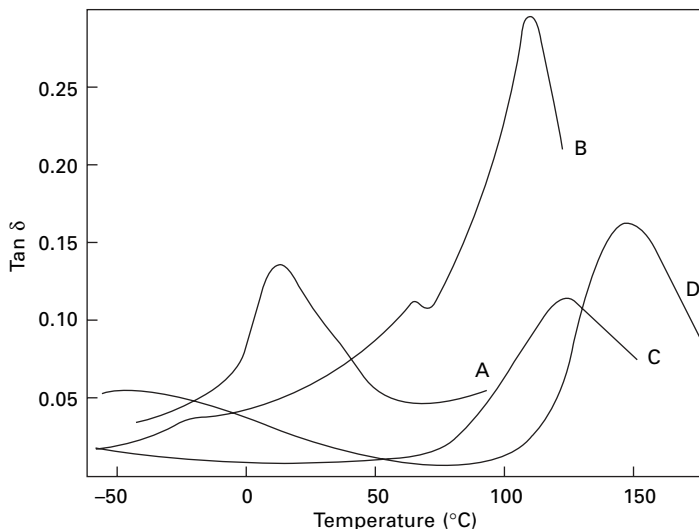
18.3.2 Observed behaviour

The dynamic and loss moduli of various polymers as measured by Takayanagi [15] are shown in Fig. 18.17. For the simplest semicrystalline polymer, polyethylene, a glass transition is shown by a sharp drop in modulus E' and peak in E'' (also shown in $\tan \delta$) around -120°C . This can be attributed to the onset of freedom of rotation around $-\text{CH}_2-$ bonds. There is then a reduction of slope of the modulus plot, which is clearer in data by Kawaguchi [17], and a trough in $\tan \delta$ before a steeper fall in modulus and increase in $\tan \delta$ over a long temperature range towards melting. In polystyrene, which is too stiff at room temperature to be useful as a textile fibre, there is a single transition at around 100°C in plots that show the major influence of crystallisation.

Polypropylene has a single transition near room temperature, which is also shown by the peak in $\tan \delta$ in dynamic bending in Fig. 18.18. This accounts for the sluggishness of its response. Any cyclic deformation is damped by the large energy absorption. The transition will be due to the onset of bond rotation, occurring at a higher temperature than in polyethylene because of the bulky side group.



18.17 Dynamic mechanical properties of various polymers. Upper lines are real (dynamic) and lower lines are imaginary (loss) moduli. From Hearle [16] based on data from Takayanagi [15].

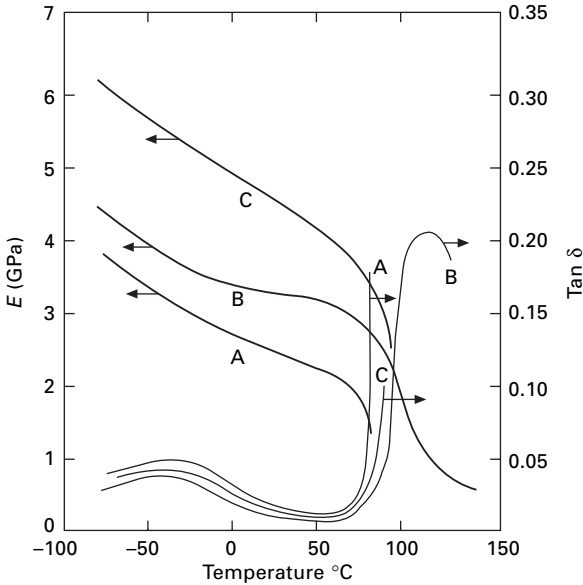


18.18 Tan δ measured in dynamic bending of fibres at 0% r.h. at frequencies of 200–300 Hz: A polypropylene; B acrylic fibre; C nylon 6.6; D polyester fibre.

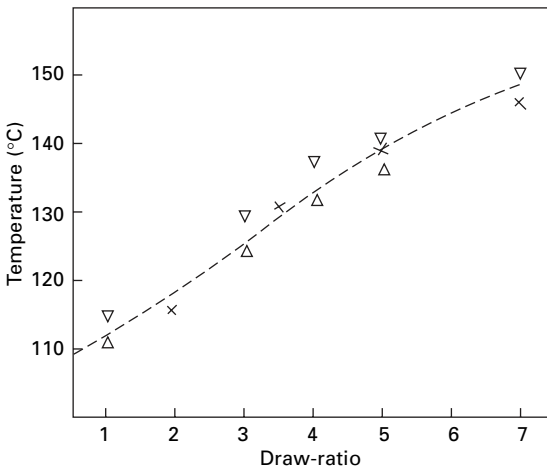
Nylon 6 shows two low-temperature peaks in E'' , which correspond to the peak in polyethylene but reflect bonds becoming free at different temperatures. Similar peaks in $\tan \delta$ are reported by Kawaguchi [17] and, in nylon 66, by Bell and Murayama [7] film at slightly lower temperatures, though this may be due to different test conditions. In rapidly quenched film, referred to in the above discussion of multiple melting as form I, the low-temperature transition was split between two peaks, but in slowly cooled film, form II, the whole transition was in the higher of the two peaks. Polyester shows a single peak in the low-temperature region.

The low-temperature peaks are of academic interest, but the peak at about 70 °C in nylon and 120 °C in polyester has great practical relevance to the behaviour of the fibres in processing and use. The transition curves are influenced by crystallinity and orientation, as shown by the results for polyester fibre in Fig. 18.19. The variation of the transition temperature (as indicated by a maximum in $\tan \delta$) with draw-ratio in polyester fibres is shown in Fig. 18.20 Davis [21] found that there was a change with time in polyester held at 150 °C at a stress of 5.5 mN/tex. The storage modulus increased and $\tan \delta$ decreased by about 10%, approaching equilibrium after 30 minutes. He also showed that the storage modulus was about 30% higher in an annealed fibre than in a direct spun fibre. In a paper on the relation between the transition and dye diffusion, Davis [22] showed that both storage and loss moduli are higher for nylon 66 in glycerol than in water and decrease as the amount of water in a glycerol/water mixture increases.

In addition to the fairly large transitions shown up by large peaks in the loss modulus, there may be minor transitions, causing small peaks or shoulders. These may be due to other deformation mechanisms, though Moseley [23] attributed a large collection of small peaks at large strain amplitudes to non-linearity of response, and Dumbleton and Murayama [24] showed that lack of uniformity in a fibre could cause



18.19 Dynamic modulus and $\tan \delta$ of PET as measured by Kawaguchi [18] at about 100 Hz: A, undrawn, 2% crystallinity; B, undrawn, 50% crystallinity; C, drawn 5 \times , 25% crystallinity.



18.20 Effects of draw-ratio on temperature of maximum $\tan \delta$ for polyester fibres, from data by Meredith [19] and Kondo *et al.* [20].

the appearance of extra peaks. Kveder and Rijavec [25] report dynamic modulus and loss data for partially oriented and drawn nylon 66 yarns.

The two transitions are also shown in dielectric properties of polyester film as described in Section 21.6, which includes the combined influence of temperature and frequency.

The influence of water on the transitions is shown by the work of van der Meer [26, 27], as illustrated in Fig. 18.21. In dry viscose rayon, there appears to be a transition somewhere above 200 °C, but in wet rayon it shifts to below 0 °C. In nylon 6, the transition falls from about 80 to 10 °C; and there is a slight effect even in polyester fibres. The change in the position of the $\tan \delta$ peak of nylon 6.6 with relative humidity is shown in Fig. 18.22.

Figure 18.23 demonstrates how the peak in $\tan \delta$ can be traversed by varying relative humidity, instead of temperature or time. The acrylic fibre has a large transition near 100 °C, which is shown in Fig. 18.18. The large decrease in stiffness is shown by the dramatic changes in stress–strain curves in Fig. 18.24. Experimental demonstration of the transition just below 100 °C was given by Rosenbaum [28], who found sharp changes in axial thermal expansion, breaking extension and creep rate. In this material, the mobility is mainly restricted by the intermolecular forces caused by the strong electric dipoles in the $-\text{C}\equiv\text{N}$ groups, and the transition occurs when freedom of relative movement of chains in less-ordered regions becomes possible. Another transition, at a slightly higher temperature, will be due to a similar effect in the ordered regions. However, the individual chains still remain stiff enough for the fibre to be solid, and a further increase in mobility occurs at a considerably higher temperature when the chain changes from its regularly coiled, cylindrical, rod-like form to a more flexible, random coil. Results for some natural polymer fibres are shown in Fig. 18.25.

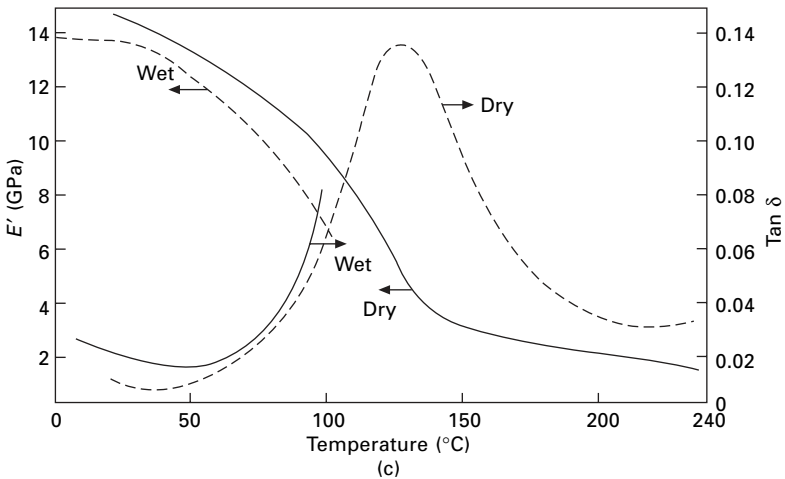
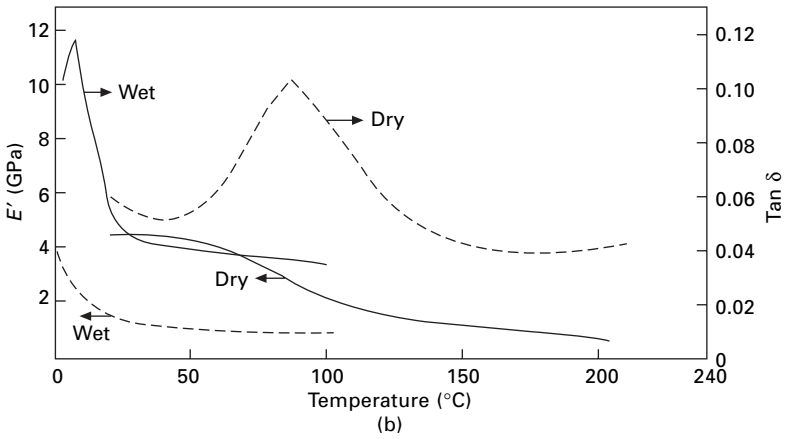
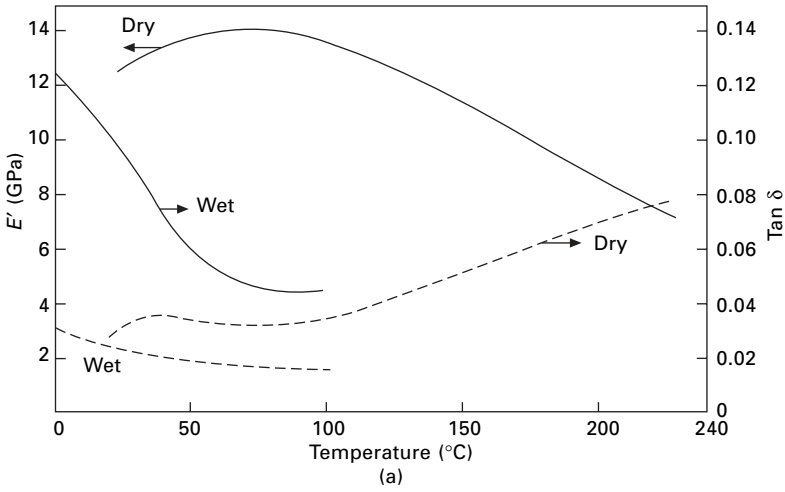
The low modulus and high extensibility of elastomeric fibres depend on their glass transition temperature being below the working temperature. Measurements of dynamic mechanical properties by Houston and Meredith [30], illustrated in Fig. 18.26, show a rather sharp transition for natural rubber between -50 and -20 °C but a more spread-out transition for the spandex fibre *Lycra* from about -80 to $+20$ °C.

18.3.3 A comparison of temperature effects

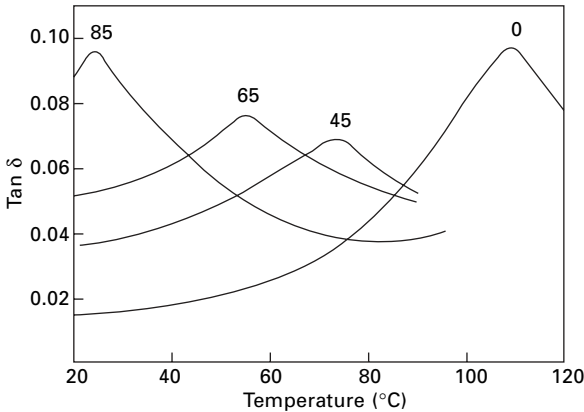
Hearle [31] suggested that an ideal set of transitions for a fibre material was of the type shown in Fig. 18.27. The low-temperature transition (A) gives some freedom to the non-crystalline regions, and thus gives moderate extensibility and high toughness to the fibre, without making it too soft and extensible. The working region near room temperature is free of transitions. The greater freedom required to allow crystallisation to occur appears at the higher transition (B). Then the melting point (C) is higher still but well below the temperature of chemical degradation.

These properties are shown, in considerable measure, by nylon and polyester fibres, except that the higher transition in wet nylon does come down to room temperature, and chemical degradation impinges on the melting point. The latter effect means that the material must not be kept in the molten state, certainly in the presence of oxygen, for any length of time. Even appreciably below the melting point, prolonged exposure can cause a loss of strength, as indicated by the results in Table 18.3.

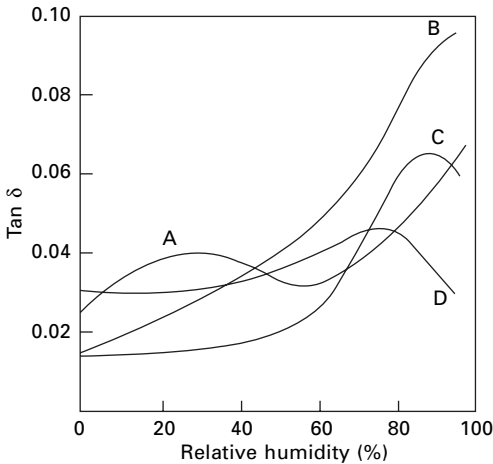
Where there is a single glass-to-rubber transition, the fibres are too soft if the transition is below room temperature, as in polyethylene, or too stiff and brittle if



18.21 Variation of E' and $\tan \delta$ with temperature wet and dry: (a) viscose rayon; (b) nylon 6; (c) polyester fibre.



18.22 Effect of temperature on $\tan \delta$ for nylon at various humidities. From Meredith [19].

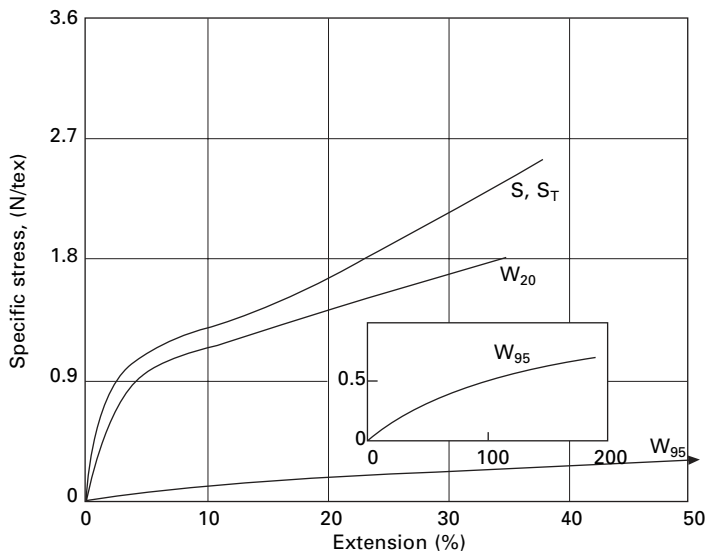


18.23 Effect of relative humidity at 20°C on $\tan \delta$: A, viscose rayon; B, nylon 6.6; C, nylon 6; D, *Acrilan* acrylic fibre.

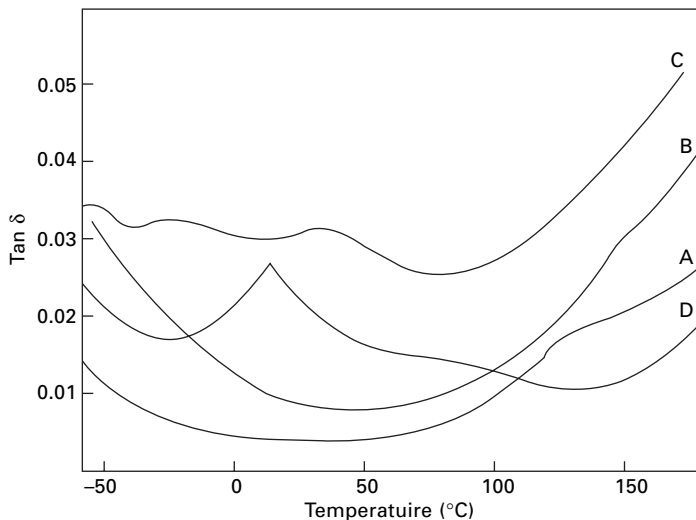
the transition is above room temperature, as in polystyrene. If the transition straddles room temperature, as in polypropylene, the properties are acceptable but not ideal.

In fibres that are not melt-spun, the above requirements are not as critical, although in one way or another there must be some freedom in the structure at room temperatures and a greater freedom at higher temperatures. Moisture often plays a part in this.

All the fibres made from linear polymers are fundamentally thermoplastic (as distinct from crosslinked polymers, which are not), but in some, such as cellulose, the thermoplastic character cannot be exhibited because chemical decomposition, leading to charring or burning, sets in first. Acrylic fibres and wool are on the borderline, where both effects occur at similar temperatures.



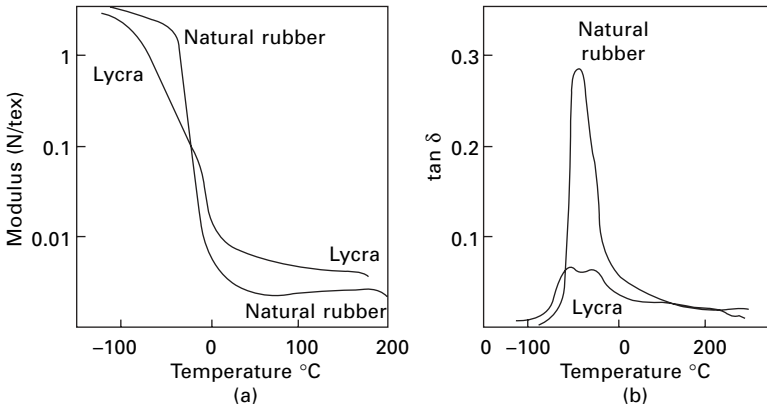
18.24 Stress–strain curves of *Courtelle* acrylic fibre. S, 65% r.h., 20 °C as received; S_T, 65% r.h., 20 °C, after water at 95 °C; W₂₀, in water at 20 °C, as received; W₉₅, in water at 95 °C, as received.



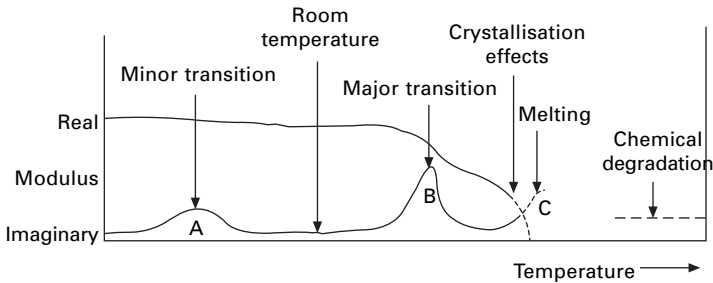
18.25 Dynamic loss of some natural polymer fibres at 0% r.h. in dynamic bending: A, mercerised cotton; B, viscose rayon; C, secondary acetate; D, wool. From Meredith [29].

18.4 Transitions in keratin fibres

As can be expected from their complex multilevel structure, the transitions in wool and other keratin fibres are complicated. There are three defined transitions, which are reviewed by Wortmann [33]. All are strongly dependent on regain as well as



18.26 Dynamic mechanical response of elastomeric fibres: (a) dynamic modulus; (b) $\tan \delta$ [30].



18.27 Transitions in an 'ideal' fibre. From Hearle [31].

Table 18.3 Loss of strength on prolonged exposure of high temperatures [32]

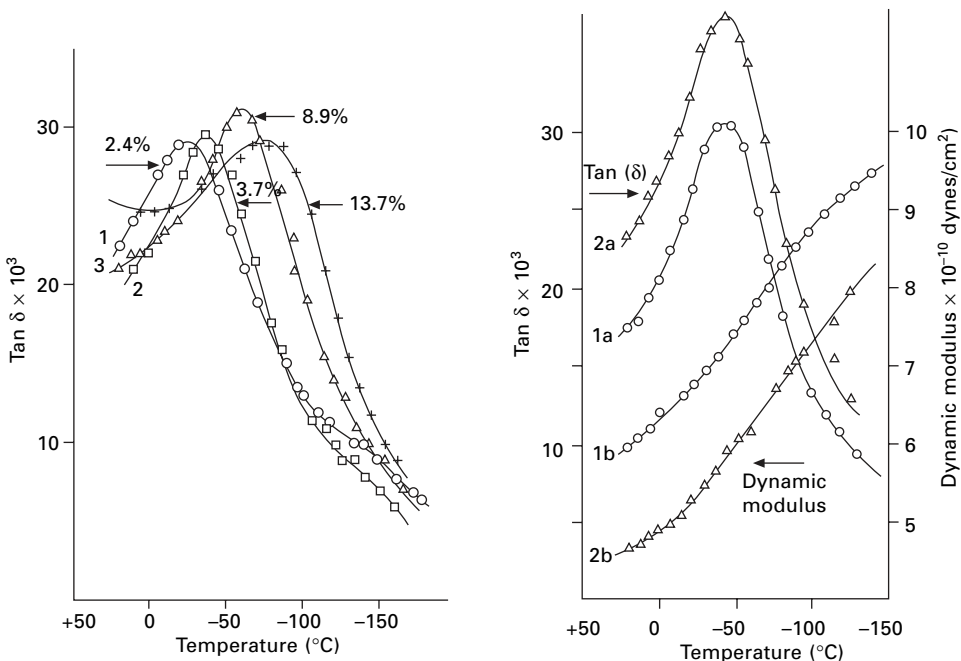
Fibre	Percentage strength retained			
	After 20 days		After 80 days	
	At 100 °C	At 130 °C	At 100 °C	At 130 °C
Viscose rayon	90	44	62	32
Cotton	92	38	68	10
Linen	70	24	41	12
Glass	100	100	100	100
Silk	73	—	39	—
Nylon	82	21	43	13
Polyester, <i>Terylene</i>	100	95	96	75
Acrylic, <i>Orlon</i>	100	91	100	55

temperature. In increasing temperature, these are referred to as β , α^1 and denaturation transitions. The α -transition is also called the glass transition, but it is more instructive to regard the glass-to-rubber transition as occurring in two stages at the β and α transitions.

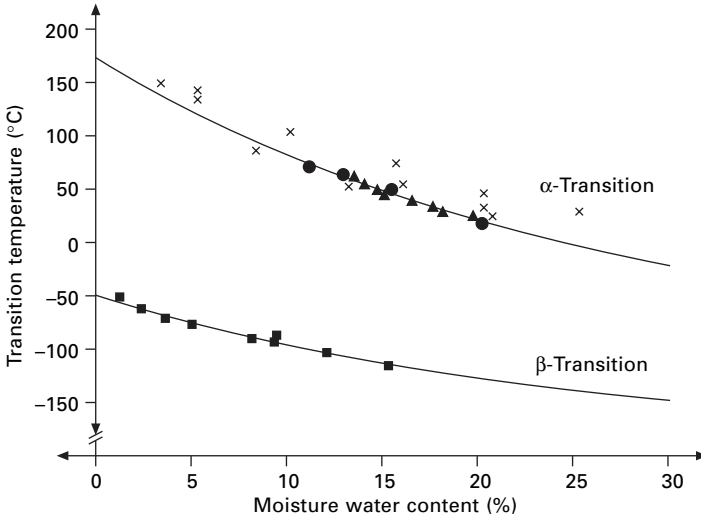
¹Not to be confused with the mechanically induced $\alpha \leftrightarrow \beta$ transition in helical crystals.

Druhala and Feughelman [34, 35] investigated the β -transition by cyclic tensile testing and found a peak in $\tan \delta$ at about -40°C in horsehair in a fairly dry state (2.4% regain), dropping to about -90°C at 13.7% regain, (Fig. 18.28(a)). This is similar to the low-temperature transition in nylon, which, as indicated in Fig. 20.15, is associated with freedom of rotation around covalent bonds. In proteins both main chain and side chain bonds are immobile below the transition region. A comparable measurement on rhinoceros horn, Fig. 18.28(b), shows the decrease in modulus at the transition. The variation in the transition temperature is shown by the lower curve in Fig. 18.29.

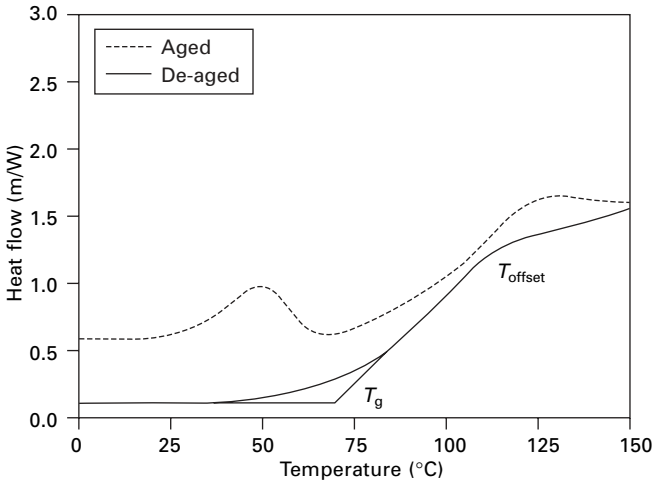
Wortmann *et al.* [37] investigated the α -transition by measuring the recovery from cohesive torsional set as mobility was induced. They found the transition at 175°C in dry wool decreasing with increasing moisture content as shown by the upper curve in Fig. 18.29. The behaviour is similar to that of nylon, which has a transition going from around 100°C when dry to near 0°C when wet. Phillips [38] and Kure *et al.* [39] studied the transition by DSC. As shown in Fig. 18.30, a sample of wool, referred to as aged, has an endothermic peak at 50°C , which presumably reflects the release of some temporary set in the amorphous matrix. This is followed by an increase in the heat flow rate, namely an increase in specific heat, between 75 and 125°C , which is interpreted as a glass transition. If the sample is heated to the final temperature and then cooled, the endotherm at 50°C is no longer present in a subsequent



18.28 (a) $\tan \delta$ for low-temperature transition in horsehair at 110 Hz at different regains. (b) Modulus and $\tan \delta$ for rhinoceros horn: 1a and 1b cut parallel to growth; 2a and 2b cut perpendicular to growth. From Druhala and Feughelman [34].



18.29 Change of transition temperatures with moisture content with lines for the Fox equation, from Wortmann [33], with data from Druhala and Feughelman ■ [34, 35], Rosenbaum ▲ [36], Wortmann *et al.* ● [37] and Phillips × [38].



18.30 DSC traces for wool. From Kure *et al.* [39].

DSC trace, but the heat flow at the glass transition is still present. In wool, the temperatures are higher in the dry material, and run into the temperatures of denaturation. Phillips [38] found that an endotherm at 60 °C was present in a fibre aged for 52 days at 20 °C, disappeared after rapid cooling, and reappeared in a trace after 15 days at 20 °C.

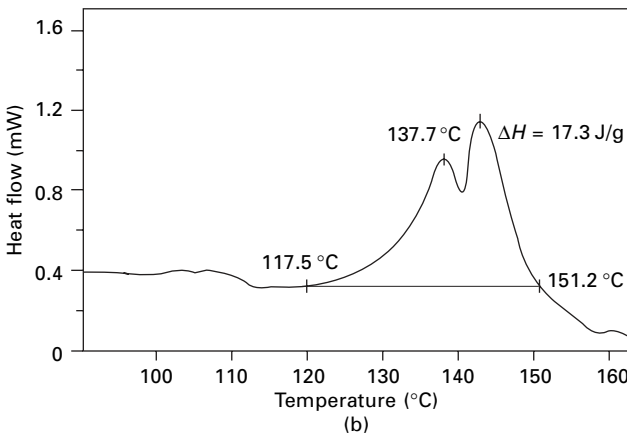
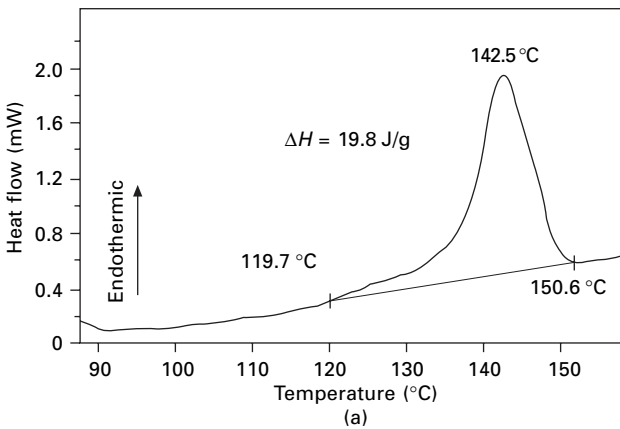
Wortmann *et al.* [33, 37, 40] has shown that for both wool and human hair the β and α transition temperatures T_t vary with moisture content according to the simple mixture equation proposed by Fox [41] as shown in Fig. 18.29:

$$\frac{1}{T_t} = \frac{m_1}{T_{t1}} + \frac{m_2}{T_{t2}}$$

where m_1 and m_2 are the mass fractions and T_{t1} and T_{t2} relate to dry and wet wool.

By fitting and extrapolating the experimental data, the α -transition in wool has $T_{\alpha1} = 174^\circ\text{C}$, which is in agreement with torsional data by Menefee and Yen [42], and $T_{\alpha2} = -148^\circ\text{C}$, which agrees with values found for ice and glassy water ($m_1 = 0$ and $m_2 = 1$) [43, 44]. For the β -transition, $T_{\beta1} = -49^\circ\text{C}$ and $T_{\beta2} = -210^\circ\text{C}$.

The highest temperature transition can be studied by high-pressure DSC in order to maintain water in the material. Wortmann and Deutz [45, 46] report measurements on eight keratinous materials. Figure 18.31 shows a single endotherm peak at 143°C in mohair and double peaks in wool at 138 and 143°C . The transition is interpreted as a ‘melting’ of the helical crystalline fibrils, though it is influenced by restraints from the amorphous matrix. It is called *denaturation*, since it is an irreversible process. The enthalpy $\Delta H = 17.1 \text{ J/g}$. If heating is stopped just past the first peak in wool and



18.31 DSC curves for (a) mohair and (b) merino wool. ΔH = denaturation enthalpy From Wortmann and Deutz [45].

the fibre is then rapidly cooled, a tightly crimped coil is formed. This indicates that the first transition occurs in the ortho-cortex, which has super-contracted, and the second transition occurs in the para-cortex, which has a higher cystine content. Differences in denaturation temperatures in different keratins are attributed to the varying cystine concentrations in the matrix.

The denaturation temperature decreases from 210 °C in the dry state to 150 °C at a moisture content of 25% [47, 48]. Wortmann [33] considers various explanations for the effect of water, but concludes that there is a gap in understanding that requires further investigation.

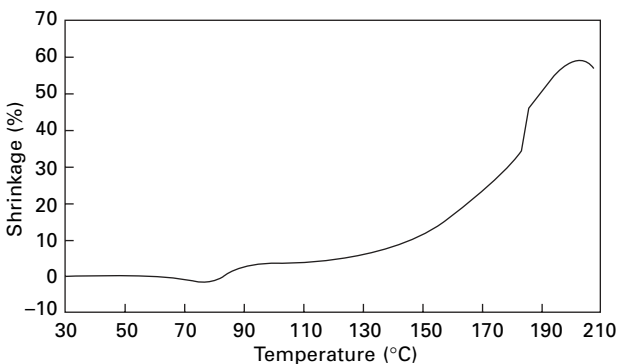
18.5 Thermomechanical responses

18.5.1 Thermomechanical analysis

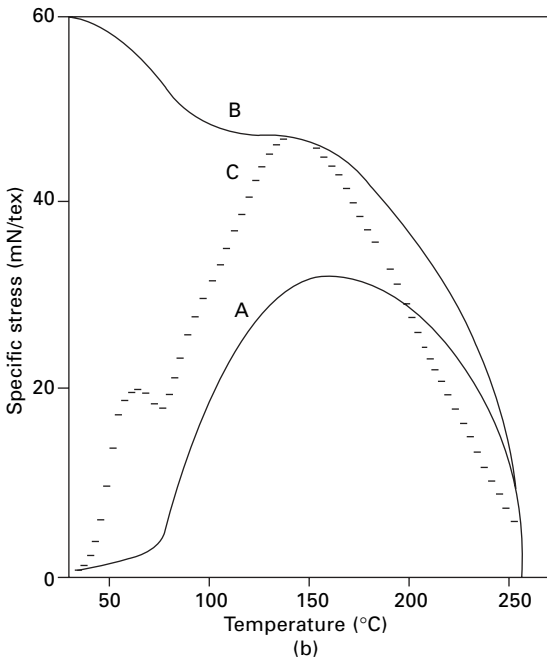
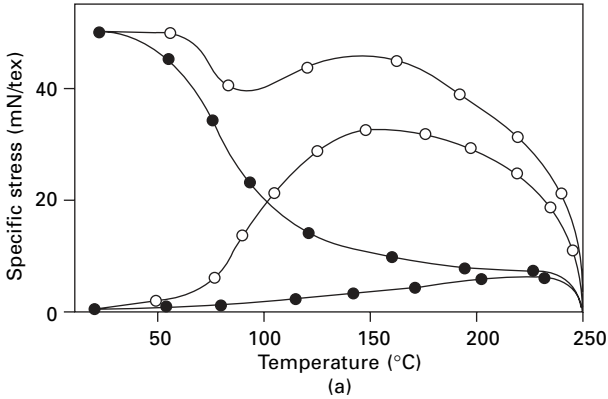
TMA is another way of studying thermal changes in materials. Specimens are held under constant tension and the length changes monitored. Commercial instruments, such as the Mettler Thermomechanical Analyser, have attachments for fibre testing. The simplest response gives a measure of the coefficient of thermal expansion. With fibres, the interest is more in reversible or irreversible shrinkage and in the step changes at transitions, though these are not as clear as the peaks in DMA. Buchanan [49] gives an extensive account of the dependence of thermal shrinkage on the prior history of nylon and polyester fibres.

Figure 18.32 is a typical TMA trace in a paper on the structural characterisation and properties of polyvinyl chloride (PVC) fibres [50]. The rise between 80 and 90 °C is a second-order transition, which is followed above 130 °C by an elastomeric thermal shrinkage as the structure loosens up. The trace terminates with a slight lengthening, which is due to the fibre extending under the applied tension as it becomes softer in the approach to melting.

The tendency to contraction, but not expansion, can be studied by the alternative procedure of measuring tension changes at constant length. Figure 18.33(a) shows shrinkage force measurements for a polyester (PET) yarn [51]. From a low pre-tension, the shrinkage force increases over the lower transition range from 75 to



18.32 TMA trace of drawn PVC fibre. From Kim and Gilbert [50].



18.33 Shrinkage force measurement of a polyester (PET) yarn (15 tex, 48 filaments). (a) Heated at 25 °C/min from pre-tensions of 0.5 mN/tex and 50 mN/tex for yarn as made ○ and for yarn pre-treated at 180 °C for 20 s at 5 mN/tex ●. (b) For fibre as received: A and B are standard shrinkage force tests; C is equilibrium shrinkage force. From Berndt and Heidemann [51].

150 °C and then falls as the fibre softens. Pre-treatment at 180 °C almost eliminates the shrinkage tension. The tension has dropped to almost zero at 250 °C, which can be taken as one measure of the melting point. A stepwise approach to the equilibrium shrinkage force (Fig. 18.33(b)), shows a maximum at 60 °C, which is attributed to a ‘classically defined glass transition’.

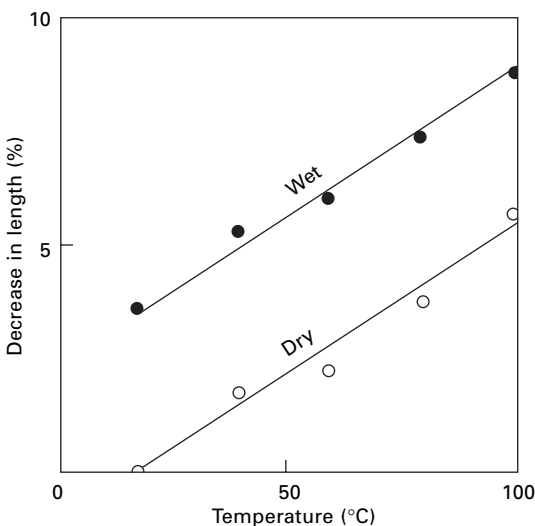
18.5.2 A flexible thermomechanical analyser for fibres

Sikorski and coworkers [52–54] describes a thermomechanical analyser that was specially developed for fibres and incorporates twisting as well as tensile changes. There were later enhancements, particularly in software for computer control, data retrieval and data processing [55]. The fibre specimen is clamped between jaws that are contained within a heating chamber and connected by rods to external functions. Temperature is controlled and can be rapidly changed by mixing streams of hot and cold air through a valve controlled by a stepper motor. Two more stepper motors control specimen length and twist. Tension is measured by a piezoelectric transducers for fast response and a strain-gauge transducer for quasi-static measurements. Torque measurement by the new transducer was described in Section 17.3.2. Twist was measured by an optical encoder and extension by an LDVT. With this tester, a great variety of test sequences can be studied.

18.5.3 Irreversible shrinkage

In addition to the reversible changes of dimensions with temperature, which occur in all materials, many fibres show an irreversible contraction or sometimes an irreversible expansion on heating. What happens depends on the prior process history of the fibre, so that manufacturers can supply nylon and polyester fibre in high- or low-shrinkage variants.

Figure 18.34 shows the irreversible changes in length of typical nylon fibres with increasing temperature. In order to achieve the same effect, the temperatures must be about 70 °C greater dry than in steam. In nylon fibres as produced, the shrinkage in boiling water is usually about 10%, but the value is very sensitive to subsequent heat



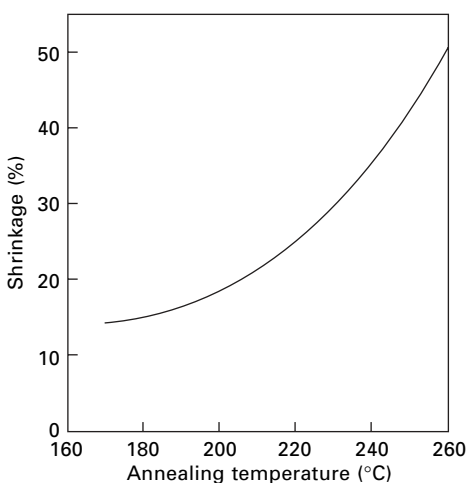
18.34 Irreversible shrinkage of nylon on heating [56].

treatments, and examples of the range of values are shown in Table 18.4. Similar effects are observed in polyester fibres, and spontaneously extensible fibres can be made by appropriate thermomechanical treatments. The more rapid shrinkage that occurs as the melting point of nylon is approached is shown in Fig. 18.35.

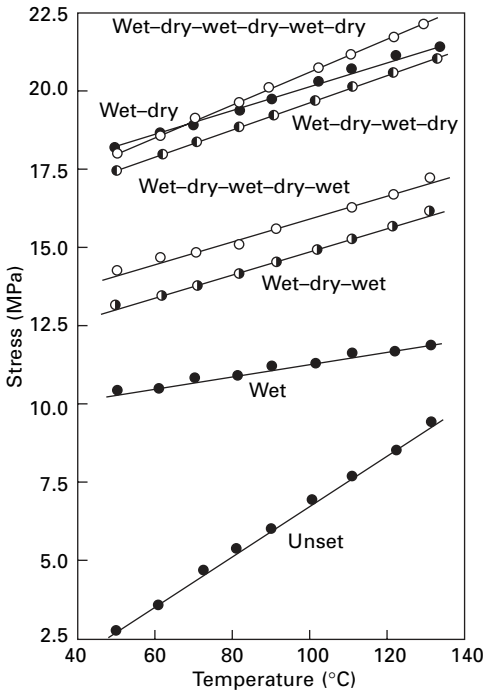
As an alternative to measuring shrinkage, the increase in tension on heating fibres at constant length may be observed. Some examples of studies on nylon 6 are shown in Fig. 18.36. The unset fibre shows a rapid build-up in tension. Corresponding to the tendency to irreversible shrinkage there is an irreversible build-up of tension, so that subsequent lines lie at a higher level. The positive slope of these lines corresponds to the reversible contraction, and is another manifestation of the occurrence of rubber elasticity in nylon. However, the results are also remarkable for the fact that successive setting treatments, wet at 120 °C and dry at 170 °C for 30 min, cause the lines to shift to progressively higher tension levels, the values always being highest when the final

Table 18.4 Shrinkage of 7.8 tex nylon 6.6 yarn in boiling water [57]

Treatment	Tension (N)	Shrinkage % in boiling water
As received		9
Dry heat (°C)		
200	0	0
200	0.1	2
200	0.3	7
200	0.5	6
200	0.75	8
160	0.1	5
240	0.1	4
160	0.5	9
240	0.5	5



18.35 Length changes in the experiments of Dismore and Statton [58] on annealing nylon 6.6.



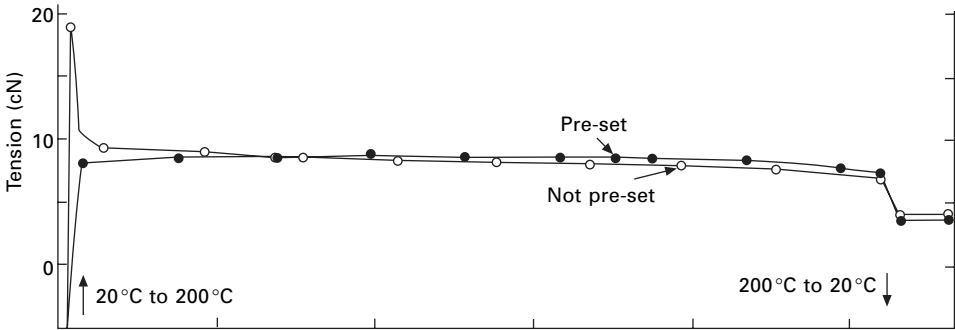
18.36 Tension-temperature curves for nylon 6 fibres, as produced and after successive setting treatments at 130 °C wet and 170 °C dry. From Koshimo [59].

treatment was wet. This demonstrates that complicated and continuing structural changes can occur in repeated treatments.

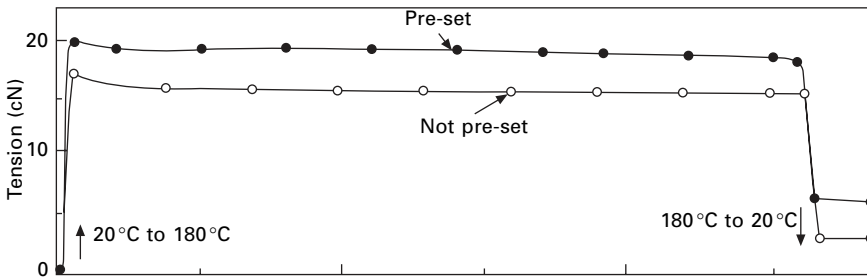
Mukhopadhyay and Hearle [60] report tests with the flexible thermomechanical analyser, which show that it is necessary to avoid artefacts due to expansion and contraction of the rods linked to the jaws. With a modified procedure, Fig. 18.37 shows shrinkage tension measurements of polyester (PET) and nylon 6. The general pattern is a rapid rise in tension followed by some stress relaxation. The fall in tension on cooling corresponds to a reversible contraction on heating. The residual tension corresponds to the irreversible shrinkage. Figure 18.38 shows that the high spike in the curve in Fig. 18.37(a) is due to the shrinkage tension in unset polyester peaking at 180 °C during the rise in temperature.

Acrylic fibres that have been stretched, for example, by stretch-breaking, and left with a 'permanent' extension, will contract severely on heating. This is the analogue of swelling recovery in rayon, which was discussed in Section 15.6. The plastic deformation of the structure is released when it is freed at the higher temperature. High-shrinkage fibres of this type are used in combination with non-contracting (or already contracted) fibres in high-bulk yarns.

The main mechanisms giving rise to an irreversible shrinkage are probably the following.

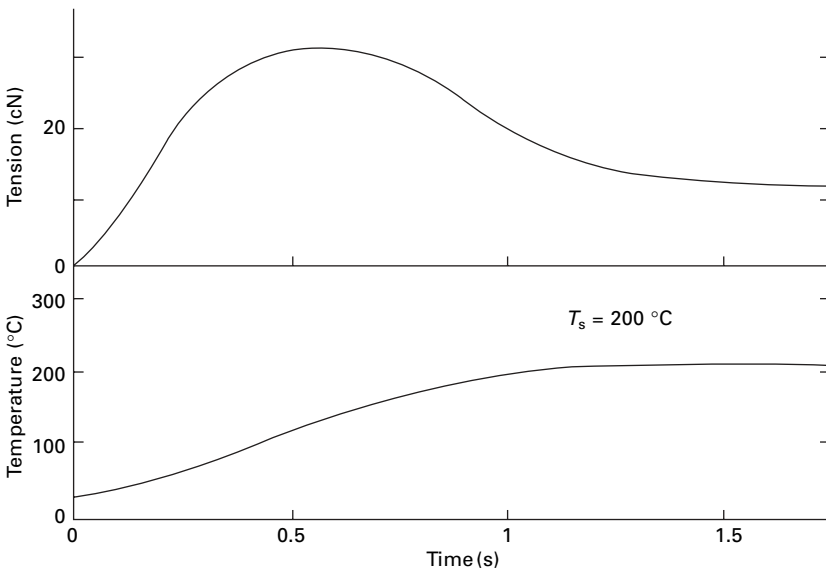


(a)



(b)

18.37 Shrinkage–tension plots for fibres rapidly heated, held at constant temperature and then cooled. (a) Polyester (PET) monofilament, 88 μm diameter, heated to 200 $^{\circ}\text{C}$, as received and pre-set at 180 $^{\circ}\text{C}$ for 30 mins. (b) Nylon 6 monofilament, 85 μm diameter, heated to 180 $^{\circ}\text{C}$, as received and pre-set at 160 $^{\circ}\text{C}$ for 30 mins. From Mukhopadhyay [61].



18.38 Expansion of the timescale in the initial part of Fig. 18.37(a). From Mukhopadhyay [61].

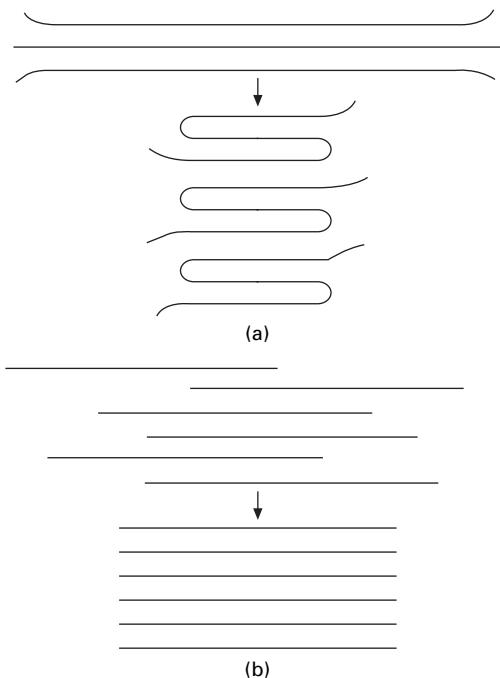
- Oriented non-crystalline material, resulting from the original drawing of the fibre or from mechanical hysteresis or from heating under tension, will revert to an unoriented or less oriented state when it is loosened by heating.
- The annealing of crystalline regions may reduce their length, as indicated in Fig. 18.39. This will certainly be true if the chain molecules fold in order to crystallise better, but it may also be true when they move relatively so as to come into better register.
- Small crystallites may melt, with the chains shrinking axially to a random coil. Recrystallisation elsewhere will tend to stabilise the shortened form.

18.5.4 Other property changes

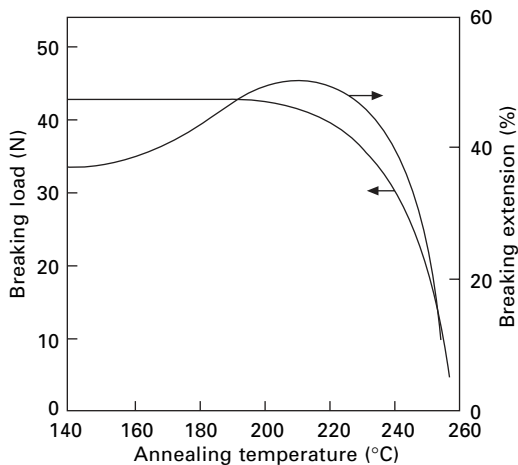
Accompanying the thermal shrinkage, there are many other changes in properties, and a full account of the effects in synthetic fibres has been given by Statton [62].

Figure 18.40, which comes from the same experimental series as Fig. 18.35, shows that, up to about 190 °C in nylon 6.6, there is little change in strength but an increase in breaking elongation, which can be accounted for as being due to the addition of the thermal shrinkage to the breaking extension. But the more rapid shrinkage above 190 °C is accompanied by a loss in strength and a corresponding reduction in breaking elongation.

The dyeing behaviour of fibres is altered in complicated ways by heat treatments.



18.39 Length changes that may occur on annealing of crystalline regions with (a) chain-folding and (b) rearrangement of chains.



18.40 Changes in strength and breaking extension in the experiments of Dismore and Statton on annealing nylon 6.6 [58].

Thus, in some experiments on nylon 6, exposure at about 120 °C causes an increase in dye uptake, but for temperatures above 190 °C there is a decrease: the rates of dye diffusion also change. This connection shows the need for great uniformity of heat treatments if dye faults are to be avoided.

The structural changes observed by Dismore and Statton [58] in the nylon samples for which observations are shown in Figs 18.35 and 18.40 included some increase in crystallinity (as indicated by the X-ray orientation index) but a reduction in dynamic modulus, an increased intensity of small-angle X-ray diffraction and an increase in long-period diffraction, and more fluid-like mobility as indicated by nuclear magnetic resonance (NMR) results. These results suggest that the crystalline regions are becoming larger and more perfect, while remaining oriented, with the non-crystalline material becoming less oriented and more mobile.

Gupta [63] summarises a number of papers on the effect of heat-setting polyester (PET) yarns at various temperatures both free to shrink and at constant length. The fibres were structurally characterised by wide- and narrow-angle X-ray diffraction, polarising optical microscopy, infrared spectroscopy and electron microscopy. The properties reported on are density, sonic modulus, boiling water shrinkage, tensile stress–strain response, recovery from elongation and uptake of disperse dye.

18.6 Setting

18.6.1 Technical importance and characteristic features

The ability to set fibres, namely to stabilise their state either in an existing form or after deformation, has major effects in processing and use. Traditionally, this was carried out on natural fibres by ironing, which combines pressure, heat and, most importantly, drying. The advent of synthetic fibres, which could be heat-set, revolutionised the technology. Fabrics could be heat set, either in a smooth form or

in sharp creases or pleats. To a considerable degree, the set was held during use and laundering, which gave 'non-iron', 'drip-dry' and 'wash-and-wear'. Processing continuous filament yarns to give bulk, stretch and texture was the most important of new fibre processing operations. The 'ease-of-care' features of synthetic fibres stimulated the natural fibre community to develop setting procedures in order to compete with synthetics.

Setting can be characterised as either *temporary* or *permanent*, though the terms are somewhat loosely used. Temporary set is commonly lost in use and certainly by going back into the setting conditions and re-setting in a new form. Permanent set cannot be undone except by going to more severe conditions, if this is possible.

Setting can also be characterised by how it is achieved. This may be by chemical action. In cotton, rayon and other cellulosic fibres, chemical crosslinks between the molecules are introduced by treatment with resins. In wool, the natural cystine crosslinks are broken and re-formed in new positions. These chemical setting treatments are outside the scope of this book, except insofar as they influence physical properties. In moisture-absorbing fibres, hydrogen bonds are broken on wetting and can re-form in new positions on drying to give a temporary set. Setting on drying is seen on drying of cotton, wool or hair. It is interesting to note that K arrholm *et al.* [64] found that a more severe wrinkling in wool fabrics occurred when the relative humidity was changed while the material was in the deformed state. Finally there are the thermal transitions, which have been described in this chapter. The observation of heat setting and its interaction with moisture raises important scientific and technical questions. The whole subject of setting was discussed in detail in the book edited by Hearle and Miles [65], but important research has been done since this was published.

Any thermal transition that causes a peak in the loss modulus must give rise to a setting effect, since it implies that part of a structure that is rigid below the transition is mobile above it. If the fibre is cooled through the transition in a deformed state, then it will become rigid and be set in the new form. The secondary transitions cause temporary setting effects, since the structure is not changed. A reference state can always be reproduced by taking the fibre above the transition and cooling it free of any restraint. The transitions below room temperature are of little practical importance for setting, but the ones above room temperature do give important temporary set to fibres. At higher temperatures, but well below the melting point (around 200 °C for nylon 66 and polyester), a permanent set is achieved. Successive setting can be achieved by successive treatments under conditions that will disturb the structure once again. In nylon, industrial experience in false-twist texturing indicates that it is necessary to go to more severe conditions of temperature or stress to re-set the fibre. In polyester, second-stage heating, which gives yarns with high bulk but low stretch, is carried out at lower temperatures than in the first heater where the yarn is set in the twist state prior to untwisting. The definition of *permanent set* appears to be weaker in polyester than in nylon.

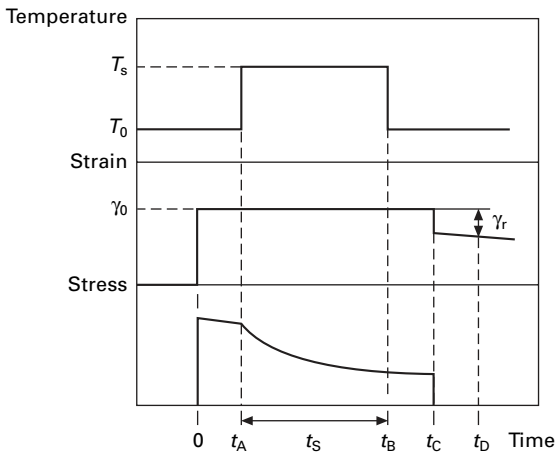
It must be remembered that any thermal treatment severe enough to cause a permanent heat-set will also cause the mechanism of temporary set to operate. A subsequent less severe treatment, for example, in boiling water, will release the temporary set but not the permanent set. Fibres set under tension will therefore show

a shrinkage when later heated. The temporary set may also act as the material cools down. On first unwinding a textured yarn from a package, it will not show any texture, but on exposure to heat, the temporary set will be released and the bulk will develop. The texture can also be developed by ‘milking’ the yarn, namely by repeated tensioning.

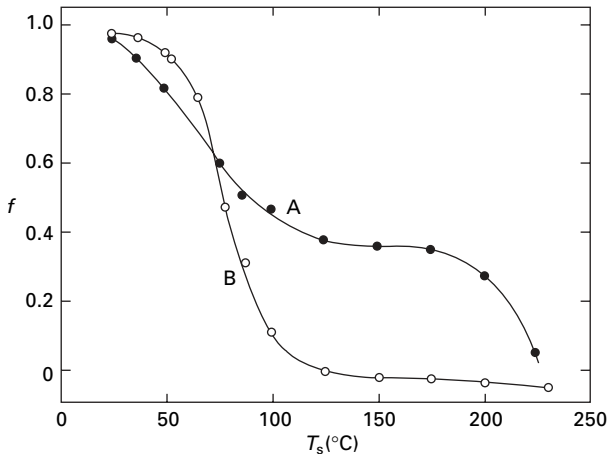
18.6.2 Heat setting of polyester and nylon

An important series of experiments on the heat setting of polyester (PET) monofilaments was reported by Salem [66] and Buckley and Salem [67, 68]. The monofilaments had been melt-extruded in the laboratory and drawn 5× to give a diameter of 51 μm (27 dtex). Any pre-setting was carried out with the fibre taut at constant length. The setting sequence is shown in Fig. 18.41. For torsional experiments, after releasing any initial twist, specimens were clamped and twisted at constant length, transferred to heating in oil or air, then removed to room temperature and released from the clamps to allow recovery. The fractional recovery f , which is a measure of the degree of set, is defined as recovered twist/imposed twist. Thus $f = 1$ indicates no setting and $f = 0$ indicates complete set. The quoted strain value is the shear strain at the surface of the monofilament. For bending experiments, specimens were wound round *Tufnol* or glass rods and clamped for the heat-setting sequence. The quoted strain value is r/R , where r is fibre radius and R is rod diameter.

Figure 18.42 shows the interaction of two setting effects. If the material is tested as produced, the setting is apparently complete in the range of 50–120 °C. Although the recovery hardly changes, a temperature around 200 °C gives some added stability,



18.41 Heat setting sequence starting from zero stress at room temperature, through imposed changes in strain and temperature with time (with assumed stress change), followed by recovery at zero stress and room temperature where T_0 is the initial temperature, T_s is the setting temperature, t_s is the setting time and t_A , t_B , t_C and t_D are times at each stage. γ_0 is the imposed shear strain on the outside of the twisted monofilament and γ_r is this strain after release. From Buckley and Salem [68].



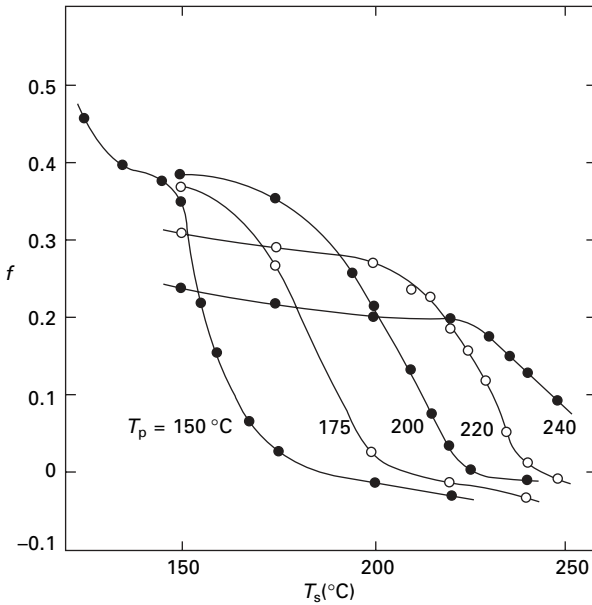
18.42 Fractional recovery of polyester monofilament in torsion plotted against setting temperature: A, pre-set at 200 °C; B, as produced. Setting time = 120 s. From Buckley and Salem [67].

which is suggested by the slight overshoot to negative values of f above 180 °C. The clear evidence comes from re-setting. A specimen that has been pre-set at 200 °C has only half the recovery in the range of 50–120 °C. The setting is completed in the range of 180–220 °C. The 50–120 °C set is associated with the transition shown in Section 18.3.2, e.g. in Fig. 18.21 or the ‘major transition’ in Fig. 18.27. It is a temporary set, which is overcome by re-heating. The ‘permanent set’, which is used in texturing and other processes, is in the 180–220 °C range. The unavoidable imposition of temporary set on any permanent setting sequence must be taken into account in interpreting the results of setting tests.

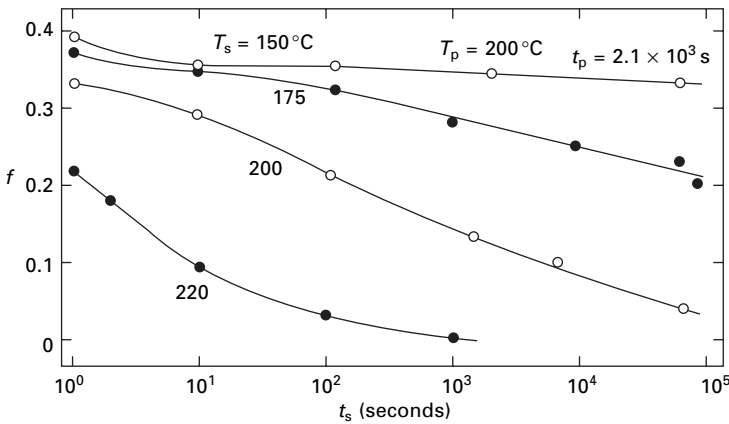
Figure 18.43 shows that the high-temperature set is moved to higher temperatures as the pre-setting temperature is increased. However, the setting starts below the pre-set temperature. Figure 18.44 shows that setting is time-dependent. A fibre pre-set at 200 °C for 35 minutes is almost fully re-set in 1 second at 220 °C, but takes one day to reach the same set at 200 °C. Re-setting occurs at 175 °C, but is much slower and still continuing after 1 day. Figure 18.45 shows that setting in bending is similar to setting in torsion. Figure 18.46 shows that setting becomes more complete as the level of deformation increases.

Mukhopadhyay [61] found a difference in clockwise and anti-clockwise heat setting of a polyester monofilament.

A more limited set of tests on nylon 66 were reported by Hearle *et al.* [69]. Figure 18.47(a) shows similar behaviour to that in Figs 18.42 and 18.43 for polyester, with a low-temperature set around 40 °C and a high-temperature set which can start at 140 °C and is complete at 180–240 °C with higher temperatures needed to overcome the pre-set. Figure 18.47(b) shows a marked difference from polyester. There is time dependence in the low-temperature set, but none in the high-temperature set. This was confirmed in tests at other setting temperatures. Some uncertainty then appears in the report. A set of tests on a different sample of nylon 66 shows time dependence in setting temperatures from 150 to 200 °C, which is similar to that of polyester.

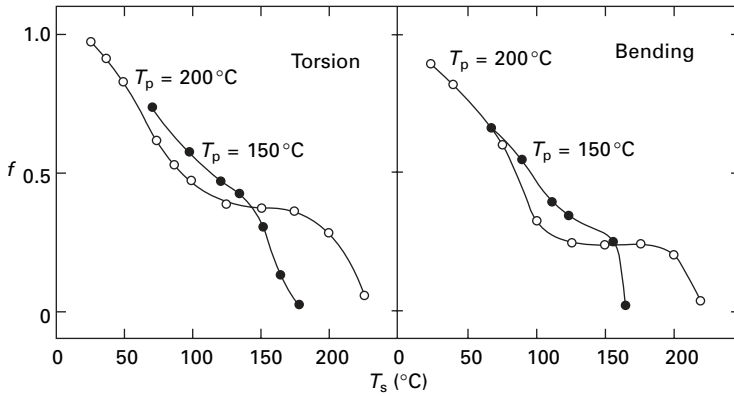


18.43 Fractional recovery of polyester monofilament in torsion plotted against setting temperature at various pre-setting temperature T_p . Pre-setting time 35 mins; setting time = 120 s. From Buckley and Salem [67].

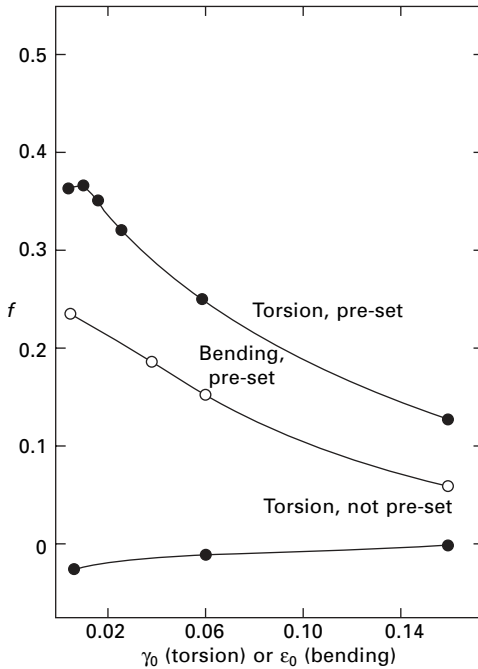


18.44 Fractional recovery of polyester monofilament in torsion plotted against setting time at various setting temperatures. Pre-set at 200 °C; setting time of 35 mins. From Salem [66].

An abundance of technological experience shows that steam setting of nylon occurs at a temperature about 80 °C below that in the dry state, corresponding to the lower melting point. Most fabric setting is carried out in superheated steam at temperatures around 120 °C compared to 200 °C for dry setting. Appreciably lower temperatures are used for nylon 6, reflecting its lower melting point.



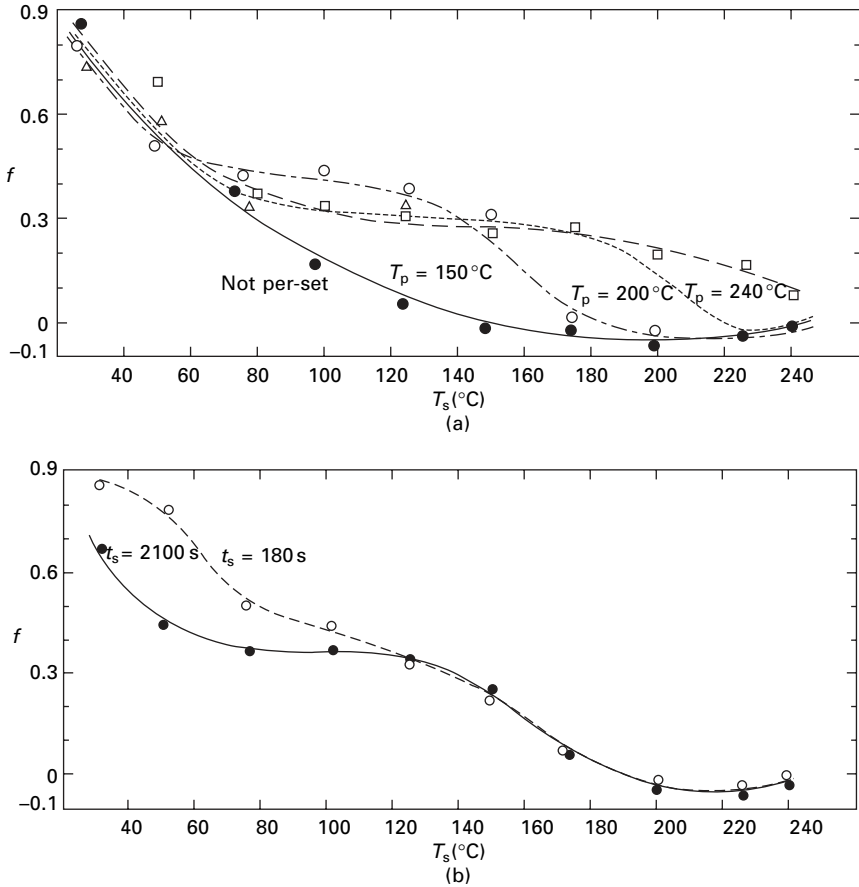
18.45 Fractional recovery of polyester monofilament plotted against setting temperature in torsion and bending at two pre-setting temperatures. Pre-set at 200 °C; setting time of 35 mins. From Buckley and Salem [68].



18.46 Strain dependence of fractional recovery in torsion and bending for polyester monofilament heat-set at 150 °C for 2 mins after pre-set at 200 °C and (in torsion) without pre-set. From Buckley and Salem [68].

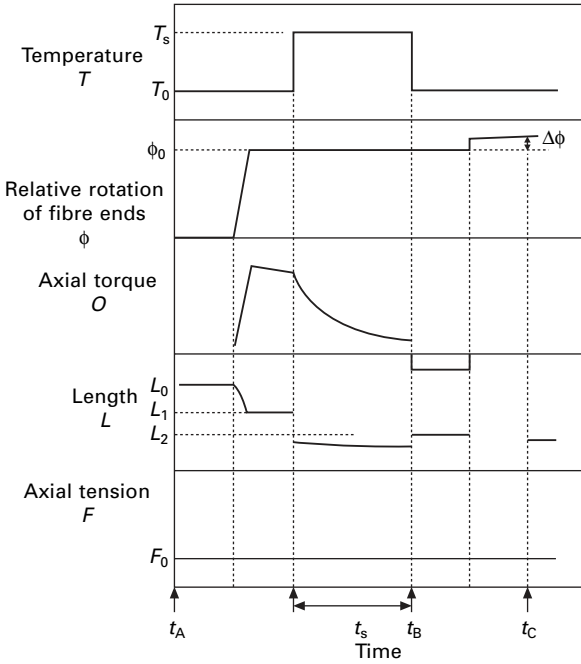
18.6.3 Overtwisting

There is a brief mention above of the occurrence of negative values of f , which implies that the set has *overtwisted* to a value greater than the imposed twist. This anomaly was reported by Arghyros and Backer [70] in their research on twist-texturing.

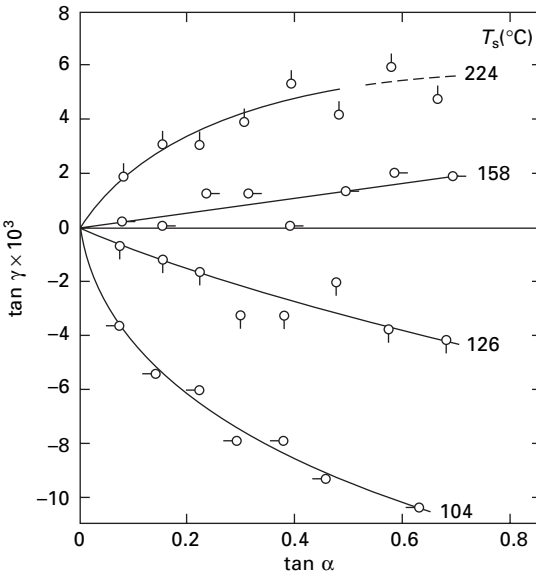


18.47 Fractional recovery in heat-setting of nylon 66. (a) Plotted against setting temperature for various pre-set temperatures. Pre-set of 2100 s; set time of 120 s. (b) Plotted against setting temperature for set times of 180 and 2100 s. Pre-set at 150 °C for 2100 s.

Figure 18.48 shows a sequence of changes in twisting, heating, cooling and releasing at constant tension by Buckley *et al.* [71]. Note the contraction in length on both twisting and heating and some length recovery on release. The data were reported in terms of tangents of the shear angle α at the surface during setting and of an angle γ , which is the difference between α and the shear angle after release, namely the shear angle associated with the overtwist $\Delta\phi$ in Fig. 18.48. As shown in Fig. 18.49, there is a positive overtwist given by $\tan \gamma$ for setting above about 150 °C, and a negative value of $\tan \gamma$, which implies incomplete setting, for lower temperatures. The overtwist increases with increased imposed twist. Similar results were found with other samples of polyester and nylon. The overtwist decreased with increased tension and $\tan \gamma$ became negative at higher tensions. Overtwist was decreased by pre-setting. Repetition of the setting sequence, by clamping, heating, cooling and releasing, shows *twist-climbing* with the overtwist increasing without more twist being inserted.



18.48 Sequence of changes in test of overtwisting. T , ϕ and F are independent variables; O and L are dependent variables; $\Delta\phi$ is the overtwist. From Buckley *et al.* [71].



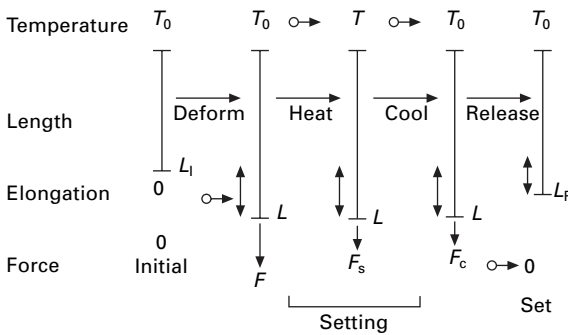
18.49 Overtwist of polyester monofilament plotted against imposed twist for various setting temperatures. α is shear angle at surface during setting; γ is difference from α after recovery (corresponding to $\Delta\phi$ in Fig. 18.48).

Buckley *et al.* [71] show that the phenomenon of overtwisting can be explained by the length changes and thermo-elasticity of an oriented polymer. A quantitative analysis follows a treatment of the thermoviscoelasticity of a twisted yarn [72].

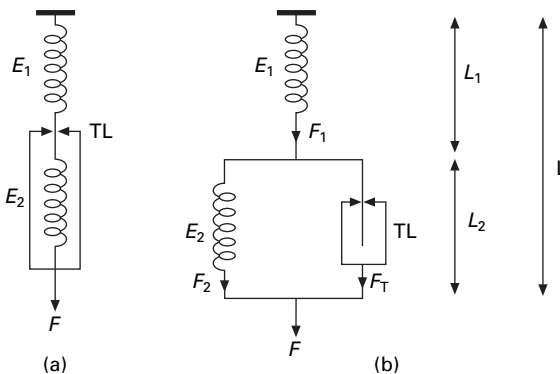
18.6.4 Phenomenological treatment of heat setting

A simplistic treatment of heat setting illuminates some of the features of an extremely complex subject. It is presented in terms of a model of force and length changes in temporary set, but other modes such as torque and twist or bending moment and curvature could be substituted. Normalised quantities, namely stress and strain, could also be used. The treatment, which predicts degree of set, is a simplification of the viscoelastic model of Buckley and Salem [67]. Other enhancements could be added to the model to take account of secondary effects, but the simple model brings out the primary features of setting.

Figure 18.50 shows a typical heat setting sequence: elongating, heating and cooling at constant length, and releasing. The terminology is as follows. F = total force; L =



18.50 Typical heat-setting sequence. F = total force, L = total length, L = total elongation. A zero subscript indicates the stress-free state, S = setting state, R = state after release.



18.51 (a) Simple model for heat-setting. (b) Expanded version showing forces and lengths.

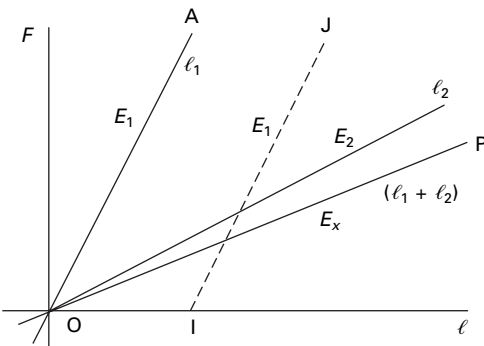
total length; l = total elongation. Subscript $[_0]$ is for stress-free state; subscript $[_S]$ is for setting state; subscript $[_c]$ is for cooled state; subscript $[_R]$ is for state after release. The degree of set is defined as set length/setting length = l_R / l_S .

The simple model, Fig. 18.51, consists of two springs, with spring constants E_1 and E_2 , in series with a thermal lock TL, which can open or close. $F_{1,2}$, $L_{1,2}$, $l_{1,2}$ are forces, lengths, and elongations for springs 1 and 2. The combined spring constant with TL open is E_x . For a series system, $E_x^{-1} = (E_1^{-1} + E_2^{-1})$. The basic assumption of the model is that setting is due to a single change between a more rigid state below a transition temperature, when TL is closed, and a more mobile state above the transition temperature, when TL is open. Setting is by release of restraint on heating and application of restraint on cooling, while the material is held at constant length. Linearity, absence of reversible expansion and contraction, time dependence, combined modes of deformation, and change in moduli except at transition are secondary features that are neglected.

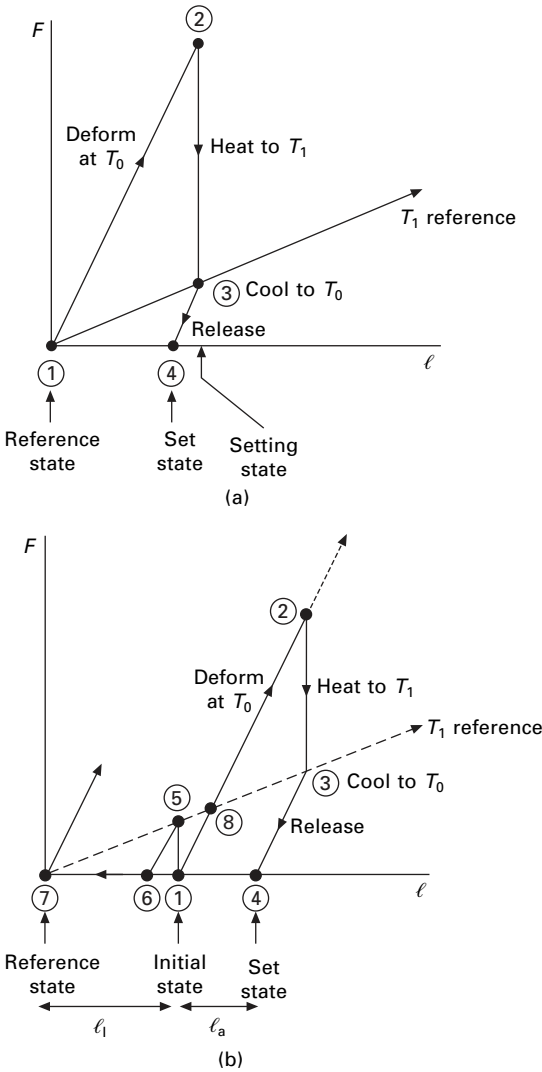
Force–elongation plots are shown in Fig. 18.52. There is a reference state at O, which is always reached if TL is opened above the transition temperature and both springs drop to zero force. With TL closed at ambient temperature, deformation would follow the line OA, or the dotted line IJ if the fibre had been set at another state. With TL open above the transition temperature, the line OP would always be followed.

A setting sequence from the reference state is shown in Fig. 18.53(a). The temperature T_0 is below the transition temperature and T_1 is above. The fibre is first extended at T_0 (1→2), and then heated to T_1 (2→3), with a consequent drop in force. (Any approach to (3) would give the same final result.) The specimen is then cooled to T_0 and released. Since TL is closed at T_0 , the recovery will be along a line with the slope E_1 . The fibre is left in the set state (4). With TL open at (3) the force is in both springs is ($E_x l_S$). When the fibre is cooled and released with TL closed, spring 2 is clamped and cannot retract, but spring 1 can recover by ($E_x l_S/E_1$). Hence:

$$\text{set length} = l_R = l_S - \left(\frac{E_x l_S}{E_1} \right) = l_S \left[1 - \left(\frac{E_x}{E_1} \right) \right] \tag{18.3}$$



18.52 Force–elongation relations. Lines from O are for initial state at temperature T_0 with TL open. Line IJ is with TL closed at intermediate state.



18.53 (a) Heat-setting sequence from initial state of model. (b) Sequences from an initial set state.

$$\text{degree of set} = \frac{l_R}{l_S} = 1 - \frac{E_x}{E_1} \tag{18.4}$$

The effectiveness of a setting operation on this simple model is determined by the ration of the modulus above the transition temperature to the modulus below the transition temperature.

Setting from a previously set state is shown by the sequence (1→2→3→4) in Fig. 18.53(b) and finished at the same set state. The sequence (1→5→6) shows the effect of holding the specimen at its initial state, heating to T_1 , cooling and releasing. Geometric modelling, which could be programmed for computing, would be the way

to follow complicated sequences. Some experimental data [73] indicates that setting of nylon and polyester monofilaments followed the predictions for temperatures up to 190 °C provided some stress relaxation was added to the model.

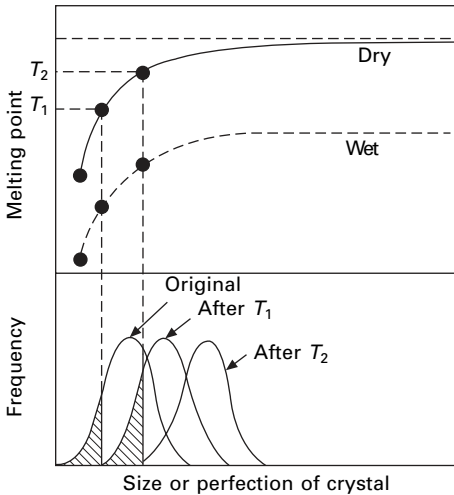
Although the model is highly simplified, it does indicate that the degree of set can be estimated from the ratio of deformability at the cool temperature to deformability at the setting temperature. For permanent setting, the model could be applied to an initial set, but the structure would then be changed and it is the deformability of the cooled structure that would be relevant. Heating again, unless it was to a higher temperature that gave full mobility, and releasing would lead back to a new reference state.

18.6.5 Setting mechanisms

Setting in cotton by introducing new bonds between molecules and in wool by switching the position of cystine bonds are clear chemical mechanisms for permanent setting of fibres in new forms, which are not changed in use. Setting by wetting and drying, with hydrogen bonds being broken and re-formed in new positions, is a clear mechanism for temporary set. The low-temperature effect in nylon and polyester fibres at *c.* 100 °C is a temporary set that can also be explained by the changed positions of hydrogen bonds or mutual attractions of benzene rings, as discussed in Section 1.1.2. The mechanism for the high-temperature ‘permanent’ setting is difficult to explain because there are so many possibilities. It is likely that various mechanisms act together, with their relative importance varying according to the type of fibre and its previous thermomechanical history. Possible mechanisms are reviewed below.

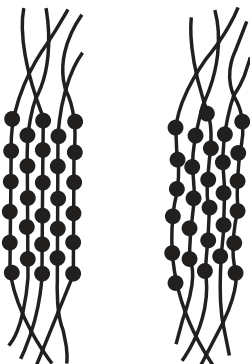
It should be re-stated that the permanent setting sequence will have the temporary set superimposed and that reversible thermal expansion or contraction will also be superimposed. Thermodynamically, permanent set must result from a transfer from one free energy minimum to another at a lower level, which is made possible by thermal vibrations. Such changes are almost always time dependent, certainly for small systems, which is another complication. It must also be remembered that it is not clear whether the high-temperature set of nylon and polyester is permanent or temporary, albeit not being overcome in normal use.

- *Larger and better crystals.* The simplest explanation is that heating leads to annealing, namely the melting of small or imperfect crystals and the growth of larger, more perfect crystals. The mechanism is illustrated in Fig. 18.54, which also shows the effect of lower melting points of wet fibres. At the start, there is a distribution of crystal sizes and perfections, which give a range of melting points. At a given temperature, the smallest crystals will melt and larger ones will be formed. The process can be repeated at successively higher temperatures, but cannot be reversed. This happens in metals, where the small crystal grains butt on to larger ones. It is more difficult to see how it would work with a distribution of polymer crystallites separated from one another without melting of the whole material. Once a fine structure of crystalline and amorphous regions is established, the pattern tends to remain. Furthermore the setting temperatures are appreciably lower than the melting temperatures.



18.54 Distributions of melting points of crystals with different sizes.

- *Defect mobility.* In metals, defects can move to the surface of crystals and disappear. This may well be a setting mechanism in polyethylene, where defects due to mis-packing of $-\text{CH}_2-$ units occur and are a cause of imperfect crystallinity. It may possibly also apply to polypropylene and other polymers with short repeats. However, as discussed in Section 1.3.2, defect models are not sensible for polymers with the long repeats found in nylon 6 or 66 and polyesters.
- *Multiple melting.* For rapidly quenched fibres, the change from form I to form II, discussed in Section 18.2.2, would certainly provide a setting mechanism. However, form II can be set, so that this cannot be a complete explanation.
- *Crystallite mobility.* A variant included in the discussion on multiple melting is that, owing to thermal vibrations, individual crystalline micelles might be able to melt and then recrystallise, as indicated in Fig. 18.55. Rather like molecules moving between liquid and vapour, most micelles would be crystalline, thus maintaining the integrity of the fibre, but a changing population would be molten.



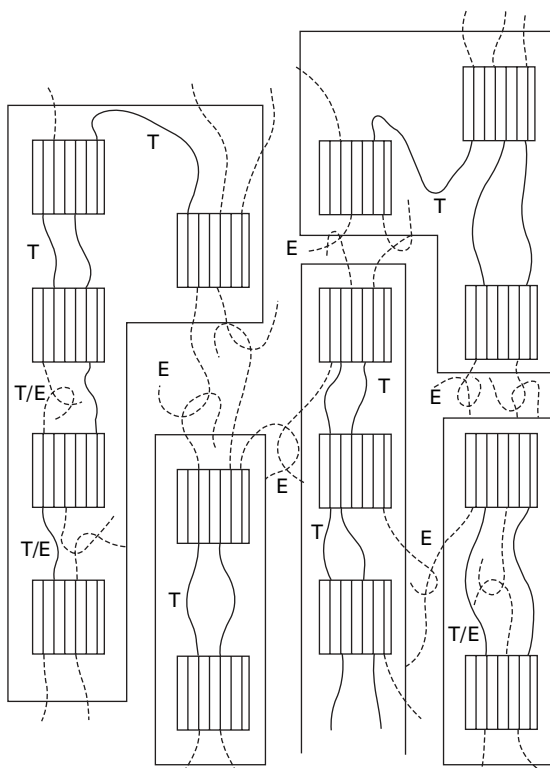
18.55 Flipping between crystalline and locally molten states.

Berry [74] has shown that small clusters of argon atoms can act in this way, flipping between the two states over a certain temperature range. If the material was deformed, the recrystallisation would take place in a slightly different form, which stabilised a new state.

- *Quantum superposition.* Hearle [75] has suggested a more speculative variant that at the setting temperature, there is a quantum superposition of ordered and disordered states. Even though the molten state was at a higher energy, the greater number of energy levels would encourage movement between the two states.
- *Movement through crystals.* Molecules passing through a crystallite will be under variable tension. The simplest case to consider is where one end is linked to the network and the other is a free end. Above a certain temperature, it is possible that thermal vibrations will give a high enough tension to pull the molecule through the crystallite. The reverse would not occur, so that a new state would be set. This effect is more likely if the fibre as a whole is under stress, though the discussion in Section 20.3.2 indicates that tie-molecules are tensioned even when there is no externally applied stress. Variants would apply if both ends are linked to the network, but in different ways, or if there is chain folding.
- *Plastic crystals.* There are more extreme options for mechanically driven setting. If a crystallite is subject to shear, layers of molecule would move relative to one another if the yield stress in shear was exceeded.
- *Drawing.* The drawing of unoriented fibres into oriented forms is a form of set induced by plastic yielding of the fine structure with rupture and re-formation of crystallites. This mechanism is obviously not applicable to drawn fibres, but it will be playing a part when partially oriented yarns are subject to draw-texturing.
- *Kink-band formation.* Another form of severe mechanical deformation is the development of kink-bands in bending or shear (see Section 17.2.5). Heating may lead to an annealing of the deformation and stabilisation in a new form.

All the above explanations relate to physical effects in the crystalline regions, with some also involving molecular segments from amorphous regions. However, there are two possible explanations that do not involve crystalline regions:

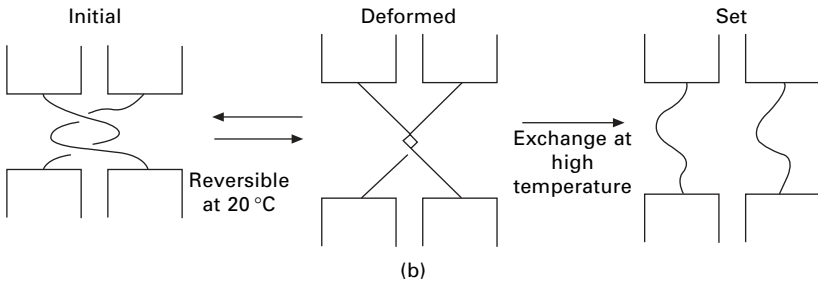
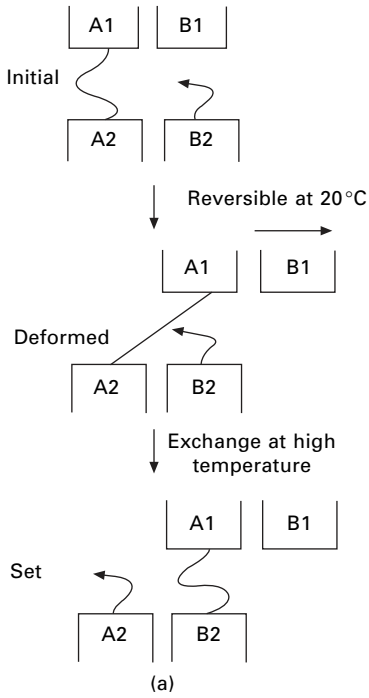
- *Entanglement reptation.* Buckley and Salem [67], citing a low molecular weight commercial polymer, propose the structure in Fig. 18.56 for polyester (PET). Some crystallites are linked together by tie-molecules to form blocks. Between the blocks, there are only entangled chain ends. It is argued that the blocks can move relative to another by viscous flow by a reptation mechanism in which molecular segments progressively move through entanglements. This is accepted behaviour for wholly amorphous polymers, and provides a simple explanation of the time dependence of setting. The explanation is plausible if there is a high degree of chain folding, as implied by the limited number of molecular segments emerging from the crystallites in Fig. 18.56. Alternatively, it is possible that, even if all crystallites are tied together, there could be reptation through entanglements in the amorphous region between crystallites.
- *Transesterification.* It is possible that there is chain scission and re-formation,



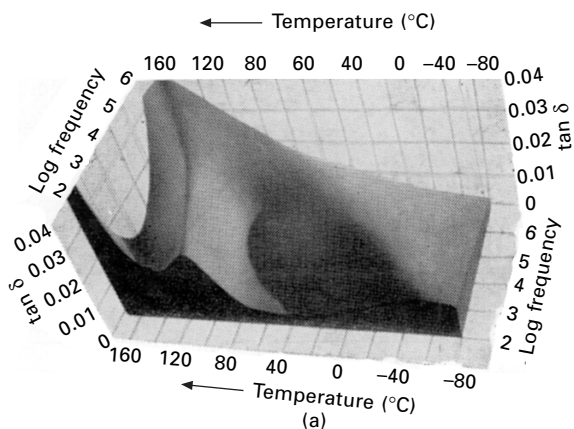
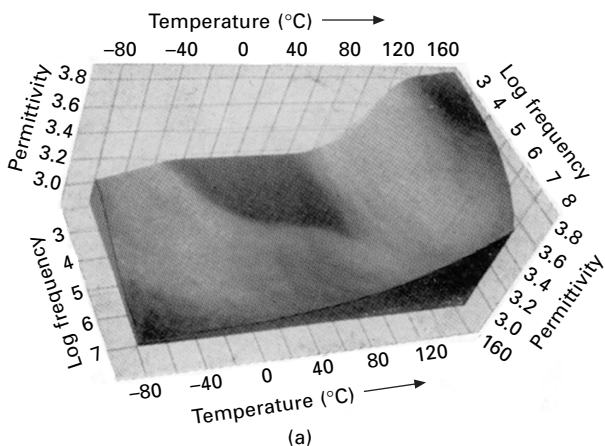
18.56 Structural model for polyester (PET) showing crystallites linked in blocks by tie-molecules (T), possibly plus entanglements (E). Separate blocks linked solely by entanglements. From Buckley and Salem [67].

which can occur in the two ways shown in Fig. 18.57. This is most likely on polyesters, where it is known as transesterification, but there would be an analogous effect in polyamides. Fakirov [76] has reviewed the solid-state reactions that would be relevant. One way of investigating the effects is by bonding together of polymer films. Quantitative information comes from studies by Kugler *et al.* [77] of the changes in length of deuterated segments of PET as measured by SANS (small-angle neutron scattering). Based on extrapolations of their data, calculations by Hearle [73] indicate that the rates of transesterification offer a plausible mechanism for heat setting of polyester.

All the mechanisms involved in heat setting of nylon 66 and polyester (PET) in the 180–220 °C region should be reflected in studies of thermal transitions. Unfortunately reported thermomechanical studies stop at about 180 °C, so that no direct observations are available. The dielectric measurements of polyester film in Fig. 18.58 do show the start of a rapid rise in $\tan \delta$ at 160 °C at low frequency. This may lead to an energy loss peak.



18.57 Two ways for changing links between crystals: (a) exchange of free end; (b) break and re-formation of tie-molecules.



18.58 Influence of temperature and frequency on dielectric properties of Terylene film (after Reddish [78]): (a) relative-permittivity solid model, (b) dissipation-factor solid model.

18.7 References

1. K. Schmeider and K. Wolf. *Kolloid-Z*, 1953, **134**, 149.
2. A. V. Tobolsky. In *Rheology* F. R. Eirich, (Editor), Volume 2, Academic Press, New York, 1958.
3. T. Murayama, J. H. Dumbleton and M. L. Williams. *J. Polymer Sci. A-2*, 1968, **6**, 787.
4. H. E. Bair, T. W. Huseby and R. Salovey. *Analytical Calorimetry*, Plenum Press, New York, 1968, p. 31.
5. S. C. Simmens. Private communication.
6. J. P. Bell, P. E. Slade and J. H. Dumbleton. *J. Polymer Sci. A-2*, 1968, **6**, 1773.
7. J. P. Bell and T. K. Murayama. *J. Polymer Sci. A-2*, 1969, **7**, 1059.
8. J. W. S. Hearle and R. Greer. *Text. Prog.*, 1970, **2**, No. 4, 68.
9. J. W. S. Hearle and R. Greer. *J. Text. Inst.*, 1970, **61**, 243.
10. J. W. S. Hearle. *J. Appl. Polymer Sci., Appl. Polymer Symp.*, 1977, **31**, 137.
11. M. S. Burnip, J. W. S. Hearle and G. R. Wray. *J. Textile Inst.*, 1961, **52**, P343.

12. S. K. Mukhopadhyay, J. W. S. Hearle and P. W. Foster. *J. Textile Inst.*, 1988, **79**, 235.
13. S. K. Mukhopadhyay. *J. Textile Inst.*, 1992, **83**, 573.
14. H. S. Kim, H. Ito, T. Kikutani and N. Okui. *J. Textile Inst.*, 1999, **90**, 508.
15. M. Takayanagi. *Mem. Fac. Engng Kyushu Univ.*, 1963, **23**, No. 1.
16. J. W. S. Hearle. *J. Polymer Sci., Part C, Polymer Symposia*, 1967, **20**, 215.
17. T. Kawaguchi. *J. Appl. Polymer Sci.*, 1959, **2**, 56.
18. T. Kawaguchi. *J. Polymer Sci.*, 1958, **32**, 417.
19. R. Meredith. In *Proceedings of Fifth International Congress of Rheology*, University of Tokyo Press, Tokyo, Japan, 1969, Volume I, p. 43.
20. A. Kondo, S. Fujino and T. Agatsuma. *Bull. Text. Res. Inst. Japan*, 1964, **6**, 11.
21. H. A. Davis. *J. Textile Inst.*, 1991, **82**, 86.
22. H. A. Davis. *J. Textile Inst.*, 1995, **86**, 332.
23. W. W. Moseley, jr. *J. Appl. Polymer Sci.*, 1964, **8**, 2095.
24. J. H. Dumbleton and T. Murayama. *J. Appl. Polymer Sci.*, 1970, **14**, 2921.
25. S. M. Kveder and T. Rijavec. *Textile Res. J.*, 1994, **64**, 495.
26. S. J. van der Meer. Doctoral Thesis, Delft, Netherlands, 1970.
27. S. J. van der Meer. *J. Text. Inst.*, 1974, **65**, 288.
28. S. Rosenbaum. *J. Appl. Polymer Sci.*, 1965, **9**, 2071.
29. R. Meredith. In *Proceedings of Fifth International Congress in Rheology* S. Onogi (Editor), University of Tokyo Press, Tokyo, Japan, 1969, Vol. 1, p. 43.
30. D. J. Houston and R. Meredith. *J. Appl. Polymer Sci.*, 1973, **17**, 3259.
31. J. W. S. Hearle. *J. Polymer Sci. C*, 1967, No. 20.
32. J. W. Illingworth. *J. Text. Inst.*, 1953, **44**, P328.
33. F.-J. Wortmann. *Int. J. Sheep Wool Sci.*, 2007, **55**, 1
34. M. Druhala and M. Feighelman. *Colloid Polymer Sci.*, 1974, **252**, 381.
35. M. Druhala and M. Feughelman. *Kolloid Z. Z. Polymere*, 1971, **248**, 1032.
36. S. Rosenbaum. *J. Polymer Sci.*, 1970, **C31**, 45.
37. F.-J. Wortmann, B. J. Rigby and D. G. Phillips. *Textile Res. J.*, 1984, **54**, 6.
38. D. G. Phillips. *Textile Res. J.*, 1985, **55**, 171.
39. J. M. Kure, A. P. Pierlot, I. M. Russell and R. A. Shanks. *Textile Res. J.*, 1997, **67**, 18.
40. F.-J. Wortmann, M. Stapels, R. Elliott and L. Chandra. *Biopolymers*, 2006, **81**, 371.
41. T. G. Fox. *Bull. Amer. Phys. Soc.*, 1956, **1**, 123.
42. E. Menefee and G. Yen. *Textile Res. J.*, 1965, **35**, 801.
43. M. Sugisaki, H. Suka and S. Saki. *Bull. Chem. Soc. Japan*, 1968, **41**, 2591.
44. M. T. Katchevsky, E. M. Jaroskiewics and J. M. V. Blanchard. *Int. J. Biol. Macromol.*, 1992, **14**, 257.
45. F.-J. Wortmann and H. Deutz. *J. Appl. Polymer Sci.*, 1993, **48**, 137.
46. F.-J. Wortmann and H. Deutz. *J. Appl. Polymer Sci.*, 1998, **68**, 1991.
47. A. R. Haly and J. W. Snaith. *Textile Res. J.*, 1967, **37**, 898.
48. J. Cao and F. Leroy. *Biopolymers*, 2005, **77**, 38.
49. D. R. Buchanan. In *Advances in Fibre Science*, S. K. Mukhopadhyay (Editor), The Textile Institute, Mandnester, 1992.
50. H. C. Kim and M. Gilbert. *Polymer*, 2004, **45**, 7293.
51. H. J. Berndt and G. Heidemann. *Colloid & Polymer Sci.*, 1980, **258**, 612.
52. M. E. Sikorski. PhD thesis, University of Manchester, 1986.
53. M. E. Sikorski and C. P. Buckley. *Proc. 35th Int. Symp. Instrument Soc. America*, Orlando, FL, 1989.
54. M. E. Sikorski, C. P. Buckley, J. W. S. Hearle and S. K. Mukhopadhyay. *Rev. Sci. Instrum.*, 1993, **64**, 1947.
55. S. K. Mukhopadhyay and L. Noui. Unpublished reports, 1991-93, University of Manchester Institute of Science and Technology.

56. M. V. Forward and H. J. Palmer. *J. Text. Inst.*, 1954, **45**, T510.
57. J. W. S. Hearle, P. K. Sen Gupta and A. Matthews. *Fibre Sci. Technol.*, 1971, **3**, 167.
58. P. F. Dismore and W. O. Statton. *J. Polymer Sci. C*, 1966, No. **13**, 133.
59. A. Koshimo. *J. Appl. Polymer Sci.*, 1965, **9**, 69.
60. S. K. Mukhopadhyay and J. W. S. Hearle. *J. Textile Inst.*, 1990, **81**, 156.
61. S. K. Mukhopadhyay. PhD thesis, University of Manchester, 1985.
62. W. O. Statton. In *The Setting of Fibres and Fabrics*, J. W. S. Hearle and L. W. C. Miles (Editors), Merrow, Watford, 1971, Chapter 4.
63. V. B. Gupta. *J. Textile Inst.*, 1995, **86**, 299.
64. E. M. K  rholm, C. O. Bostwick, G. Sil  n, and C. Kahlson. *Appl. Polymer Symp.*, 1971, No. **18**, 999.
65. J. W. S. Hearle and L. W. C. Miles (Editors). *The Setting of Fibres and Fabrics*, Merrow, Watford, 1971.
66. D. R. Salem. PhD Thesis, University of Manchester, 1982.
67. C. P. Buckley and D. R. Salem. *Polymer*, 1987, **28**, 69.
68. C. P. Buckley and D. R. Salem. *J. Appl. Polymer Sci.*, 1990, **41**, 1707.
69. J. W. S. Hearle, M. A. Wilding, C. Auyeung and R. Ihmayed. *J. Textile Inst.*, 1990, **81**, 214.
70. S. Arghyros and S. Backer. *Textile Res. J.*, 1982, **52**, 295.
71. C. P. Buckley, J. W. S. Hearle and R. Mandal. *J. Textile Inst.*, 1985, **76**, 264.
72. C. P. Buckley. *Int. J. Mech. Sci.*, 1981, **23**, 503.
73. J. W. S. Hearle., Unpublished experiments and calculations.
74. R. S. Berry. *Scientific American*, 1990 (August), **263**, 68.
75. J. W. S. Hearle. *Polymer Eng. Sci.*, 1994, **34**, 260.
76. S. Fakirov. In *Solid State Behaviour of Linear Polyesters and Polyamides* J. M. Schultz and S. Fakirov (Editors), Prentice Hall, Englewood Cliffs, N J, 1990.
77. J. Kugler, J. W. Gilmer, D. Wiswe, H. G. Zachmann, K. Hann and E. W. Fischer. *Macromolecules*, 1987, **20**, 1116.
78. W. Reddish. *Turns. Fowaday Soc.*, 1950, **46**, 459.